CONTENTS

Page

INTENTIONALLY LEFT BLANK

TABLES

Page

INTENTIONALLY LEFT BLANK

FIGURES

Page

FIGURES (Continued)

FIGURES (Continued)

INTENTIONALLY LEFT BLANK

2.3.3   Water Seeping into Drifts
[NUREG-1804, Section 2.2.1.3.3.3: AC 1(1) to (5), (7) to (9), (12), AC 2(1) to (3), AC 3(1) to (4), (6), AC 4, AC 5; Section 2.2.1.3.6.3: AC 1(6)]

The information presented in this section addresses the requirements of proposed 10 CFR 63.114(a)(1) through (a)(5), (a)(7), and (b) for conducting a performance assessment as it relates to the area of water seeping into drifts. The requirements of proposed 10 CFR 63.114(a)(6) are not referenced in this section because they are addressed by information provided in Sections 2.2, 2.3.4 to 2.3.7, and 2.3.11. Section 2.3.3 also provides information that addresses specific regulatory acceptance criteria in Section 2.2.1.3.3.3 of NUREG-1804, as shown below. According to the proposed rule change to 10 CFR Part 63, the assessment of repository performance by the total system performance assessment (TSPA) needs to consider both the first 10,000 years after disposal and the period after 10,000 years within the period of geologic stability. The same conceptual framework, including the numerical process models and rock properties, is used for predicting ambient seepage for both the first 10,000 years after repository closure and the post-10,000-year period.

With regard to water seeping into drifts, this section presents the following:

- Data from the Yucca Mountain site and surrounding region, uncertainties and variabilities in parameter values, and alternative conceptual models used in the analyses

- Specific features, events and processes (FEPs) included in the analyses, with appropriate technical bases for inclusion

- Technical bases for models used in the performance assessment.

The categories of information provided in this section, as well as the corresponding proposed 10 CFR Part 63 regulatory requirements and NUREG-1804 acceptance criteria, are presented in the table below. With regard to Acceptance Criteria 1(12) and 3(6) in Section 2.2.1.3.3.3 of NUREG-1804, no formal peer reviews were used to support development of the current seepage models discussed in Section 2.3.3. Similarly, while an expert elicitation on unsaturated zone flow was completed for the TSPA for the viability assessment (CRWMS M&O), the results were not directly relied upon to develop the current seepage models. In addition, this section does not discuss the approach used for data qualification. However, scientific analyses, model development, and data qualification activities were conducted in accordance with project procedures that comply with Quality Assurance Program requirements. The project procedures governing data qualification are consistent with NUREG-1298 (Altman et al. 1988) in keeping with Acceptance Criterion 1(12). With regard to Acceptance Criterion AC4(5), the equivalent continuum modeling approach (Pruess et al. 1990) is not used in the models described in Section 2.3.3. Acceptance Criteria 1(6), 1(10), 2(4), and 2(5) of NUREG-1804, Section 2.2.1.3.3.3 are not referenced below because they do not refer to the technical area of water seeping into drifts. These acceptance criteria, relating to components of the engineered barrier system, are addressed in Sections 2.3.5 and 2.3.6. Acceptance Criteria 1(11) and 3(5) are not referenced below because Section 2.2.1.4.1 provides the technical basis for exclusion of criticality from the TSPA.

SAR Section	Information Category	Proposed 10 CFR Part 63 Reference	NUREG-1804 Reference
2.3.3	Water Seeping into Drifts	63.114(a)(1) 63.114(a)(2) 63.114(a)(3) 63.114(a)(4) 63.114(a)(5) 63.114(a)(7) 63.114(b) 63.342(c)	Section 2.2.1.3.3.3: Acceptance Criterion 1(1) Acceptance Criterion 1(2) Acceptance Criterion 1(3) Acceptance Criterion 1(4) Acceptance Criterion 1(5) Acceptance Criterion 1(7) Acceptance Criterion 1(8) Acceptance Criterion 1(9) Acceptance Criterion 1(12) Acceptance Criterion 2(1) Acceptance Criterion 2(2) Acceptance Criterion 2(3) Acceptance Criterion 3(1) Acceptance Criterion 3(2) Acceptance Criterion 3(3) Acceptance Criterion 3(4) Acceptance Criterion 3(6) Acceptance Criterion 4 Acceptance Criterion 5 Section 2.2.1.3.6.3: Acceptance Criterion 1(6)
2.3.3.1	Summary and Overview	Not applicable	Not applicable
2.3.3.2	Ambient Seepage	See details in sections below	See details in sections below
2.3.3.2.1	Conceptual Description of Ambient Seepage Processes	63.114(a)(1) 63.114(a)(4) 63.114(a)(5)	Section 2.2.1.3.3.3: Acceptance Criterion 1(1) Acceptance Criterion 1(2) Acceptance Criterion 1(3) Acceptance Criterion 1(4) Acceptance Criterion 1(5) Acceptance Criterion 1(7) Acceptance Criterion 1(8)
2.3.3.2.2	Data and Data Uncertainty	63.114(a)(1) 63.114(a)(2) 63.114(b)	Section 2.2.1.3.3.3: Acceptance Criterion 2(1) Acceptance Criterion 2(2) Acceptance Criterion 3(1) Acceptance Criterion 3(2) Acceptance Criterion 3(3) Acceptance Criterion 3(4)

SAR Section	Information Category	Proposed 10 CFR Part 63 Reference	NUREG-1804 Reference
2.3.3.2.3	Model and Model Uncertainty	63.114(a)(1) 63.114(a)(2) 63.114(a)(3) 63.114(a)(7) 63.114(b) 63.342(c)	Section 2.2.1.3.3.3: Acceptance Criterion 3(1) Acceptance Criterion 3(2) Acceptance Criterion 3(3) Acceptance Criterion 3(4) Acceptance Criterion 4(1) Acceptance Criterion 4(2) Acceptance Criterion 4(3) Acceptance Criterion 4(4) Acceptance Criterion 5 Section 2.2.1.3.6.3: Acceptance Criterion 1(6)
2.3.3.2.4	Ambient Component of Drift Seepage Abstraction	63.114(a)(1) 63.114(a)(7) 63.114(b) 63.342(c)	Section 2.2.1.3.3.3: Acceptance Criterion 4(1) Acceptance Criterion 4(2) Acceptance Criterion 4(3) Acceptance Criterion 4(4) Acceptance Criterion 5
2.3.3.3	Thermal Seepage	See details in sections below	See details in sections below
2.3.3.3.1	Conceptual Description of Thermal-Hydrologic Processes	63.114(a)(1) 63.114(a)(4) 63.114(a)(5)	Section 2.2.1.3.3.3: Acceptance Criterion 1(1) Acceptance Criterion 1(2) Acceptance Criterion 1(3) Acceptance Criterion 1(4) Acceptance Criterion 1(5) Acceptance Criterion 1(7) Acceptance Criterion 1(8) Acceptance Criterion 1(9)
2.3.3.3.2	Data and Data Uncertainty	63.114(a)(1) 63.114(a)(2) 63.114(b)	Section 2.2.1.3.3.3: Acceptance Criterion 2(1) Acceptance Criterion 2(2) Acceptance Criterion 2(3) Acceptance Criterion 3(1) Acceptance Criterion 3(2) Acceptance Criterion 3(3) Acceptance Criterion 3(4)
2.3.3.3.3	Model and Model Uncertainty	63.114(a)(1) 63.114(a)(2) 63.114(a)(3) 63.114(a)(7) 63.114(b) 63.342(c)	Section 2.2.1.3.3.3: Acceptance Criterion 3(1) Acceptance Criterion 3(2) Acceptance Criterion 3(3) Acceptance Criterion 3(4) Acceptance Criterion 4(1) Acceptance Criterion 4(2) Acceptance Criterion 4(3) Acceptance Criterion 4(4) Acceptance Criterion 5 Section 2.2.1.3.6.3: Acceptance Criterion 1(6)

SAR Section	Information Category	Proposed 10 CFR Part 63 Reference	NUREG-1804 Reference
2.3.3.3.4	Thermal Component of Drift Seepage Abstraction	63.114(a)(1) 63.114(a)(7) 63.114(b) 63.342(c)	Section 2.2.1.3.3.3: Acceptance Criterion 5
2.3.3.4	Total System Performance Assessment Implementation of Drift Seepage	63.114(a)(1) 63.114(a)(3) 63.114(a)(7) 63.114(b) 63.342(c)	Section 2.2.1.3.3.3: Acceptance Criterion 5(1) Acceptance Criterion 5(2)
2.3.3.5	Analogue Observations	63.114(a)(1) 63.114(a)(7) 63.114(b)	Section 2.2.1.3.3.3: Acceptance Criterion 5(1)
2.3.3.6	Conclusions	Not applicable	Not applicable

In some instances, the acceptance criteria in the table above are addressed in multiple sections. The acceptance criteria for Section 2.2.1.3.3.3 of NUREG-1804, Quantity and Chemistry of Water Contacting Engineered Barriers or Waste Forms, are addressed by one or more of Sections 2.2, 2.3.3 to 2.3.7, 2.3.11 and 2.4, as described more fully in Section 2.3.5. The seepage calculation is based on an understanding of flow paths in the unsaturated zone at Yucca Mountain, which affects the quantity of seepage into drifts. Thus, the information on water seeping into drifts presented in this section not only addresses acceptance criteria given in Section 2.2.1.3.3.3 of NUREG-1804, but is also relevant for some acceptance criteria in Section 2.2.1.3.6.3 of NUREG-1804, *Flow Paths in the Unsaturated Zone*. In particular, Acceptance Criterion 1(6) in Section 2.2.1.3.6.3 of NUREG-1804 refers to the spatial and temporal variability employed in process-level models to estimate, among other parameters, seepage flux, a subject relevant to and addressed in this section. Discussions on the spatial and temporal variability employed in the seepage-process models can be found in Sections 2.3.3.2 and 2.3.3.3.

2.3.3.1   Summary and Overview

The unsaturated zone above the repository is a component of the Upper Natural Barrier (Section 2.1.2.1), which prevents or substantially reduces the rate of movement of water into the emplacement drifts. The Upper Natural Barrier therefore prevents or substantially reduces the rate of the movement of water from the repository to the accessible environment. The FEPs that affect the movement (seepage) of water from the unsaturated formation into the emplacement drifts are discussed in this section. The potential for seepage to occur, and the seepage rates, are reduced by the diversion of water around the emplacement drifts as a result of capillary forces and vaporization effects.

An integrated conceptual framework has been developed to model the diversion of water around drifts and to predict the potential for seepage. Two basic time periods are defined, with different processes accounting for seepage barrier effects. During the early postclosure stage, while seepage is affected by thermal perturbation due to the waste heat, both capillary forces and vaporization

effects will likely cause diversion of water around drifts. This period is referred to as the period of thermal seepage (Section 2.3.3.3).

Once the thermal perturbation has diminished (typically, a few hundred to a few thousand years after repository closure), water flow into the drifts is reduced by capillary barrier effects only. This period is referred to as the period of ambient seepage (Section 2.3.3.2). The basic conceptual framework for predicting ambient seepage is the same for the first 10,000 years following repository closure and the post-10,000-year period.

Several FEPS contribute to the capability of the Upper Natural Barrier to limit seepage into emplacement drifts (Section 2.1.2.1). There are two key processes that define the seepage barrier capability during the ambient seepage period:

- **Flow Diversion Around Repository Drifts**—Downward percolation flux in the near-field host rock tends to be diverted around the drift openings by capillary forces. The amount of flow diversion due to capillary forces is a function of (1) the flow characteristics and magnitude of local percolation in the unsaturated zone above the emplacement drifts; (2) permeability and capillary strength of the fractured rock mass near the emplacement drifts; and (3) geometry of the emplacement drifts and drift-wall properties (Section 2.3.3.2.1.3).

- **Water Influx at the Repository**—Water influx at the repository is seepage into emplacement drifts. This FEP is directly linked with the above FEP on flow diversion, because the downward percolation water in the host rock that is not diverted around the emplacement drifts will seep into the drifts.

The main features that influence these key ambient-seepage processes are the following:

- **Rock Properties of Host Rock and Other Units**—The capillarity and permeability of the fracture network surrounding drift openings significantly affect diversion of water around repository drifts (Section 2.3.3.2.1.3).

- **Fractures and Fracture Flow in the Unsaturated Zone**—Interconnected fractures are the main conduits for downward percolation in the near-field host rock. The detailed flow patterns in the fractures surrounding drift openings significantly affect seepage (Section 2.3.3.2.1.2).

- **Unsaturated Groundwater Flow in the Geosphere**—The magnitude and variability of unsaturated flow in the unsaturated zone define the downward percolation flux arriving at individual drifts. The characteristics and magnitude of local percolation are a key parameter for seepage (Section 2.3.3.2.1.3).

The parameters and parameter characteristics associated with the above features and processes have been determined to be important to barrier capability (Section 2.1, Table 2.1-2). Various other FEPs influence these main features and processes. A complete list of the FEPs addressed in this section is given in Table 2.3.3-1.

During the period of thermal seepage, thermal perturbation causes additional diversion of water around repository drifts. The key process affecting barrier capability caused by thermal perturbation is the following:

- **Geosphere Dryout Due to Waste Heat**—Thermal-hydrologic effects of heat from the repository reduce the rate of movement of liquid water to the emplacement drifts during the early postclosure stage (Section 2.3.3.3.1). Seepage is not expected to occur as long as boiling temperatures and dryout conditions prevail in the rock above the repository (Section 2.3.3.3.3.1). The thermal-hydrologic conditions in the near-field rock are influenced by many of the features and processes listed above for ambient seepage, in addition to the heat generation characteristics of the waste and the duration and efficiency of preclosure ventilation. Other features and processes important for thermal seepage are the condensation zone forming in the near-field rock, the two-phase flow characteristics of water and vapor, and the resaturation of the rock due to waste cooling (see discussion of FEPs in Table 2.3.3-1).

The effect of boiling and dryout in the host rock surrounding emplacement drifts contributes to barrier capability for the first few hundred to a few thousand years, depending on the location within the repository, which is a small fraction of the period of geologic stability. The parameters and parameter characteristics associated with this FEP have therefore not been specifically identified as important to barrier capability (Section 2.1, Table 2.1-2) (i.e., they are less important for barrier capability as the ambient-seepage related FEPs).

All features and processes discussed above, including their spatial variability and uncertainty, have been accounted for in the seepage predictions conducted in the TSPA, as discussed in Section 2.3.3.2 for ambient seepage and in Section 2.3.3.3 for thermal seepage.

Role of Water Seeping Into Drifts in the TSPA—Figure 2.3.3-1 schematically shows the information flow from the foundation of field and laboratory seepage-related data through different process models to the drift seepage abstraction and the TSPA drift seepage submodel. The following section briefly explains the model and abstraction components displayed in the figure, starting with the detailed process models for seepage predictions.

There are two conceptually consistent process models simulating seepage under ambient conditions: (1) the seepage calibration model; and (2) the seepage model for performance assessment. The seepage calibration model uses field test data from active seepage testing for the validation of the basic conceptual model for seepage predictions and determines seepage-relevant parameters through model calibration (Section 2.3.3.2.3.3). The basic conceptual model for seepage predictions and the calibrated parameters are transferred to the second process model for ambient conditions—the seepage model for performance assessment—which is used to predict drift seepage rates for long-term conditions at Yucca Mountain (Section 2.3.3.2.3.4). Seepage rates are calculated for a range of parameter combinations reflecting their expected spatial variability and uncertainty. Different drift shape scenarios are considered to account for drift degradation, including the possibility of complete drift collapse. Information on drift shape changes is provided by the geomechanical model simulations conducted in the drift degradation analysis (Section 2.3.4). Results from the seepage model for performance assessment are summarized in seepage flow rate tables (lookup tables). As explained in Section 2.3.3.2, these lookup tables,

together with probability distributions of seepage-relevant parameters, are used to predict repository-wide ambient seepage rates in the TSPA.

A third seepage process model, the thermal-hydrologic seepage model (described in Section 2.3.3.3), analyzes seepage behavior during the period when water-flow processes in the near-field host rock are influenced by repository heating. This process model simulates the thermally driven coupled processes in the drift vicinity—including moisture redistribution from boiling and condensation of pore water—and evaluates the combined effect of flow diversion caused by capillary forces and vaporization, respectively. The conceptual treatment of flow diversion due to capillary forces is consistent with the two ambient seepage models. The thermal-hydrologic seepage model is applied to selected simulation cases to determine transient seepage rates for a range of expected repository conditions (Section 2.3.3.3.3.1). To allow for a simple abstraction method, the thermal seepage results are compared to ambient seepage predictions, with the goal of qualitatively describing the evolution of thermal seepage in comparison to ambient seepage rates.

In addition to these three primary seepage models, two other process models provide information on seepage-relevant parameters to the drift seepage abstraction. The flow focusing model evaluates intermediate-scale heterogeneity in rock properties in order to understand how preferential-flow processes affect the local percolation flux arriving at emplacement drifts. The thermal-hydrologic-mechanical model predicts the changes in seepage-relevant parameters caused by excavation-related stress redistribution.

The drift seepage abstraction shown in Figure 2.3.3-1 assembles the input from the various data sources and process model results described above, synthesizes and simplifies this input into a coherent conceptual framework, and then feeds the necessary methods, parameters, and simplifications to the TSPA drift seepage submodel. The ambient component of seepage abstraction (Section 2.3.3.2.4) provides (1) probability distributions for seepage-relevant parameters accounting for spatial variability and uncertainty; (2) seepage lookup tables for intact and degraded drifts; (3) a methodology for determining seepage rates and estimation uncertainty from the lookup tables; (4) a distribution of flow focusing factors; (5) a methodology for categorizing drift degradation (from seismic activity) and seepage behavior based on the accumulated rockfall volume; and (6) a methodology for determining seepage after igneous intrusion and early failure events. The thermal component of seepage abstraction (Section 2.3.3.3.4) develops and justifies the methodology for calculating seepage during the time period of thermal perturbation.

As shown in Figure 2.3.3-1, information needed for the implementation of drift seepage into the TSPA is also provided by two other TSPA components; the EBS thermal-hydrologic environment submodel (SNL 2008a, Section 6.3.2), and the TSPA model for the seismic scenario class (SNL 2008a, Section 6.6). The EBS thermal-hydrologic environment submodel provides percolation flux values interpolated at various locations throughout the repository (Section 2.3.3.2.3.5), using the three-dimensional flux distributions for current and future climate states calculated by the site-scale unsaturated zone flow model (Section 2.3.2). These flux values are needed in conjunction with flow focusing factors to estimate the local percolation flux arriving at the drifts. The EBS thermal-hydrologic environment submodel also provides the evolution of drift-wall temperature at each repository location which is required to evaluate whether thermal seepage is limited by a vaporization barrier (Section 2.3.3.3.4). The TSPA model for the seismic scenario class provides

cumulative rockfall volumes in response to (single or multiple) seismic events, which are used to categorize drifts with respect to the degree of drift degradation and its impact on seepage (Section 2.3.3.2.4.2.2).

Figure 2.3.3-2 shows the information transfer among the principal model components of the TSPA nominal scenario class model. The drift seepage abstraction, using input from ambient and thermal seepage process models, provides input to the TSPA drift seepage submodel (a component of the drift seepage and drift-wall condensation submodel in Figure 2.3.3-2). The TSPA drift seepage submodel is used in the TSPA to calculate the time-dependent average seepage rate (mass of water seeping into a drift segment per time, with drift segment length corresponding to be the approximate length of a waste package plus the spacing between waste packages) and seepage fraction (number of drift segments with seepage divided by total number of drift segments) in percolation subregions under ambient and thermal conditions. The drift-wall condensation submodel, using results from the in-drift condensation model (Section 2.3.5.4.2), provides the average rate of condensation, which is combined with the drift seepage results. These results are provided to the EBS flow submodel (Section 2.3.7.1), which calculates flow rates through breached waste packages and through the invert.

FEPs in the Models Related to Water Seeping into Drifts—The technical basis and approach for analysis of each FEP included in the seepage-related models is summarized in Table 2.3.3-1. Information on the complete set of FEPs, both included and excluded, is given in Section 2.2, as listed in Table 2.2-5. Some of the FEPs included in the seepage-related models are also included in models related to climate and infiltration, unsaturated zone flow, drift degradation, and the in-drift physical and chemical environment (Sections 2.3.1, 2.3.2, 2.3.4, and 2.3.5).

Design Features Related to Water Seeping into Drifts—Those repository features, described in Section 1.3.4, which are important to seepage have been adequately represented in and incorporated into the seepage-related models, the seepage model abstraction, and the seepage calculation in the TSPA. Design features important for ambient seepage are the emplacement drift size and shape, as well as the ground support system. Consistent with Section 1.3.4.2, the ambient seepage predictions are conducted for a circular drift with a nominal 5.5 m diameter. Rock bolts and other ground support described in Section 1.3.4.4 have been shown to not significantly affect the potential for or the magnitude of seepage (Section 2.3.3.2.3.4.1; excluded FEP 2.1.06.04.0A, Flow through rock reinforcement materials in EBS, Section 2.2, Table 2.2-5). An additional design feature important for thermal seepage (and the thermally-induced mechanical or chemical processes occurring in the near-field rock) is the thermal output of the waste packages. The respective process models described in Section 2.3.3.3 use a reference thermal load (which represents average conditions over all waste packages) consistent with the nominal thermal loading conditions described in Section 1.3.1.2.5. Table 2.2-3 provides a summary as to how repository design has been included in the performance assessment. The second and last column in the table provide pointers to where in the SAR each design control parameter is utilized.

2.3.3.2   Ambient Seepage
[NUREG-1804, Section 2.2.1.3.3.3: AC 1(1) to (5), (7), (8), AC 2(1), (2), AC 3(1) to (4), AC 4, AC 5; Section 2.2.1.3.6.3: AC 1(6)]

This section describes the development, calibration, validation, and use of process models for the prediction of potential seepage into waste emplacement drifts under ambient conditions. Ambient conditions are expected over most of the time period important for the performance assessment, except for the early postclosure stages when thermal perturbation is strong because of the heat produced by the radioactive waste. The impact of thermal perturbation on seepage is discussed in Section 2.3.3.3. The ambient seepage models are developed based on a conceptual understanding of the process by which water may seep from the fractured rock into an emplacement drift. This conceptual understanding, as well as the key factors, properties, and conditions affecting seepage are discussed in Section 2.3.3.2.1. Data from active seepage testing, passive monitoring, and other observations provide the basis for the calibration and validation of the seepage process model. These data and their uncertainties are described in Section 2.3.3.2.2. The data are incorporated into a site-specific seepage process model through the seepage calibration model, which determines seepage-relevant parameters. These parameters are transferred to a conceptually consistent prediction model (the seepage model for performance assessment), which is used to calculate ambient seepage into waste emplacement drifts for a range of expected parameter combinations. The development, calibration, validation, and application of these models—as well as a discussion of model uncertainty and alternative conceptual models—can be found in Section 2.3.3.2.3. The results from the seepage prediction model are summarized in lookup tables. As described in Section 2.3.3.2.4, these tables—together with probability distributions of seepage-relevant parameters and a suitable abstraction of seepage-relevant FEPs (Table 2.3.3-1)—provide the information needed for the implementation of ambient drift seepage into the TSPA.

2.3.3.2.1   Conceptual Description of Ambient Seepage Processes
[NUREG-1804, Section 2.2.1.3.3.3: AC 1(1) to (5), (7), (8)]

In the context of Yucca Mountain seepage is defined as dripping of water into an underground opening, such as a niche, alcove, access tunnel, or emplacement drift (SNL 2007a, Section 6.1.3). Accordingly, seepage, as discussed in this section, does not include advective or diffusive vapor flow into the opening or condensation of water vapor on surfaces, which may lead to water drop formation and water drop detachment. Seepage, as defined here, does not constitute all the water potentially contacting the EBS. Furthermore, some of the water entering an underground opening may evaporate or flow along the wall and, thus, does not contribute to seepage. In-drift moisture redistribution and potential condensate accumulation are discussed in the section on the in-drift physical and chemical environment (Section 2.3.5).

In the unsaturated zone at Yucca Mountain, percolating water encountering an emplacement drift tends to be diverted around the opening because of capillary effects (Figure 2.3.3-3; Table 2.3.3-1, FEPs 2.1.08.02.0A Enhanced influx at the repository; 2.2.07.03.0A, Capillary rise in the unsaturated zone; and 2.2.07.20.0A, Flow diversion around repository drifts). Seepage occurs when percolation flux exceeds the seepage threshold (the minimum percolation flux required to initiate seepage). A nonzero seepage threshold indicates that water may be excluded due to capillary diversion. This capillary-diversion effect reduces the amount of water entering an emplacement drift, or prevents dripping altogether. The seepage flux averaged over a sufficiently large area

(i.e., that of an emplacement drift section with the length of a waste package) will always be equal to or less than the local percolation flux.

2.3.3.2.1.1   Significance of Seepage for Repository Performance

The rate and distribution of seepage from the unsaturated zone above the repository (a component of the Upper Natural Barrier) into the emplacement drifts affect performance in different ways. The number of waste packages contacted by water, the corrosion performance of the features that make up the EBS, the dissolution and mobilization of radionuclides, and the release and migration of radionuclides to the unsaturated zone below the repository (a component of the Lower Natural Barrier) are all influenced by seepage (Section 2.3.5). Partial or complete diversion of water around the emplacement drifts due to capillary diversion, in combination with vaporization during the thermal period, reduces or prevents seepage into the emplacement drifts. In addition, flow diversion around drifts results in development of a low-saturation and low-flux zone beneath the emplacement drift (Figure 2.3.3-4), which may delay the transport of released radionuclides from the emplacement drift to the unsaturated zone, but has been excluded from TSPA on the basis of low consequence (Excluded FEP 2.2.07.21.0A, Drift shadow forms below repository, in Section 2.2, Table 2.2-5).

2.3.3.2.1.2   Description of Ambient Seepage Process

Seepage is a process that occurs at the interface between the Upper Natural Barrier and the EBS. As a result, the amount and distribution of seepage is not only affected by the hydrogeological properties and flow conditions in the fractured host rock, but also by the repository design (drift geometry), construction method (excavation effects, drift surface roughness), and the operating conditions within the drifts (e.g., heat load and ventilation). Figure 2.3.3-4 schematically depicts the potentially significant processes and factors affecting seepage for both an intact drift and a partially collapsed drift. Some of the processes and factors shown in Figure 2.3.3-4 are insignificant and thus are excluded from further consideration (e.g., ground support, see excluded FEP 2.1.06.04.0A, Flow through rock reinforcement materials in EBS, Section 2.2, Table 2.2-5). Others (such as film flow and matrix imbibition (Table 2.3.3-1; FEPs 2.2.07.09.0A, Matrix imbibition in the unsaturated zone; and 2.2.07.18.0A, Film flow into the repository)) are not explicitly simulated, but are accounted for and therefore included in the seepage models through the estimation of effective seepage-relevant parameters (Section 2.3.3.2.1.5). A third group of processes (such as ventilation and evaporation effects) are considered when necessary (e.g., during model calibration), but conservatively are not included in the prediction of ambient seepage (as explained later in this section). The treatment of processes and factors shown in Figure 2.3.3-4 that are considered relevant for seepage assessment, and the identification of the key seepage-relevant parameters, are discussed in Section 2.3.3.2.3.

The source of seepage water is deep percolation in the unsaturated zone, which in turn depends on the precipitation and infiltration patterns at the surface. At Yucca Mountain, the majority of precipitation is inhibited from infiltration into the unsaturated zone by surface runoff and evapotranspiration. On the basis of the values in Tables 2.3.1-17, 2.3.1-18, and 2.3.1-19, the infiltration on average ranges from about 8% (average of present-day climate conditions) to about 10% (average of glacial-transition climate conditions) of the precipitation expected over the repository area. Infiltrating water percolates downward in the unsaturated zone as local percolation

flux, driven by gravity and capillary forces. As this water percolates to depth within the unsaturated zone, it is spatially redistributed, as described by the site-scale unsaturated zone flow model (Section 2.3.2).

The detailed flow path within the unsaturated zone is determined by the degree of fracturing, fracture geometry, orientation, connectivity, and the hydrogeologic properties of the fractures and the matrix (Table 2.3.3-1, FEPs 1.2.02.01.0A, Fractures; 2.2.03.02.0A, Rock properties of host rock and other units; and 2.2.07.08.0A, Fracture flow in the unsaturated zone). Depending on these factors, the water in the unsaturated fracture network generally concentrates along discrete flow paths or channels. Tilted contacts between hydrogeologic units (especially between welded and nonwelded tuffs), as well as heterogeneity in rock properties, affect the overall flow pattern and change the frequency and spacing of flow channels (Section 2.3.2). Flow channeling and dispersion of flow paths also occur within rough-walled fractures where asperity contacts and locally larger fracture openings lead to small-scale redistribution of water within the fracture plane. Flow focusing (Section 2.3.3.2.3.5) impacts seepage because seepage depends on the local, rather than the average, percolation flux (SNL 2007a, Section 6.6.5; BSC 2004a, Section 6.8).

Rock formation properties around the emplacement drifts are altered as a result of mechanical, thermal, and chemical processes, which in turn may affect seepage. Stress redistribution during drift excavation leads to local opening or partial closing of fractures and, potentially, the creation of new fractures (SNL 2007a, Sections 6.3.2 and 6.6.3) (Table 2.3.3-1, FEP 2.2.01.01.0A, Mechanical effects of excavation and construction in the near field). Fracture apertures may also be changed by the thermal expansion of the rock matrix. Finally, the local chemical environment, which is altered by evaporation and thermal effects, will lead to dissolution and precipitation of minerals, affecting flow properties of the fracture system and fracture–matrix interaction (SNL 2007a, Section 6.3.2). These conditions lead to a flow pattern around an emplacement drift that is different from that in the undisturbed formation under ambient conditions.

In addition, as percolating water approaches the emplacement drifts, it encounters different thermal conditions over time that affect the amount of water that can seep into the drifts. During preclosure, ventilation removes heat and moisture from the surrounding rock (Table 2.3.3-1, FEP 1.2.02.02.0A, Faults). In most repository locations, near-drift rock temperatures rise above the boiling point of water after closure, resulting in a dryout zone, a two-phase transition zone, and a condensation zone. The effects of these thermal perturbations on flow and seepage are discussed in Section 2.3.3.3. As the radioactive decay heat dissipates, rock temperatures eventually decrease to below the boiling point of water, rewetting occurs, and seepage becomes possible. While there may be irreversible changes in the near-field host rock due to coupled effects, the impact on the quantity of long-term water seeping into the drifts is minor (Section 2.3.3.3.3.4).

Percolating water that reaches the immediate vicinity of the drift wall may be prevented from seeping into the drift because the water has the tendency to be held in the pores on account of capillary forces. This induces a local saturation buildup in the formation within the region closest to the drift crown, leading to a pressure gradient in the direction tangential to the drift circumference. If the tangential permeability and the capillarity of the fracture network within this region are sufficiently high, all or a portion of the water is diverted around the emplacement drift under partially saturated conditions. Conversely, if the capillarity of the formation is relatively weak, tangential permeability is low, or the local percolation flux is high, the water potential in the

formation may be higher than that in the emplacement drift, allowing water to exit the formation and enter the emplacement drift. At the emplacement drift surface, the water either evaporates, follows the inclined rough wall in a film, or forms a drop that may grow and eventually detach. For modeling purposes, only water that drips is defined as seepage to be explicitly modeled by the seepage model for performance assessment (SNL 2007a, Section 6.1.3). Evaporation from the drift wall is included in the seepage calibration model to account for ventilation effects that impacted the observed seepage rates; however, it is not considered in the seepage model for performance assessment, because relative humidity in the drift under ambient postclosure conditions is expected to be close to 100%. This assumption leads to slightly higher and conservative seepage predictions. Film flow is accounted for by estimating an effective, seepage-related parameter from seepage tests that reflects film flow processes (BSC 2005a, Section 6.2.1.1.2).

As discussed in Section 2.3.4, emplacement drifts degrade with time as a result of seismic activity, potentially leading to rock mass damage and rockfall in emplacement drifts (Table 2.3.3-1, FEP 1.2.03.02.0D, Seismic-induced drift collapse alters in-drift thermohydrology). The resulting changes in drift shape and size affect the potential for seepage. Drift degradation furthermore leads to changes in seepage-relevant rock properties in the drift vicinity (SNL 2007a, Section 6.3.1). An abstraction methodology was developed that accounts for all the above effects (Section 2.3.3.2.4), based on seepage modeling predictions for moderately degraded as well as fully collapsed drifts (Section 2.3.3.2.3.4).

Seepage is also affected by igneous intrusions into emplacement drifts (Table 2.3.3-1, FEP 1.2.04.03.0A, Igneous intrusion into repository), which are likely to introduce strong thermal, mechanical, and chemical perturbations within the drifts and the surrounding rock (Section 2.3.11.1). Given the uncertainties in predicting seepage processes under such conditions (SNL 2007a, Section 6.5.1.7), the TSPA drift seepage submodel does not account for the possible capillary-barrier effects above magma-filled drifts. Instead, seepage is conservatively set to the local percolation flux arriving at the drift (Section 2.3.3.2.4.2).

In summary, the rate of water dripping into an emplacement drift is expected to be less than the local percolation rate because (1) the dryout zone around the drift reduces liquid water flow, potentially preventing water from reaching the drift surface (SNL 2007a, Section 6.3.2); (2) the capillary barrier diverts water around the drift; (3) water may flow along the emplacement drift wall without dripping into the opening; and (4) water may evaporate from the drift surface (BSC 2004b, Section 6.3.1). Therefore, even if the seepage threshold were exceeded and seepage occurred, the seepage flux would be lower than the local percolation flux by the amount of water that is diverted around the drift, evaporates, or flows as a film along the drift surface. This ambient seepage representation applies to the period during which rock temperatures are below the boiling point of water, and before the drift geometry may change due to drift degradation in a seismic event. In the case of full drift collapse, when the original openings have filled with rubble rock material, capillary effects are still expected to cause flow diversion at the interface between the solid rock and the rubble-filled drift (Section 2.3.3.2.3.4.2).

2.3.3.2.1.3   Factors and Properties Affecting Ambient Seepage

The factors affecting ambient seepage include (1) the magnitude of the local percolation flux; (2) rock properties, including the strength of the capillary forces in the fractures and the tangential

permeability and connectivity of the fracture network in the immediate vicinity of the emplacement drift; (3) the emplacement drift size and shape, as well as the local topography of the rough emplacement drift wall; and (4) the thermodynamic conditions in the emplacement drift (specifically in-drift relative humidity). Some of these factors are affected by the construction method and ground-support system; they determine excavation effects in the formation, small-scale emplacement drift surface roughness, and the likelihood and geometry of breakouts. The relative humidity in the drift affects the evaporation potential. The treatment of these factors and their incorporation into the base-case seepage conceptual model are discussed below. Drift degradation and drift collapse in response to seismic events change the drift size, drift geometry, and the potential presence of rubble in the drift, which in turn affect the effectiveness of the capillary barrier. These factors are discussed in Section 2.3.3.2.1.4.

Percolation Flux—The magnitude of the percolation flux is an important factor determining seepage (Table 2.3.3-1, FEP 2.1.08.01.0A, Water influx at the repository). Seepage is initiated if the local percolation flux in individual flow channels and the accumulation of water from these channels near the emplacement drift crown exceed (1) the vaporization potential during the thermal period; (2) the diversion capacity of the capillary process; (3) the evaporation potential within the emplacement drift; and (4) the capacity of films to carry water along the emplacement drift surface. It is the local percolation flux rather than the large-scale average flux that controls the onset of seepage (SNL 2007a, Sections 6.3.1 and 6.6.5).

The source of percolation flux is net infiltration at the ground surface, stemming from precipitation events (Section 2.3.1). As infiltrating water percolates through the unsaturated zone, the flow patterns change depending on the heterogeneous properties of the hydrogeologic units (Section 2.3.2). Percolation flux in the TCw hydrogeologic unit occurs mostly in fractures before entering the PTn hydrogeologic unit (BSC 2004c, Section 6.1.2; BSC 2004d, Section 7.9.1). With its high matrix porosity and low fracture frequency, and the existence of tilted layers of nonwelded vitric and bedded tuff, the PTn unit diverts some percolating water into fault zones. It also dampens downward-moving transient pulses from surface infiltration events (SNL 2007b, Section 6.9). Below the PTn is the TSw hydrogeologic unit, which is a thick, densely fractured unit consisting of layers with different lithologic properties that will host the repository. Because of the presence of the PTn, the large-scale percolation flux distributions in the TSw predicted by the site-scale unsaturated zone flow model are considered to be steady within a given climate period, but changes in percolation flux due to climate change are accounted for (Section 2.3.2) (Table 2.3.3-1, FEPs 1.3.01.00.0A, Climate change, and 1.4.01.01.0A, Climate modification increases recharge). The climate states considered are the present-day climate (0 to 600 years after emplacement), the monsoon climate (600 to 2,000 years), and the glacial-transition climate (2,000 to 10,000 years). Percolation flux during the post-10,000-year time period is based on the proposed revision to 10 CFR 63.342(c), where a log-uniform distribution is prescribed defining the spatially-averaged percolation flux through the repository footprint.

Heterogeneities in rock properties of the hydrogeologic units occur on various scales. As seen in Figure 2.3.3-5, large-scale heterogeneities can divert water (e.g., along contacts between hydrogeologic units) and concentrate it into local features (e.g., faults (FEP 1.2.02.02.0A in Table 2.3.3-1)). Intermediate-scale heterogeneities, which are not resolved by the site-scale unsaturated zone flow model, are likely to redistribute water as it percolates downwards, resulting in an average, local percolation flux on the scale of an emplacement drift that is either higher or

lower than the flux averaged on the scale of the larger gridblock used in the site-scale unsaturated zone flow model. This intermediate-scale flow redistribution is captured by a distribution of so-called flow focusing factors, which are defined as the ratio of the drift-scale to the mountain-scale percolation flux. Flow concentration on this intermediate scale is referred to as flow focusing. Flow simulations using the flow focusing model that calculates flow focusing factors (Section 2.3.3.2.3.5) show that flow becomes more focused within tens of meters of the top of the model. The effects of flow focusing change at interfaces between hydrogeologic units, leading to some additional redistribution of flow (BSC 2004a, Section 6.8).

Flow channeling and diversion of flow paths also occur within each rough-walled fracture, where asperity contacts and locally larger fracture openings lead to small-scale redistribution of water within the fracture (BSC 2004b, Section 6.3; SNL 2007a, Section 6.3.1). In addition to spatial flow-channeling effects, temporal fluctuations with a wide frequency spectrum and a range of amplitudes may exist. The flux in a flow channel may be near steady state or episodic, ranging from high-frequency fluctuations triggered by small flow instabilities to intermediate variabilities in percolation fluxes in response to changing weather conditions to long-term variations from climate changes. Since the small-scale, high-frequency fluctuations occur on the spatial and temporal scale of the liquid-release tests used for model calibration, these effects are included in the estimates of seepage-relevant parameters. As pointed out earlier, long-term variations in percolation flux due to climate changes are accounted for explicitly by using different flux distributions (Table 2.3.3-1; FEPs 1.3.01.00.0A, Climate change; and 1.4.01.01.0A, Climate modification increases recharge), while intermediate variabilities in response to precipitation events have been determined to be insignificant due to the presence of the PTn unit (Excluded FEPs 2.2.07.05.0A, Flow in the UZ from episodic infiltration; and 2.1.08.01.0B, Effects of rapid influx into the repository, in Section 2.2, Table 2.2-5).

The impact of lithophysal cavities on flow and seepage is twofold: (1) lithophysal cavities are essentially obstacles to water flow because capillary processes divert water flow around the cavities and focus the flow into regions between the cavities; and (2) lithophysal cavities intersected by the drift lead to a rough drift ceiling, potentially creating seepage points at local low points on the ceiling. Both effects promote seepage (BSC 2004b, Section 6.3.3.5). They are accounted for in the seepage calculation through the use of calibrated capillary-strength parameters (Section 2.3.3.2.3.2).

Rock Properties—Heterogeneities in rock properties occur on various scales that affect flow and seepage. The key rock properties determining the effectiveness of the capillary diversion are the capillary strength and the permeability tangential to the emplacement drift wall. Larger values of capillary strength and tangential permeability both lead to a higher seepage threshold (i.e., more diversion around the drift opening and, therefore, less seepage), while lower values result in a higher potential for seepage (BSC 2004b, Section 6.3.3.2).

In the model developed for ambient seepage predictions, rock properties are represented by a set of process-relevant, scale-dependent, and model-related parameters. As discussed in Section 2.3.3.2.3, capillarity and permeability are to be considered effective parameters determined by matching the model to data that contain information about the seepage process. In general, however, a fracture with a small aperture has relatively low permeability and strong capillarity (and vice versa for a fracture with a wide aperture). This negative correlation reduces the probability of

encountering parameter combinations that would lead to extreme (low or high) seepage behavior, making seepage in porous rocks relatively uniform across different geologic units. While the negative correlation between permeability and capillary strength is evident if considering a single fracture, such a correlation may not necessarily apply to a fracture system. A given permeability for fractured rock may result from a network consisting of a few large fractures or, alternatively, a network of many small, well-connected fractures. A network with few large fractures would exhibit relatively weak capillarity, while a network with many small fractures would have stronger capillarity. If the predominant fracture orientation is aligned with the longitudinal drift axis (Section 2.3.3.2.3.2, Figure 2.3.3-6), little or no tangential permeability is available, and seepage is increased. For flow diversion to occur, the fracture system must have sufficient connectivity and permeability to provide the necessary effective diversion pathways in a tangential direction around the emplacement drift (SNL 2007a, Section 6.3.1). The seepage relevant capillary strength parameter is an effective continuum parameter that implicitly accounts for additional factors affecting seepage. Factors that are lumped into the effective capillary strength parameters include (1) the continuum capillarity of a network of rough-walled fracture; (2) capillary rise within axially oriented fracture segments intersected by the drift; (3) small scale drift wall roughness (including effects of lithophysal cavities); and (4) capillary adsorption of water along the drift wall leading to film flow.

Because of excavation, stress is redistributed, and fractures generally dilate near the crown of the emplacement drift. Such fracture dilation depends on the orientation of the fracture set and occurs within approximately one emplacement drift radius. An increase in fracture aperture causes an increase in fracture permeability and a decrease in capillary strength. The ambient seepage models use excavation-disturbed rock properties in the simulation of seepage (BSC 2004b, Section 6.5.2; SNL 2007a, Section 6.6.3). Rock properties may also be affected by repository heat (Section 2.3.3.3) and the related thermal-hydrologic-chemical-mechanical effects, which are discussed in Sections 2.3.3.3.3.4 and 2.3.5.

Emplacement Drift Geometry and Drift-Wall Properties—Drift size and geometry affect the seepage threshold and the seepage rate. Generally, a large emplacement drift exhibits a significantly lower seepage threshold compared to a small opening. With larger emplacement drifts, more water accumulates in the high-saturation region near the emplacement drift boundary because the water needs to move over a longer diversion distance around the wider opening (Philip et al. 1989). The size of emplacement drifts is strongly affected in the case of drift collapse, as discussed in Section 2.3.3.2.1.4.

The effectiveness of a capillary diversion is greatest if the shape of the cavity follows an equipotential surface (Philip et al. 1989). Breakouts in the drift ceiling caused by rockfall and drift degradation may change the emplacement drift geometry locally and lead to local low points in the ceiling, which may trap water, reduce or prevent flow diversion, and initiate seepage (Section 2.3.3.2.1.4). In addition, small-scale surface roughness increases seepage if the amplitude of the irregularity is comparable to the boundary-layer thickness, which is determined by the capillary rise in the fractures and is on the order of a few centimeters (BSC 2004b, Section 6.3.3.3). Accounting for small-scale surface roughness in the seepage predictions is explained in Section 2.3.3.2.3.2.

In-Drift Conditions—The relative humidity in the emplacement drift is the key factor that determines the evaporation potential, which in turn affects the amount of liquid water at the drift wall that is available for drop formation and seepage. The evaporation potential may change in response to active and passive drift ventilation, which determines the temperature, relative humidity, and the thickness of the diffusive boundary layer at the drift surface (BSC 2004b, Sections 6.6.1.3 and 6.6.1.4). Under the long-term conditions for which ambient seepage is evaluated for the TSPA, relative humidity is expected to be close to 100%, resulting in a negligible effect on seepage. However, ventilation and evaporation effects have to be accounted for in the analysis of data collected during active seepage testing (Section 2.3.3.2.2.1). The seepage rate data used for the estimation of seepage-relevant parameters (Section 2.3.3.2.3.3) are reduced by the amount of water that evaporated, which depends on the evaporation potential and the wetted area at the drift wall exposed to evaporation.

The development of wet spots on the ceiling during active seepage testing, and their relation to in-drift conditions, have been studied in several niches and along the Enhanced Characterization of the Repository Block (ECRB) Cross-Drift (Section 2.3.3.2.2.1.1). The tests showed that temporal reduction of the size of the wet spot during continued water release from above was related to increased evaporation as a result of changes in the ventilation regime. The effects of ventilation on seepage test data were addressed by (1) increasing relative humidity in the testing area (using bulkheads, end curtains, and humidifiers); (2) monitoring relative humidity and evaporation from a free water surface (pan experiments); and (3) including evaporation in the seepage calibration model used to analyze seepage-rate data (Sections 2.3.3.2.2.1 and 2.3.3.2.2.2). Similar effects on seepage are expected during the preclosure period, in which both heat and moisture are removed by forced ventilation.

2.3.3.2.1.4   Drift Degradation Effects

Drift degradation and related drift shape changes can be caused by seismic activity, as explained in Section 2.3.4. Seismic events of varying peak ground velocities (PGVs) have been evaluated in *Drift Degradation Analysis* (BSC 2004e). One of the conclusions from the geomechanical studies is that the degradation results are fundamentally different between nonlithophysal and lithophysal rocks.

In the hard, strong, jointed rock of the nonlithophysal units, damage to drifts will be mostly limited to the local gravitational drop of rock blocks (wedge type rockfall) at the drift roof, which is controlled by the geological structure. Except for this effect, emplacement drifts in nonlithophysal units are expected to remain mostly intact openings, with the horizontal extent of the drifts essentially unchanged (BSC 2004e, Figures 6-108 through 6-114). In most cases, as shown later, local rockfall has no considerable impact on seepage. Only if topographic lows would form at the drift ceiling (where percolation water could accumulate as lateral flow diversion is not possible), the seepage probabilities and rates would increase compared to nondegraded drifts (SNL 2007a, Sections 6.4.2.4.2 and 6.2.3[a]).

More significant drift degradation is predicted for the relatively deformable lithophysal rock. In lithophysal units, seismic events with large PGVs will lead to complete collapse of emplacement drifts, with rubble rock material filling the enlarged opening (BSC 2004e, Section 6.4.2.2.2) (Table 2.3.3-1, FEP 1.2.03.02.0D, Seismic induced drift collapse alters in drift thermohydrology).

In such conditions, seepage is defined as the flow of liquid water from the fractured formation into the rubble-filled opening. Drift collapse can lead to seepage behavior that is much different from that in intact drifts (SNL 2007a, Sections 6.4.2.4.2 and 6.2.2[a]). The larger size and possibly different shape of a collapsed drift can reduce the potential for flow diversion. In addition, the capillary barrier behavior at the drift wall can be affected by the rubble rock blocks filling the opening, as the capillary strength inside the opening is different from the zero capillary strength condition in the initially open drift. Finally, as discussed before, drift degradation can lead to changes in the permeability and capillary strength of the fractured rock in the vicinity of the rubble filled openings, which are caused by fracture dilation or the generation of new fractures.

2.3.3.2.1.5   Modeling Approach

A number of numerical models have been developed to (1) help understand the ambient seepage process; (2) to determine site specific, seepage relevant formation parameters; and (3) to predict seepage into intact and degraded waste emplacement drifts. These drift scale seepage models are linked to other models on different scales; specifically, the site scale unsaturated zone flow model and the scale-transition models provide flow focusing factors. Quantitative and qualitative results from these process models are used in the seepage abstraction to arrive at a reasonable approach to handling seepage in TSPA calculations. Using this approach, the processes that are implicitly or explicitly accounted for include (1) the mountain-scale distribution of percolation flux; (2) the intermediate-scale and small-scale channeling of flow in the fracture network, including possible high-frequency fluctuations; (3) the drift-scale capillary diversion; (4) the microscale phenomena of film flow, drop formation, and drop detachment at the emplacement drift surface where water leaves the formation and enters the emplacement drift; and (5) the local thermodynamic environment in the emplacement drift influencing the potential for evaporation (e.g., relative humidity) (BSC 2004b, Section 6.3.3 and 6.3.4).

Seepage-relevant model parameters on the drift scale are determined using the seepage calibration model (Section 2.3.3.2.3.3), which simulates the liquid-release tests described in Section 2.3.3.2.2.1. A second model—the seepage model for performance assessment (Section 2.3.3.2.3.4)—is conceptually consistent with the seepage calibration model; it simulates seepage into waste emplacement drifts for combinations of the parameters that are most significant for predicting ambient seepage.

To support the modeling approach for ambient seepage, liquid release tests were performed at rates below and above the seepage threshold. The tests covered the conditions expected under ambient percolation conditions, which are typically below the threshold at which seepage becomes possible. The tests also covered localized, high flux conditions that could result from wetter future climates and could induce seepage. As a result, the chosen approach focuses on the relevant emplacement drift and waste package scale (BSC 2004b, Section 6.1.1).

Conducting active seepage tests in the repository host rock units and on a scale that approximates an emplacement drift section assures that data are generated that contain relevant information about the seepage processes to be predicted. Moreover, the consistency between calibration data and the prediction variable minimizes potential conceptual differences between the seepage calibration model and the seepage model for performance assessment. Finally, uncertainties and variabilities

inherent in the seepage process are addressed by a probabilistic treatment of seepage in the TSPA, based on uncertainty in parameters affecting seepage (Sections 2.3.3.2.3.6, 2.3.3.2.4, and 2.3.3.4).

2.3.3.2.2   Data and Data Uncertainty
[NUREG-1804, Section 2.2.1.3.3.3: AC 2(1), (2), AC 3(1) to (4)]

This section describes the data from the field tests and laboratory experiments that support the development of the two ambient seepage process models, the ambient component of the drift seepage abstraction, and the TSPA drift seepage submodel. Measurement uncertainties in these data are also discussed.

Tests to characterize seepage that were conducted in various niches and the ECRB Cross-Drift provide the primary data used for the seepage calibration model (BSC 2004b, Section 6.5.1). In addition to seepage tests, a section of the ECRB Cross-Drift and Alcove 7 were closed off to eliminate ventilation effects in order to provide data for seepage under natural percolation conditions (BSC 2004f, Section 6.10). Moisture monitoring in these drift sections, and observations related to evaporation and condensation effects, are described in Section 2.3.3.2.2.2.

2.3.3.2.2.1   Seepage Testing

The bulk of the data for understanding ambient seepage comes from two testing programs conducted in the Exploratory Studies Facility (ESF) and the ECRB Cross-Drift (BSC 2004b, Section 6.5.1):

- **Niche Studies**—Short drifts, or niches, ranging from 6.3 to 15.0 m in length, were constructed in the Tptpmn unit and the Tptpll unit for use in a variety of tests (BSC 2004b, Section 6.5.1).

- **Systematic Borehole Testing Program**—The systematic borehole testing program was initiated to complement the niche studies and to provide for systematic hydrologic characterization by performing air injection and liquid-release tests in approximately 20-m-long boreholes drilled at a 15° angle upward and parallel to the drift axis into the crown every 30 m along the ECRB Cross-Drift (BSC 2004f, Section 6.11).

Multiple liquid-release tests (Section 2.3.3.2.2.1.1) were performed in Niches 2, 3, 4, and 5 (also referred to as Niches 3650, 3107, 4788, and 1620, respectively), and in the systematic testing boreholes (SYBT-ECRB-LA#1 to #3) to study seepage behavior and to characterize seepage-related properties in different units and under different conditions. Test locations in niches and the location of the ECRB Cross-Drift are illustrated in Figure 2.3.3-7. Seepage-rate data collected during those liquid-release tests were used to calibrate the seepage calibration model (Section 2.3.3.2.3.3) for the determination of seepage-relevant formation parameters (BSC 2004b, Section 6.5.3). In addition, air injection tests (Section 2.3.3.2.2.1.2) were conducted to determine permeability distributions needed to develop the seepage calibration model and the seepage model for performance assessment (BSC 2004b, Section 6.5.2).

Because evaporation at the drift wall affects seepage, other studies were done to monitor and at times control the drift relative humidity under various conditions (Section 2.3.3.2.2.1.3) (BSC

2004b, Section 6.5.4). Another study investigated capillary diversion by performing mass balance calculations using test data collected in Niche 5, along with associated modeling results to account for components of the mass balance equation that could not be measured directly (Section 2.3.3.2.2.1.4). A liquid-release test on the fault and fracture network between Alcove 8 and Niche 3 was conducted (Section 2.3.3.2.2.1.5).

2.3.3.2.2.1.1   Liquid-Release Tests

As part of the niche studies program, drift-scale liquid-release tests were initiated in 1997 to investigate potential seepage into an underground opening representing an emplacement drift. Niches were constructed at various locations along the ESF and the ECRB Cross-Drift. Boreholes were drilled above the niches prior to and after the niches were excavated, in order to facilitate characterization of the rock using air injection tests and investigation of seepage processes using liquid-release tests. The locations of the niches were chosen to represent different hydrogeologic units where emplacement drifts will be located. Additional liquid-release tests were conducted as part of the systematic borehole testing program (BSC 2004f, Section 6.1.1; BSC 2004b, Section 6.5.3).

The effectiveness of the capillary diversion and the presence of a threshold percolation flux were examined using liquid-release tests, in which water was released at various rates from a short section of a borehole above the opening. Any water that migrated from the borehole to the crown and dripped into the opening was captured and measured. Seepage processes were observed and resulting seepage rates were measured using liquid-release tests in multiple borehole intervals at Niches 2, 3, 4, and 5, and in three systematic testing boreholes (SYBT-ECRB-LA#1 to #3). To evaluate the seepage response to different percolation fluxes and different initial conditions, multiple liquid-release tests were conducted in the same borehole interval using different release rates—above and below the seepage threshold—with different time delays between individual test events. Only a small amount of water was released in early tests conducted in Niche 2. To reduce the impact of the effects of water storage in the rock formation, and to test a more representative portion of the fracture network involved in flow diversion around the opening, later tests in Niches 3, 4, and 5, and along the ECRB Cross-Drift, used significantly more water to reach near steady seepage conditions (BSC 2004b, Section 6.5.3). These later tests are used for parameter estimation purposes, as described in Section 2.3.3.2.3.3. Ventilation and evaporation effects were mitigated or accounted for, as discussed in Section 2.3.3.2.2.1.3.

Figure 2.3.3-8 shows an example of contours of the wetting front spreading across the Niche 4 crown during a liquid-release test over a period of about 12 days. In this test, water issued from the formation through fractures and microcracks spread along the rough and dusty surface.

Figure 2.3.3-9 presents seepage rates measured in Niche 4 during a different liquid-release test, showing that they stabilize after about four days of continuous water injection. These stabilized seepage rates indicate that there are no relevant changes to the partitioning of injected water between flow diversion around the niche and storage in the formation on the one hand, and seepage on the other hand. (Note that due to the relatively short distance between the water release point and the niche crown, it is unlikely that water bypasses the niche. Bypassing of the niche and seepage collection system may have occurred in the Alcove 8–Niche 3 seepage test bed, as discussed in

Section 2.3.3.2.2.1.5.) In this example, because of the high release rate, a near-steady seepage rate developed that was approximately half the release rate.

2.3.3.2.2.1.2   Air Injection Tests

To understand the small-scale permeability variation that is important for seepage processes, air injection tests were conducted in the same boreholes above niches where seepage liquid-release tests were later performed. Air injection tests estimate the permeability of the fractured rock by isolating a short section of a borehole (in this case about 1 ft), using an inflatable packer system and then injecting compressed air at a constant rate into the isolated injection interval. The pressure buildup in the injection interval (and in nearby similarly isolated observation intervals) was monitored until steady conditions were reached, typically within a few minutes. Air injection was terminated after reaching steady pressures, and the decline in air pressure was then monitored as it recovered to its initial pretest condition. Air-permeability values were derived from the steady pressure data using the modified Hvorslev approach (LeCain 1995; BSC 2004f, Section 6.1.2.1) to obtain fracture permeability. The air permeabilities are considered representative of the intrinsic fracture continuum permeability because the fractures are essentially dry during air injection testing, and the contribution of matrix gas flow is negligible because of low overall matrix permeability and high liquid saturation (BSC 2004f, Section 6.1.2.1).

The air injection tests were conducted before and after excavation of the niches. The results showed that permeability around the niches was affected by excavation (BSC 2004f, Section 6.1.2.2.1; Wang and Elsworth 1999). Because seepage is determined by the formation properties and excavation effects in the immediate vicinity of the opening, postexcavation air-permeability data are used for calculation of seepage into emplacement drifts. Different excavation methods can result in varying degrees of excavation effects. Niches used in seepage testing were excavated using a Road-Header Alpine Miner, whereas systematic tests in the ECRB Cross-Drift are in a section excavated with a tunnel-boring machine. Since local postexcavation permeabilities are used to model each test, no bias is introduced in seepage calibration (BSC 2004b, Section 6.5.2). Emplacement drifts will be excavated using a tunnel-boring machine (Section 1.3.4.3). Qualitative evaluation of the effects of excavation on fracture propagation into the excavated wall indicates that, in general, the Alpine Miner and the tunnel-boring machines induce new fractures to similar depths (less than 10 cm into the wall) and, thus, would affect fracture permeability and capillary strength to a similar extent (SNL 2007a, Section 6.6.3). The uncertainty band for sampling fracture permeability in the drift seepage abstraction accounts for spatial variability and various sources of uncertainty, including uncertainty due to effects of excavation (SNL 2007a, Section 6.6.3).

The ambient seepage models do not directly use the flow rate and pressure data measured during the air injection testing; instead, the permeability values derived from these data are used to describe the small-scale heterogeneity distributions incorporated in the seepage models (Section 2.3.3.2.3.3). The variation of permeability measurements between different niche locations is also used to describe the intermediate-scale variability of this parameter in the drift seepage abstraction (Section 2.3.3.2.3.6.2). Uncertainties in permeability values stem from uncertainties in the measured airflow rate and pressure data and the analytical method used to derive the permeability values from these data. The airflow rate was measured using four different mass flow controllers, each of which covered a portion of the total response range of 1 to 500 standard L/min full scale (BSC 2004f, Appendix A2). Each flow mass controller has a maximum error of 10% of its full scale

(BSC 2004f, Appendix A2). Instrumentation error of the pressure sensors was about 0.3 kPa, which is negligible (BSC 2004f, Appendix A2). Short-circuiting of gas flow between adjacent boreholes was minimized by the design of the tests, thereby rendering the measurement uncertainty insignificant (SNL 2007a, Section 6.6.3.3). Uncertainty due to the effects of excavation methods on excavation disturbed permeability is included in the range of uncertainty used in the drift seepage abstraction (SNL 2007a, Section 6.6.3).

2.3.3.2.2.1.3   Relative Humidity Monitoring

Reduced relative humidity due to ventilation in the seepage testing sections of niches and the ECRB Cross-Drift leads to partial or complete evaporation of the water that reaches the wall of the opening, thus affecting seepage. To diminish, control, and quantify this effect, test sections of niches were isolated from the main access drifts by bulkheads. In some tests, humidity in the isolated niches was artificially increased by humidifiers to reduce the evaporation potential. Finally, evaporation pans were installed to directly measure the evaporation potential (BSC 2004f, Section 6.2.1.3).

The measured evaporation rates and a related sensitivity analysis indicate that evaporation effects in the closed off niches are insignificant, and that corrections to the seepage rate data used by the seepage calibration model are not needed (BSC 2004b, Section 6.7). In contrast, the relative humidity in the open ECRB Cross-Drift is significantly lower and exhibits relatively strong fluctuations, depending on weather and ventilation conditions. On the basis of observations from initial liquid-release tests in the open ECRB Cross-Drift, subsequent liquid-release tests included measurement of relative humidity and evaporation rates to estimate and correct for the effects of ventilation on measured seepage (BSC 2004f, Sections 6.2.1.3.5.3, 6.10.1.2.1, and 6.11.3.6; BSC 2004b, Sections 6.5.4 and 6.6.1.3). In the seepage calibration model, evaporation was numerically simulated using the measured humidity as a time-varying boundary condition in the drift. A potential bias in the estimated seepage parameters due to evaporation effects was thus eliminated (BSC 2004b, Section 6.7).

High-humidity and low-evaporation conditions are expected to prevail during the postclosure period after the heat load and associated temperature rise have dissipated and the sealed repository has equilibrated with the surrounding rock (BSC 2004f, Section 6.2.1.3.2). Therefore, evaporation effects are (conservatively) not considered in the seepage model for performance assessment used for the prediction of ambient seepage (Section 2.3.3.2.3.4).

2.3.3.2.2.1.4   Mass Balance in Niche 5

The flow-diversion capability of the capillary barrier is the mechanism that leads to the absence of seepage into waste emplacement drifts or seepage fluxes that are significantly lower than the local percolation flux. Although not required to characterize seepage behavior, obtaining a complete mass balance during a liquid-release test is a means to directly assess the flow-diversion capability of a drift excavated from an unsaturated fractured formation. Calculating this mass (or rate) balance in a transient test requires estimation of the following components: the amount of water that (1) is injected; (2) seeps into the opening; (3) evaporates from the rock surface and the collection system; (4) is stored in the formation between the injection point and the opening; (5) bypasses the opening through known and unknown geologic features; and (6) is diverted around the opening on account of the capillary-barrier effect (BSC 2004b, Section 6.8).

Components 1 and 2 can be measured with sufficient accuracy. Reliable estimates of Component 3 can be obtained from relative humidity or evaporation-rate measurements. The tests can be run to near-steady-state conditions to minimize Component 4, and a rate balance (as opposed to a mass balance) can be performed. Measuring Components 5 and 6 requires capturing the water in a secondary water collection system at the side or below the drift (BSC 2004b, Section 6.8).

To measure Components 5 and 6, water was collected in a slot at the side of the niche during two seepage tests conducted in Niche 5 (BSC 2004f, Sections 6.2.1.3.5 and 6.6.2.3). While qualitative evidence was obtained for capillary diversion of water around the niche, it was not possible to accurately measure the amount of water diverted around and arriving at the side of the niche because of difficulties in excavating the slot and installing the capture system (BSC 2004f, Section 6.2.1.3.5; BSC 2004b, Section 6.8). The seepage calculations, therefore, rely on (1) established understanding of the physics underlying flow diversion by capillary processes; (2) extensive site-specific and seepage-relevant characterization data; (3) qualitative evidence demonstrating flow diversion and water exclusion due to capillarity; (4) calibration and validation of a physically based process model that includes all components of the mass balance; and (5) propagation of uncertainty and variability in a probabilistic treatment of seepage for the TSPA (SNL 2007a, Sections 6.4 through 6.7 and 7).

2.3.3.2.2.1.5   Alcove 8–Niche 3 Testing

Evaluation of seepage is among the multiple objectives of the studies performed in the Alcove 8–Niche 3 test bed. Water was released into a fault and the fracture network from various infiltrations plots within Alcove 8, which is located within the Topopah Spring Tuff upper lithophysal zone (Tptpul) next to the ECRB Cross-Drift (Figure 2.3.3-10). Approximately 20 m below Alcove 8, Niche 3 was excavated from the ESF main drift within the Topopah Spring Tuff middle nonlithophysal zone (Tptpmn). The Tptpul-Tptpmn contact is at about 3 m above Niche 3 (BSC 2004f, Section 6.12; Salve 2005). Niche 3 was equipped with trays for seepage collection. In addition, boreholes surrounding Niche 3 were instrumented with sensors to detect the arrival of the wetting front.

Water was continuously released, over a period of 216 days, from a 3 m-by-4 m infiltration plot on the floor of Alcove 8. The infiltration plot was divided into 12 separate subplots, each having a 1 m-by-1 m area. Ponded conditions occurred in these infiltration plots over most of the test duration. The spatial and temporal variability in infiltration rates into the fractured rock was continuously monitored. In Niche 3, the water collected in individual compartments of the tray system provided information about the temporal and spatial distribution of seepage from the ceiling of Niche 3 (BSC 2006, Section 6.1.1).

During the last 125 days of this test, the system reached a quasi-steady state, where only 10% of the total volume of the liquid released from the entire infiltration plot on Alcove 8 seeped out of the fractured rock through the niche ceiling (Zhou et al. 2006). The remaining water that was released was stored in the fractured rock, bypassed the niche, or was diverted around the opening on account of the capillary barrier effect. Although storage effects and bypassing may be considerable factors contributing to the low seepage-to-percolation ratio, these results demonstrate that seepage is likely to be smaller than the local percolation flux (SNL 2007a, Section 7.2[a]), which is consistent with the findings from the liquid-release tests described in Section 2.3.3.2.2.1.1 and the associated

modeling studies (Section 2.3.3.2.3). This result was obtained despite the fact that seepage was promoted due to fairly extreme test conditions (ponded infiltration conditions in Alcove 8; small distance from the source of infiltration in Alcove 8 to the potential seepage location in Niche 3), which result in downward fluxes towards Niche 3 that are much higher than ambient percolation fluxes for current or future climate conditions. The infiltration rate reported for Subplot 12, for example, was 15 l/day at the end of test stage 2, which translates into 5,475 mm/yr over the 1 m × 1 m area of the subplot (BSC 2006, Section 6.1.2). For comparison, the present-day net percolation fluxes over the repository area (10 percentile infiltration scenario) are on the order of a few millimeter per year (Section 2.3.2, Figure 2.3.2-38).

2.3.3.2.2.1.6   Summary of Active Seepage Testing

Active testing was performed to understand the seepage process on the scale of an emplacement drift segment and to characterize seepage-relevant properties of the host rock. Recognizing that permeability, capillary strength, and the local percolation flux are key parameters affecting seepage, a series of tests were conducted that examined these factors. Liquid-release tests were performed at various locations, using release rates above and below the seepage threshold (Section 2.3.3.2.2.1.1). Air injection tests provided location-specific estimates of fracture permeability and its small-scale, as well as intermediate-scale, spatial variability (Section 2.3.3.2.2.1.2). To account for the expected impact of ventilation effects on observed seepage rates, relative humidity was controlled and monitored (Section 2.3.3.2.2.1.3). The data collected in four niches and three boreholes drilled into the crown of the ECRB Cross-Drift provided the basis for the estimation of seepage-relevant, site-specific, and model-related parameters on the scale of interest, and for the validation of the models used for the prediction of ambient seepage (Section 2.3.3.2.3.3). In addition, the flow-diversion capability of the open drift due to the capillary-barrier effect was further examined in Niche 5 (Section 2.3.3.2.2.1.4) and in the Alcove 8–Niche 3 test bed (Section 2.3.3.2.2.1.5). This comprehensive testing program provides the technical basis for the process modeling (Section 2.3.3.2.3) and abstraction (Section 2.3.3.2.4) of ambient seepage. Data from passive hydrologic testing and monitoring (Section 2.3.3.2.2.2), and observations of seepage under natural conditions (Section 2.3.3.2.2.3), supplement the information gained from active testing.

2.3.3.2.2.2   Moisture Monitoring in the ECRB Cross-Drift and Alcove 7

2.3.3.2.2.2.1   Passive Hydrologic Tests

Forced ventilation may have prevented the direct observation of seepage in the ESF main drift and the ECRB Cross-Drift (Section 2.3.3.2.2.3). In an attempt to observe seepage under natural flow conditions, the terminal section of the ECRB Cross-Drift was closed off by a series of bulkheads to minimize ventilation effects (Figure 2.3.3-11). The 918-m drift section is located in the Topopah Spring lower lithophysal (Tptpll) and the lower nonlithophysal (Tptpln) tuff units; the drift section is intersected by the Solitario Canyon Fault (BSC 2004f, Figure 6-108). Within the isolated sections between the bulkheads, barometric pressure, relative humidity, and temperature were measured at various stations to provide information on moisture dynamics. Psychrometers were installed along seven boreholes to measure the water potential and the initial extent and later rewetting of the dryout zone in the fractured rock. Electrical resistance probes were laid out at 0.5 m intervals to measure saturation changes along the drift wall. Six water collectors were installed. Periodically, the bulkhead doors isolating the nonventilated sections were opened for observations and sampling of

liquid water from the water collectors. Water samples from the collectors and from other locations in the tunnel were analyzed to evaluate whether the water originated from seepage or condensation based on the composition measured (Section 2.3.3.2.2.2.4) (BSC 2004f, Section 6.10.3).

Moisture monitoring similar to that described above has been conducted in Alcove 7 since 1998 (see Figure 2.3.3-7 for location of Alcove 7). Bulkhead doors were installed 64 and 132 m from the entrance of the alcove. Ambient temperature, barometric pressure, and relative humidity were monitored. The bulkheads were opened after being closed for extended periods. Evidence of moisture was observed, including drip spots on the drip collection sheets, moisture drops on the utility lines and on the shotcrete around the bulkheads, and moisture spots in the dust on one instrument enclosure. The rock in the crown had a dark, moist appearance, and the fractures in the rib appeared wet (BSC 2004f, Section 6.10.4).

2.3.3.2.2.2.2   Evidence of Ventilation Effects

Evidence of effects of forced ventilation in exploration drifts provides a basis for predicting their effects on repository performance (Table 2.3.3-1, FEP 1.1.02.02.0A, Preclosure ventilation). The observations of changes in water potential, saturation, and in-drift atmospheric conditions after closure of the bulkheads can be used to confirm the impact of ventilation and reduced relative humidity on the hydrologic conditions in the immediate vicinity of the drift. Under ventilated conditions, the matrix is partially dried out up to a few meters from the drift surface. Even though the relative humidity increases rapidly after closing the bulkheads in the ECRB Cross-Drift (BSC 2004f, Figure 6-112), the water potential data indicate that the rewetting of the matrix is a slow process. Figure 2.3.3-12 shows water potentials as a function of time and distance from the drift surface. Low water potentials up to a distance of about 1.5 m from the borehole collar indicated the extent of the dryout zone as a result of drift ventilation. After installation of the bulkheads, water potentials increased over a period of 1.5 years, indicating a tendency to return to preventilated conditions (Figure 2.3.3-12).

2.3.3.2.2.2.3   Observations Related to Wet Zones

Wet zones observed in the closed-off sections of the ECRB Cross-Drift provide information regarding potential seepage and in-drift moisture redistribution. Within the entries behind the bulkheads, droplets and other indications of moisture were observed on rock bolts, ventilation ducts, utility conduits, wire meshes, and painted patches of tunnel walls. Puddles of water were observed on the conveyor belt, and drip cloths showed evidence of dripping. Observed rust spots and organic growths, associated with organic introduced materials, indicated the prolonged presence of moisture (BSC 2004f, Section 6.10.2.2).

The visual observations of moisture on impervious (nonporous) surfaces, plus the chemical analyses of collected samples described below, suggest that the moisture originated from condensation. The near-100% relative humidity in the ECRB Cross-Drift (BSC 2004f, Figure 6-112) and local thermal gradients, partly induced by the operating heat from electrical equipment in the closed-off drift sections (BSC 2004f, Section 6.10.2.2), are the likely causes for the observed condensation.

2.3.3.2.2.2.4   **Chemical and Isotopic Water Analyses**

Chemical and isotopic analyses were conducted on the water samples collected during the periodic entries into the nonventilated sections of the ECRB Cross-Drift. Analyses were performed with the objective of determining the origin of the moisture observed in the closed-off sections of the ECRB Cross-Drift. The chemical analyses included major anionic and cationic constituents (e.g., bromide, chloride, and lithium) (BSC 2004f, Section 6.10.3).

The initial water samples collected from the puddles on the conveyor belt were dark in color. Because the surface of the conveyor belt contained dust and rock fragments, the chemical analyses of these samples did not provide meaningful information about the source of water found in the puddles. Subsequent samples were taken from clean containers placed on top of the conveyor belt. These samples were found to be low in chloride and silica content, which is characteristic of condensate. The samples were also found to lack the chemical signature of the water introduced during construction (20 mg/L of lithium bromide was added to construction water as a tracer). Although these data do not rule out the possibility of seepage (mixed waters), they indicate that observed moisture originated primarily from condensation (BSC 2004f, Section 6.10.3).

The hydrogen isotope composition (δD, ratio of the molar concentration of deuterium isotope relative to the more common isotope of hydrogen) and oxygen isotope composition (δ^{18}O, ratio of the molar concentration of ^{18}O relative to the more common isotope^{16}O) were also analyzed. The δD values ranged from -48‰ to -90‰, and the δ^{18}O values ranged from -3‰ to -10.7‰. These values distinguish the water samples from construction water, which has lower values. The lag time between opening of bulkheads and sample collection (3 to 4 hours) is sufficient to result in a significant degree of evaporation of the samples. As shown in Figure 2.3.3-13, the samples from the ECRB Cross-Drift are shifted from the global meteoric water line. The offset is characteristic of waters that have undergone some degree of evaporation and subsequent condensation (BSC 2004f, Section 6.10.3.2). The same degree of shift was observed for both the samples containing dust and rock fragments, and for the relatively clean samples, which indicates approximately the same amount of evaporation and subsequent condensation. The chemical analyses of water collected in the nonventilated ECRB Cross-Drift, as well as visual observations, indicate that condensation is the primary source of the dripping water, with minimal contribution from seepage (BSC 2004f, Section 6.10.3).

2.3.3.2.2.2.5   **Summary of Moisture Monitoring in Drifts**

Observations of hydrologic and thermodynamic conditions in the nonventilated drifts and in the nearby rock lead to the following conclusions:

- Effects of forced ventilation have a significant impact on seepage, mainly through evaporation of potential seepage water at the drift surface but also through the development of a dryout zone around the opening (Section 2.3.3.2.2.2.2).

- Once ventilation effects are reduced or eliminated, the relative humidity of the initially dry in-drift environment generally recovers rapidly to conditions dictated by moisture conditions in the rock (Section 2.3.3.2.2.2.2).

- Variable temperature and relative humidity in closed-off drift sections facilitate in-drift moisture redistribution processes, including condensation of water on surfaces, which may induce dripping (Section 2.3.3.2.2.2.3). Section 2.3.5.4 provides details on these processes and how they are accounted for in the TSPA.

- The presence of water on nonporous surfaces and the chemistry of water samples indicate that the water accumulations in the ECRB Cross-Drift originated from condensate (Section 2.3.3.2.2.2.4).

These observations are consistent with the conceptual understanding of seepage as implemented in the ambient seepage models discussed in Section 2.3.3.2.3.

2.3.3.2.2.3   Observation of Seepage Under Natural Conditions

2.3.3.2.2.3.1   Impact of Forced Ventilation on Seepage

The evaporation potential of the dry drift air in response to forced ventilation has a strong impact on seepage under natural ambient conditions (Table 2.3.3-1, FEP 1.1.02.02.0A, Preclosure ventilation). Seepage can only occur when the amount of percolating water is large enough to overcome evaporation. This has evidently not been the case in any of the ventilated openings in the rock units below the PTn unit at Yucca Mountain, as no unambiguous evidence of dripping from natural percolation water has ever been observed (SNL 2007a, Section 7.1.1[a]). The significant evaporation potential of the dry drift atmosphere is evident not only from theoretical considerations, but also from (1) temporal observations of wet spots observed at the drift crown during liquid-release tests conducted in the ECRB Cross-Drift (BSC 2004f, Section 6.10.2.2); and (2) the fact that a damp-looking feature observed along a the vertical end wall immediately after the dry excavation of Niche 1 (also referred to as Niche 3566) dried up within a few hours (BSC 2004f, Section 6.2.1.2; Wang et al. 1999) before a bulkhead could be installed to increase the relative humidity in the opening.

2.3.3.2.2.3.2   Direct Observation of Seepage into the ESF South Ramp

Seepage has been observed over a limited time period in the South Ramp area of the ESF, in the fractured welded tuff above the PTn unit. During the period between October 2004 and February 2005, unusually heavy precipitation occurred in the Yucca Mountain area—12.75 inches, which is about 3.5 times the recent nine-year average of 3.64 inches, taken over the same time period between October and February (BSC 2005b, Section 2.3). On February 28, 2005, Yucca Mountain Project personnel working in the South Ramp of the ESF observed, in select areas, wet spots on the main drift's crown, ribs, and invert. This field observation is considered to be the first unambiguous evidence of seepage under ambient conditions.

As shown in Figure 2.3.3-14, wet areas were identified between Stations 75+62 and 75+82, Stations 75+92 and 76+07, and Stations 77+48 to 77+53. Several factors have contributed to the occurrence of seepage in the South Ramp section of the ESF (SNL 2007a, Section 7.1[a]). Most importantly, the heavy rainfalls are believed to have induced large infiltration fluxes percolating down towards the tunnel. The area above the South Ramp has a relatively thin soil cover, and the distance from the land surface to the ESF is relatively small in the seepage section (less than 75 m vertical distance).

Also, as opposed to most other sections along the ESF and the ECRB Cross-Drift, the South Ramp is not overlain by bedded or nonwelded tuffs (such as the PTn). The PTn has a higher storage capacity and permeability, and thus is able to imbibe water and dampen episodic infiltration events. In contrast, the nonlithophysal units present above the seepage location are welded and highly fractured, resulting in fast flow through the fracture network. In summary, the high precipitation rates combined with thin soil cover led to pulses of high infiltration and percolation fluxes, which migrated through the fracture network and—due the absence of the nonwelded PTn unit—arrived at the ESF South Ramp without significant dampening. These fluxes were higher than the seepage threshold and the evaporation potential, thus inducing seepage.

The section of the ESF South Ramp that has no overlying layers of bedded or nonwelded tuffs (PTn) is approximately 300 m long, from Station 75+80 to the South Portal (at Station 78+77). Assuming (1) that each of the wet areas identified in Figure 2.3.3-14 actually resulted in drop formation and drop detachment (as opposed to film flow along the drift surface) and (2) that—for wet areas extending more than 5 m in axial direction—at least one dripping location exists for every 5 m of continuous wet area, approximately 13% of the drift section experienced seepage (SNL 2007a, Section 7.1[a]). These observations were used for a seepage abstraction validation study Section 2.3.3.4.3.

2.3.3.2.2.4   Summary of Data and Data Uncertainty

Data needed to develop the conceptual understanding, process models, and abstraction of ambient seepage were obtained through active seepage testing (Section 2.3.3.2.2.1), moisture monitoring (Section 2.3.3.2.2.2), and direct observations of seepage (Section 2.3.3.2.2.3). Active testing provided data for the development, calibration, and validation of the ambient seepage process models described in Section 2.3.3.2.3. The spatial variability of seepage-relevant properties is examined by performing air injection and liquid-release tests at multiple locations. Efforts were made to reduce the impact of systematic errors (such as those arising from evaporation, storage effects, and scale discrepancies) by controlling and monitoring relative humidity and by performing long-term experiments on the scale of interest. Measurement uncertainty (which is considered relatively small) and uncertainties related to model simplifications or spatial variability considerations are propagated through the seepage calibration model, the seepage model for performance assessment, and the abstraction methodology (Section 2.3.3.2.3.6). Additional data from the fractured host rock were used to corroborate the conceptual understanding of the capillary barrier effect and flow diversion capability of an emplacement drift.

2.3.3.2.3   Model and Model Uncertainty
[NUREG-1804, Section 2.2.1.3.3.3: AC 3(1) to (4), AC 4(1) to (4), AC 5; Section 2.2.1.3.6.3: AC 1(6)]

2.3.3.2.3.1   General Approach for Ambient Seepage Modeling

The general approach followed to arrive at a calibrated and validated predictive seepage model is based on the recognition that (1) detailed simulation of individual seeps is not necessary to estimate average seepage rates into waste emplacement drifts; rather, calculated seepage rates can be averaged in time and over an emplacement drift section that approximates the length of a waste package, which is the spatial scale of interest; (2) calibration to data from seepage experiments

provides confidence that the relevant processes are captured in a direct manner (i.e., they do not need to be indirectly inferred from secondary information or data); (3) individual factors affecting seepage can be combined into effective parameters; (4) estimating effective parameters compensates for processes and features that are not explicitly considered in the model; and (5) the estimated parameters can be directly used in the seepage model for performance assessment (BSC 2004b, Section 6.3.4).

The main advantage of this modeling approach is that it relies directly on seepage-rate data, which contain information about the relevant processes. The calibration data (seepage rates on the scale of a drift section) are similar to the quantity of interest for the subsequent simulations (emplacement drift seepage). The consistency between the seepage calibration model used to derive seepage-relevant parameters and the seepage model for performance assessment (used to simulate ambient seepage) minimizes conceptual differences (BSC 2004b; BSC 2004a).

The two ambient seepage models are based on data that capture seepage-relevant processes under in situ conditions. Some of these data are directly used to develop and calibrate the models. Air permeabilities are used to generate and condition heterogeneous permeability fields for the two models. Evaporation rate and relative humidity data are used to determine the evaporative boundary layer thickness, which is needed by the seepage calibration model to account for evaporation effects that impacted seepage data collected in the ventilated ECRB Cross-Drift. Seepage rate data measured during liquid-release tests are the principal data used for calibration of the seepage calibration model. Additional seepage rate data are used for testing the capability of the seepage calibration model to estimate seepage under different conditions and at different locations (BSC 2004b, Section 7).

The development of the two ambient seepage models involves the following steps (BSC 2004b, Section 6.3.4; BSC 2004a; BSC 2004f, Section 6):

1. Geostatistical parameters of the permeability field are determined from the results of air injection test data.

2. Multiple realizations of the permeability field are generated, each of which is consistent with the geostatistical properties of the measured air permeabilities representing the excavation-disturbed zone in the drift vicinity.

3. A numerical model (i.e., the seepage calibration model) is developed for the simulation of liquid-release tests conducted in niches and along the ECRB Cross-Drift.

4. Capillary strength parameters are determined by calibrating the seepage calibration model against data from liquid-release tests.

5. The seepage calibration model is tested by comparing simulated seepage rates to observed data from seepage experiments not used for model calibration. This step provides confidence that the model is capable of predicting the seepage behavior above and below the seepage threshold.

6. The seepage model for performance assessment, which is conceptually consistent with the seepage calibration model, is developed for simulating seepage into emplacement drifts.

7. Emplacement drift seepage is evaluated for ranges of percolation flux, capillary strength, and permeability that bracket the range expected to be sampled during the probabilistic seepage evaluation in the TSPA (BSC 2004a, Section 6.3.7, Table 6-3). These three parameters represent the key factors affecting ambient seepage into intact emplacement drifts. These parameters were identified as seepage-relevant by means of a sensitivity analysis (BSC 2004b, Section 6.6.3.1).

8. The results are combined in the ambient component of the drift seepage abstraction, providing the basis for a probabilistic evaluation of seepage in the TSPA.

The following sections describe the development of the drift-scale models used to estimate seepage-relevant rock properties, and to generate the seepage lookup tables, which are passed through the drift seepage abstraction for use in the TSPA calculations.

2.3.3.2.3.2   Conceptual and Numerical Models of Seepage

The ambient seepage process models consider three-dimensional, drift scale flow through the unsaturated fracture network. The fractured rock is conceptualized as a single, heterogeneous continuum with effective fracture permeabilities assigned to each gridblock using geostatistical methods, conditioned on the permeabilities determined from air injection tests (Section 2.3.3.2.2.1.2). The potential contribution of the matrix to seepage is not explicitly simulated, as there is very limited flow through the matrix, and the capillary barrier effects are strong due to the strong matrix capillarity.

Although the permeability structure comprises a network of discrete fractures, the continuum approach is appropriate for simulating unsaturated flow and seepage because it is capable of predicting observed seepage behaviors and seepage rates. In a network of randomly oriented fractures, flow diversion around openings occurs primarily within fracture planes. Diversion of water through multiple fractures arises only if a fracture is too short, and the flow path within a fracture plane is interrupted. In this case, water is diverted into the next connected fracture, if available. This fracture is again unlikely to be perfectly parallel to the drift axis, allowing the in-plane flow diversion process to continue. The situation is schematically illustrated in Figure 2.3.3-6, which shows two fractures intersecting a drift. In Figure 2.3.3-6a, the two fractures are aligned with the drift axis. This specific and unlikely fracture orientation prevents flow diversion and increases the likelihood of seepage. In Figure 2.3.3-6b, the fractures are approximately perpendicular to the drift axis. In this case, flow diversion occurs within the fracture plane, which is a process that is appropriately captured by a heterogeneous fracture continuum model, even for a single fracture. In-plane flow occurring in multiple fractures can be readily combined and described by an effective fracture continuum.

The geologic units that constitute the host rocks of the repository horizon are within the crystal-poor member of the Topopah Spring Tuff, which comprises strongly fractured, lithophysal and nonlithophysal rock units. The nonlithophysal rocks-the Topopah Spring Tuff middle

nonlithophysal (Tptpmn) and lower nonlithophysal (Tptpln) units-comprise roughly 15% of the emplacement area. The lithophysal rocks-the Topopah Spring Tuff upper lithophysal (Tptpul) and middle lithophysal (Tptpll) units-comprise approximately 85% of the emplacement area (about 80% of the emplacement is within the Tptpll) (SNL 2007a, Section 6.6.1). The fracture inventory of these units has been extensively characterized from geological mapping and scanline surveys along the ESF and the ECRB Cross-Drift as well as from borehole cores and video logs (Mongano et al. 1999). The information gathered in the scanline surveys includes location, orientation, trace length, width, and roughness for fractures with a trace length greater than 1 m.

A network of long, relatively closely spaced joints generally characterizes the Tptpmn unit. The highest degree of fracturing is associated with joint sets that have average fracture spacing of less than 60 cm. Average trace lengths in the Tptpmn unit are between 2.54 m and 3.23 m for the different joint sets. These trace lengths are relatively long compared to the fracture spacing, suggesting that the Tptpmn unit features a well-connected fracture system, with numerous large fractures longer than 1 m. In addition, there are shorter fractures that have not been included in the line surveys and fracture analyses, but would increase fracture connectivity. The Tptpln unit is similar in fracture characteristics (joint sets, spacing, trace lengths) to the Tptpmn unit (SNL 2007a, Section 6.6.1). Based on the line surveys, the apparent fracture intensity in the lithophysal units is approximately five times smaller than in the Tptpmn unit, and about two times smaller than in the Tptpln unit. However, the Tptpll unit has abundant short-length, interlithophysal fractures, with spacing on the order of inches, which are not recorded in the line surveys and thus not reflected in the above average characteristics. The Tptpll unit has fracture characteristics different from the nonlithophysal units, but nevertheless features a well-connected fracture system, which comprises less intense fracturing with longer fractures, but very intense fracturing with short fractures (SNL 2007a, Section 6.6.1). Fracture network connectivity has been independently determined at the drift scale through cross-hole air injection tests, which support the fracture survey conclusions that fractures networks are well connected within the rocks units selected to host the repository (Section 2.3.3.2.2.1.2).

Given the significance of in-plane flow diversion around the drift in combination with relatively high fracture density, a three-dimensional, heterogeneous fracture continuum model is an appropriate conceptualization and is used as the basis for the ambient seepage models developed to analyze seepage data from liquid-release tests and to predict seepage into emplacement drifts (BSC 2004a, Section 6.3.1; BSC 2004b, Sections 6.3.2 and 6.6.2.2; Finsterle 2000).

To determine seepage-relevant parameters, models that simulate liquid-release tests are developed and calibrated to seepage data collected in the niches in the ESF drift and in the ECRB Cross-Drift (Section 2.3.3.2.2.1.1). The calibration process (Section 2.3.3.2.3.3) yields effective capillary strength parameters that not only represent the flow diversion capacity of the underground openings, but also include (1) the effects of film flow along the drift surface; (2) small-scale drift wall roughness; (3) effects of the discrete fractures terminating at the drift ceiling; (4) the effect of drift excavation on the apertures; and (5) in the case of lithophysal units, the presence of lithophysal cavities. Because the liquid-release tests have been conducted, once the seepage-relevant parameters are determined and the model is validated, ambient seepage predictions into intact and degraded emplacement drifts can be performed (Section 2.3.3.2.3.4).

As discussed above, the impact of small-scale drift wall roughness is implicitly accounted for in the calibrated capillary strength parameter. Small-scale roughness corresponds to wall imperfections on the order of a few centimeters, as one can typically expect in drifts excavated with a tunnel boring machine (such as the ECRB Cross-Drift or the future emplacement drifts, Section 1.3.4.3). Therefore, the seepage simulations for the liquid-release tests in the ECRB Cross-Drift, as well as the predictive seepage simulations for emplacement drifts, are conducted without explicit consideration of drift wall roughness (i.e., with the drifts represented as circular openings). More irregular shapes are observed in the niches, which have been excavated using a Road-Header Alpine Miner and have imperfections on the order of a few decimeters. These decimeter-scale irregularities are not implicitly accounted for in the calibrated capillary strength parameter; rather, they are explicitly represented in the numerical grids used for the niche simulation of the seepage calibration model (Figure 2.3.3-15) (BSC 2004b, Section 6.3.3; BSC 2004a, Section 6.1; SNL 2007a, Section 6.4).

The conceptualization and approach described above are suitable for simulations of seepage averaged over an emplacement drift section equivalent to the length of one waste package. The seepage calibration model used for reproducing seepage-rate data from liquid-release tests, and the seepage model for performance assessment used for simulating seepage into emplacement drifts, solves the Richards equation (Richards 1931) for saturated–unsaturated flow through porous materials. The van Genuchten–Mualem constitutive relations describe the capillary pressure and relative liquid permeability in the fracture continuum as a function of liquid saturation (van Genuchten 1980; BSC 2004b, Section 6.6.1).

To account for small-scale heterogeneity, the spatial structure of the air-permeability data is analyzed, and the resulting geostatistical parameters are used to generate multiple realizations of a spatially correlated permeability field, which are conditioned on the permeabilities measured in borehole intervals. The permeability fields are eventually mapped onto the numerical grid; an example is shown in Figure 2.3.3-15. The numerical grids created for the simulation of liquid-release tests by the seepage calibration model represent an appropriate section of the formation around the injection interval, including the emplacement drift (BSC 2004b, Section 6.6.2.2). For a small number of gridblocks, the statistically sampled permeability may be greater or smaller than the measured range, which is consistent with the probability distribution used to represent the data and the application of scaling relationships.

Evaporation from the drift and niche surfaces is accounted for in the seepage calibration model runs for the ECRB Cross-Drift systematic testing and Niche 5 testing. The model specifies a time-dependent water-potential boundary condition based on Kelvin's equation, where the thickness of the diffusive boundary layer is determined from evaporation experiments at the seepage test location (BSC 2004b, Sections 6.6.1.3 and 6.6.1.4).

In summary, the ambient seepage process models describe the FEPs relevant for simulating unsaturated zone flow and seepage into underground openings at Yucca Mountain (BSC 2004b, Section 6.2; BSC 2004a, Section 6.2). The processes are captured explicitly by solving the physically based governing equations. The degree of complexity of the models is appropriate for the simulation of average seepage on the scale of an approximately 5 m long emplacement drift segment. Small-scale features and processes, including discrete-fracture flow behavior, surface roughness, and film flow, are captured in effective model-related parameters determined from

site-specific data that reflect the seepage process on the appropriate scale. Calibration of the seepage calibration model against seepage-rate data, and the consistent conceptualization of the seepage model for performance assessment, make this a valid and reasonable approach to characterizing and calculating seepage at Yucca Mountain (BSC 2004b, Section 6.3; BSC 2004a, Section 6.3).

2.3.3.2.3.3   Model Calibration and Validation

The seepage calibration process model is calibrated against seepage-rate data from numerous liquid-release tests conducted in several boreholes at locations in both the middle nonlithophysal zone and the lower lithophysal zone. Seepage data collected early in the testing period were not used for purposes of model calibration, because they were affected by storage of water in the rock formation and the properties of a few fractures connecting the injection interval with the opening. These fractures are not necessarily representative of the fracture network that is activated in flow diversion around the entire opening under steady-state conditions. To obtain more accurate results, data obtained at later times are used for calibration of the seepage calibration model because they are more representative of near-steady-state conditions and are less influenced by storage effects. Consequently, the seepage data obtained later in the test better reflect average conditions on the scale of interest (BSC 2004b, Section 6.6.3.2).

Eighty-one liquid-release tests conducted in Niches 2, 3, 4, and 5, and the systematic testing area in the ECRB Cross-Drift, are simulated with the seepage calibration model (BSC 2004b, Table 6-5 and Sections 6.6.3 and 7.2.2). In addition, evaporation effects are accounted for when simulating seepage into the open, ventilated ECRB Cross-Drift. An example of the simulated saturation distribution at the end of liquid-release tests conducted in Niche 5 and the ECRB Cross-Drift is depicted in Figure 2.3.3-16 (BSC 2004b, Sections 6.5.3 and 6.6.3). Measured seepage-rate data from 22 liquid-release tests performed in boreholes above Niches 3, 4, and 5, and along the ECRB Cross-Drift (BSC 2004b, Table 6-5 and Section 6.5.3), are used to calibrate the seepage calibration model and to estimate the seepage-relevant, model-related van Genuchten capillary strength parameter. Most of the remainder of the seepage-rate data from liquid-release tests is used to validate the seepage calibration model (BSC 2004b, Table 6-5 and Sections 6.6.3 and 7.2.2).

Examples of seepage-rate data and calibrated model results for the liquid-release tests conducted along the ECRB Cross-Drift and in Niche 5 are shown in Figure 2.3.3-17. For the tests conducted along the ECRB Cross-Drift (Figure 2.3.3-17a, b, and c), a significant component of the fluctuations in both the simulated and observed seepage rates results from the variation in relative humidity and the evaporation potential in the ventilated drift, which was appropriately captured by the seepage calibration model. No such fluctuations were observed in the Niche 5 test (Figure 2.3.3-17d), where relative humidity was approximately constant at about 85% (BSC 2004b, Section 6.6.3.3).

The capillary strength parameter for each tested borehole interval is determined by calibrating the seepage calibration model against multiple tests using different liquid-release rates. Some of these release rates induced a local percolation flux that was above the seepage threshold (i.e., water dripped into the opening and yielded seepage-rate data used for calibration and validation of the seepage calibration model). However, tests performed below the seepage threshold were also used for calibration and validation in combination with tests that did result in seepage. These low-injection-rate seepage tests provide results at conditions similar to the natural percolation

fluxes that are below the seepage threshold and yield zero seepage in agreement with observations in exploration drifts and niches. Only high-infiltration climate or strong flow focusing causes the natural local percolation flux to exceed the seepage threshold, leading to seepage (BSC 2004b, Section 8.1). For example, record-breaking precipitation and relatively fast flow through fractured welded tuff contributed to a seepage event in the South Ramp area of the ESF (Ziegler 2005).

Figure 2.3.3-18 shows examples of validation runs in which seepage rates for liquid-release tests conducted in Niche 3 at different injection rates are simulated with the seepage calibration model using a single parameter set. Measured seepage data that were not used in model calibration serve the function of model validation. The results show that, for the tests at low injection rates (corresponding to the top four plots in Figure 2.3.3-18) where little or no seepage is predicted, the seepage calibration model always overestimates seepage and, therefore, provides conservative values with respect to effects of seepage.

Results for seepage tests with relatively high injection rates (corresponding to the bottom four plots in Figure 2.3.3-18) show that measured seepage is generally within the 95% uncertainty band, and less than the mean simulated seepage except for the tests conducted on October 11, 1999 (the bottom right plot in Figure 2.3.3-18), in which the measured seepage falls close to the upper bound of the uncertainty band and is more than the simulated seepage. The injection rates used in these tests were significantly greater than the background percolation flux, in order to achieve a measurable seepage amount in a reasonable amount of time. The observations in three of the bottom four tests yield results comparable to the model results, which provides additional confidence concerning the reliability of the seepage calibration model (BSC 2004b, Section 7.3). Only the fourth test yields seepage rates that are slightly larger than the relatively narrow uncertainty band (BSC 2004b, Section 7.3).

In summary, the capillary strength parameters determined from high-rate liquid-release tests provide an appropriate basis for seepage calculations under low and high natural percolation fluxes. Validation demonstrates that the seepage calibration model satisfactorily predicts the behavior above and below the seepage threshold (Figure 2.3.3-18). The measured seepage-rate data (1) fell within the range of the predicted seepage rates in all test cases for the Tptpll, and in almost all test cases for the Tptpmn, or (2) were lower than the predicted seepage rates in a few cases; i.e., the model prediction was conservative (BSC 2004b, Section 7.4). The data were marginally higher than the relatively narrow uncertainty band in two longer-term tests and in three short-term tests in Niche 2, which are considered of minor relevance (BSC 2004b, Section 7.4). The successful validation of the seepage calibration provides confidence that seepage into large underground openings can be reliably predicted for conditions that are different from those used for model calibration. The seepage model for performance assessment, which has the same conceptual basis as the seepage calibration model, is therefore validated for its intended purpose, which is the calculation of ambient seepage into waste emplacement drifts (Section 2.3.3.2.3.4).

The analysis of seepage-rate data for model development, and the determination of seepage-relevant parameters, is summarized as follows (BSC 2004b, Section 8.1):

- The testing and modeling approach provides the conceptual basis and parameters for the seepage model for performance assessment. The approach consists of analyzing seepage by means of the seepage calibration model, which is calibrated against seepage-rate data

from liquid-release tests conducted within the principal repository host units (Tptpmn and Tptpll).

- The variability of seepage-relevant parameters has been examined by performing liquid-release tests at various sites along the ESF and the ECRB Cross-Drift, and is incorporated into the drift seepage abstraction.

2.3.3.2.3.4   Prediction of Ambient Seepage

2.3.3.2.3.4.1   Seepage into Intact Emplacement Drifts

While the seepage calibration model simulates liquid release tests and seepage into niches and into the ECRB Cross-Drift for calibration and validation purposes, the seepage model for performance assessment evaluates total seepage into a section of an emplacement drift under ambient postclosure percolation conditions (BSC 2004a, Section 6.3.1). Isothermal flow simulations are performed over wide ranges of key parameters that bracket the range of parameters expected to be evaluated during the probabilistic TSPA calculations (Section 2.3.3.2.3.3). The key parameters affecting ambient seepage are the effective capillary strength parameter, permeability, and local percolation flux imposed at the upper model boundary (BSC 2004b, Section 6.3.3). These parameters were identified as seepage-relevant, based on the general understanding of the flow diversion and seepage process (Section 2.3.3.2.1.3; Philip et al. 1989), and by means of a formal sensitivity analysis (BSC 2004b, Section 6.6.3.1). The seepage calibration model and the seepage model for performance assessment are conceptually consistent, meaning that the basic conceptual framework and the calibrated parameters are transferred from the validated model to the predictive model. The main differences between the two models are in the model geometry (future emplacement drifts are slightly larger than niches), the flux boundary conditions (the seepage tests were operated with artificial water release in addition to natural percolation), and the range of key parameters considered (the seepage calibration model used key parameters specific to each test location, while the seepage model for performance assessment was applied to wide ranges of parameter combinations to encompass the seepage conditions near all future emplacement drift segments). Furthermore, evaporation from the drift wall is included in the seepage calibration model to account for ventilation effects that impacted the observed seepage rates. Evaporation is not considered in the seepage model for performance assessment, because relative humidity under ambient postclosure conditions is likely to be close to 100%.

The seepage model for performance assessment is a three-dimensional, drift-scale, predictive model employing a stochastic continuum representation of the small-scale heterogeneity of fractured rock in the drift vicinity (BSC 2004a, Section 6.3). Applying a percolation flux at the top of the model, the steady-state seepage flux is obtained. The calculation is repeated for different parameter combinations and different realizations of the underlying stochastic permeability field. Results are provided in the form of lookup tables that give seepage rates and related seepage estimation uncertainty as a function of the three key parameters (i.e., effective capillary strength parameter, permeability, and percolation flux) (BSC 2004a, Section 6.6.1). During a probabilistic TSPA calculation, values of key input parameters are sampled from their respective probability distributions, and the corresponding seepage rate is extracted from these lookup tables. Sensitivity analyses are performed to examine the impact of the standard deviation and correlation length describing the small-scale heterogeneity of the permeability field (BSC 2004a, Section 6.6.2).

Example results from the seepage model for performance assessment are illustrated in Figure 2.3.3-19. The figure gives contours of the simulated mean seepage percentage into an emplacement drift with a diameter of 5.5 m as a function of the capillary strength parameter and the mean fracture permeability for selected percolation fluxes between 1 and 1,000 mm/yr. These percolation fluxes are local and include flow focusing. The seepage percentage (the ratio between the seepage rate and the percolation flux arriving over the footprint of the considered drift segment) indicates the flow diversion capability of the capillary processes at the emplacement drift surface. As expected, the seepage percentage is large for small capillary strength, small permeability, and large percolation flux. In these extreme cases, seepage may approach 100% (i.e., there is no flow diversion at the drift wall), and the entire percolation flux seeps into the drift. At the other end of the spectrum, the seepage percentage is small for the cases with strong capillarity, large permeability, and small percolation flux. In many of these cases, there is no seepage; the entire percolation flux is diverted around the drift by capillary forces because the percolation flux is below the critical percolation flux. The critical percolation flux is the flux that corresponds to the seepage threshold for the given combination of permeability and capillary strength parameter (SNL 2007a, Sections 6.1.3, 6.4.2, and 6.6).

The model domain length along the drift axis considered in the seepage model for performance assessment is 5.1 m. In other words, the seepage model for performance assessment results—such as the seepage rate—represent the seepage conditions predicted for a drift section comprising one 5.0 m long waste package plus the 0.1 m gap spacing between waste packages. The length of the waste package corresponds to the rounded length of the 44-BWR and 21-PWR waste packages considered in previous designs. With the introduction of the transportation, aging, and disposal (TAD) canisters for commercial spent nuclear fuel (SNF), which is about 5.85 m long (SNL 2007c, Table 4-3), the average length of all waste packages plus gap increases to about 5.614 m. This, in turn, increases the seepage rate that waste packages may potentially encounter, and may also increase the seepage fraction. As discussed in *Total System Performance Assessment Model/Analysis for the License Application* (SNL 2008a, Appendix P13[a]), the seepage rates are expected to increase by approximately 10% with increased waste package length, while it is shown that a change in seepage fraction has little effect on annual dose. Therefore, the overall effect of increasing the waste package length is considered minor (SNL 2008a, Appendix P13[a]).

The seepage model for performance assessment is also used to simulate the potential effect of rock bolts in the drift ceiling on seepage (BSC 2004a, Section 6.5). Several rock bolts scenarios are examined in a sensitivity analysis, including cases representing both grouted and ungrouted boreholes. It is shown that these features have a minor effect on seepage, and can be excluded in the TSPA drift seepage submodel (Section 2.2, Table 2.2-5, for excluded FEPs 1.1.01.01.0B, Influx through holes drilled in drift wall or crown; and 2.1.06.04.0A, Flow through rock reinforcement materials in EBS).

2.3.3.2.3.4.2   Seepage into Degraded Emplacement Drifts

The above ambient seepage predictions represent the conditions in idealized intact drifts. This section describes the seepage predictions conducted to evaluate the effects of drift degradation, using the seepage model for performance assessment with a specific model setup that accounts for drift geometry changes caused by seismic activity (BSC 2004a, Section 6.6.3; SNL 2007a,

Section 6.4.2.4.2). Two drift profile scenarios are considered that cover the range of degradation results expected in the nonlithophysal and lithophysal repository rocks (Section 2.3.3.2.1.4).

Nonlithophysal Rock—The first drift profile scenario is for drifts where isolated wedge type rockfall has occurred, representing degraded conditions in nonlithophysal rock. Otherwise, the drifts remain intact openings with the horizontal extent essentially unchanged. Seepage calculations are conducted for two selected drift profiles, based on model results from the drift degradation analysis. For the considered drift profiles the average seepage rates—as well as the average seepage threshold calculated—are almost identical to the no degradation cases (BSC 2004a, Section 6.6.3). This result indicates that the impact of local geometry changes at the drift ceiling need not be explicitly addressed, as long as individual breakouts are not so ubiquitous (e.g., as a result of multiple seismic events) that many topographic lows would form at the ceiling. It follows that the seepage lookup table derived for the intact (idealized circular) drift can also be used to calculate seepage rates into moderately degraded drifts with local rockfall.

No seepage simulations are available for drift profiles with significant degradation, e.g., with several fallen wedges and multiple topographic lows at the roof. Since seepage may increase considerably in such cases, the predictions from the intact-drift lookup table cannot be used. It is therefore necessary to set seepage to an upper-bound value given by the local percolation flux arriving at the drift. In other words, it is assumed that there is no flow diversion capacity for drifts with multiple fallen wedges and topographic lows (Section 2.3.3.2.4).

Lithophysal Rock—The second drift profile scenario is for completely collapsed drifts, as expected in lithophysal rock in response to severe (or multiple) seismic events. During collapse, the rock mass above an underground opening disintegrates into a number of fragments that fall down and eventually fill the open space. The situation after drift collapse, as predicted by drift degradation analyses, can be categorized as follows (Section 2.3.4): The original opening has increased in size to about double the initial diameter (i.e, about 11 m diameter), and is filled with fragmented rubble with large voids. The solid wall rock surrounding the rubble filled opening is intact, but may have increased permeability and reduced capillary strength because of the dynamic motion and the stress redistribution (see discussion below). The rubble-filled opening is referred to hereafter as a "collapsed drift," although technically there is no drift after collapse.

For seepage predictions, the various collapsed-drift profiles provided by the drift degradation analyses in *Drift Degradation Analysis* (BSC 2004e, Appendix R) are idealized as rubble-filled openings of circular shape with a diameter of 11 m (SNL 2007a, Figure 6-4[a]). The seepage model for performance assessment is configured for these conditions using a modified model geometry with an 11 m wide opening embedded in the stochastic continuum domain that represents the heterogeneous fractured rock in the drift vicinity. A capillary-strength parameter of 100 Pa is used within the opening, and is representative of the small capillarity of the rubble material. Systematic seepage simulations are conducted with the seepage model for performance assessment to evaluate the capillary-barrier behavior at the interface between the 11 m wide rubble-filled opening and the surrounding rock. The calculation is repeated for the parameter combinations evaluated in the intact drift simulations, and a seepage lookup table is developed specific for collapsed drifts similar in structure to the one developed above. In the case of drift collapse, this lookup table needs to be used instead of the lookup table for intact or moderately degraded drifts.

Example seepage results illustrating the impact of drift collapse on seepage are presented in Figure 2.3.3-20, where seepage percentage contours for intact and collapsed drifts are plotted as a function of permeability and capillary strength, using a local percolation flux of 5 mm/yr. The seepage percentages obtained in the collapsed drift scenario are considerably higher than those for intact drifts, which is caused by the larger size of the collapsed drift (reducing the effectiveness of flow diversion around the drift) and the nonzero capillary strength in the rubble filled drift (reducing the effectiveness of the capillary barrier) (SNL 2007a, Section 6.4.2.4.2). Nevertheless, the simulation results demonstrate that most of the percolation flux is still diverted around the collapsed drift for most of the considered parameter range.

Hydrologic Property Changes—Geomechanical simulations have been conducted to determine the impact of drift degradation on the hydrologic properties in the drift vicinity (BSC 2004g, Section 6.8). Model results indicate that moderate degradation is not expected to cause any relevant rock-property changes, compared to the initial excavation disturbed conditions. Drift collapse, on the other hand, is expected to cause changes in the hydrologic properties, with fracture permeability increases and fracture capillary strength decreases in the relevant area above the drift crown. A local permeability increase would result in less seepage because of enhanced flow diversion around the collapsed drift, whereas a local capillary strength decrease would result in more seepage, since the capillary barrier is weakened. As discussed in *Abstraction of Drift Seepage* (SNL 2007a, Section 6.4.4.1.2), the net result of these counteracting property alterations is relatively small (i.e., the interpolated seepage rates using the adjusted properties for collapsed drifts are similar to the interpolated seepage rates using the initial excavation-disturbed properties). Thus, reasonable estimates of seepage into degraded or collapsed drifts can be derived when the seepage calculation uses the initial properties of the excavation-disturbed zone around drifts (i.e., when the calculation does not explicitly address changes to these properties caused by the drift degradation and collapse).

Drift Degradation Characterization for Seepage—How emplacement drifts can be categorized regarding the different degradation and seepage scenarios introduced above is explained in Section 2.3.3.2.4.2.

2.3.3.2.3.4.3   Seepage Predictions for Alcove 8–Niche 3 Tests

Numerical modeling of the flow and seepage processes in the Alcove 8–Niche 3 tests (Section 2.3.3.2.2.1.5) was conducted to evaluate the conceptual model for seepage predictions, as discussed in the preceding sections. Seepage modeling was conducted in two stages (BSC 2006, Sections 6.2 and 6.3.1). First, the infiltration rate and seepage data from early tests were used to calibrate the model in order to obtain site-specific rock properties. The calibrated model was then used to predict results for subsequent tests. Figure 2.3.3-21 shows the results for observed and simulated total seepage rates in comparison to total infiltration rates. There is an overall good agreement between observations and simulations for the calibration period (0 to 210 days) and the prediction period (after 210 days). Some disagreements observed in the late testing stage (after 550 days) are attributed to scrubbing of the infiltration plots, which may have released in-fill or dust particles into the fractured rock (BSC 2006, Section 6.2.4). The data and modeling evaluation supports the conceptual approach for predicting seepage in the unsaturated rocks at Yucca Mountain. Note that these data were not directly used for the seepage calibration effort described in

Section 2.3.3.2.3.3, because of the larger separation between the infiltration and observation levels, which may allow some of the infiltrating water to migrate laterally and bypass Niche 3.

2.3.3.2.3.5   Percolation Flux and Flow Focusing

The magnitude and spatial distribution of local percolation fluxes at the repository horizon significantly affect seepage into emplacement drifts. The larger the local percolation flux, the greater the potential for seepage to occur and the larger the amount of water that can seep into emplacement drifts.

For ambient flow conditions, the three-dimensional spatial flux distributions in the unsaturated zone are provided by the site-scale unsaturated zone flow model (SNL 2007b). This model calculates flow fields accounting for climate changes and related uncertainties, variability in net infiltration, the effects of different stratigraphic units, and the presence of faults (Section 2.3.2.2) (Table 2.3.3-1, FEPs 1.3.01.00.0A, Climate change; 2.2.03.01.0A, Stratigraphy; 1.2.02.02.0A, Faults; and 2.2.07.02.0A, Unsaturated groundwater flow in the geosphere). Climate changes expected during the pre-10,000-year period are represented using the flux distributions for three future climate states, namely the present-day climate, the monsoon climate, and the glacial-transition climate. The flux distribution during the post-10,000-year period is based on the proposed revision to 10 CFR 63.342(c), where a log-uniform distribution is prescribed defining the average percolation flux through the repository. These flux distributions are interpolated by the multiscale thermal-hydrologic model (Section 2.3.5.4.1) (SNL 2008b) to determine downward flux values consistent with repository locations used for in-drift thermal-hydrologic calculations. However, because of the large model area used to determine the percolation flux distributions and the related interpolated values, the spatial resolution is much coarser than the extent of drift-scale seepage models (Figure 2.3.3-5), and layer-averaged properties are used within stratigraphic units (Sections 2.3.2 and 2.3.5.4.1). Intermediate-scale heterogeneity that may lead to focusing of flow is not represented. To bridge the gap in scale between the mountain-scale models providing percolation fluxes and drift-scale seepage models, the local percolation flux relevant for seepage is estimated from the interpolated percolation flux multiplied by a flow focusing factor (SNL 2007a, Section 6.7.1.1). (Table 2.3.3-1, FEPs 2.1.08.01.0A, Water influx at the repository; and 2.2.07.04.0A, Focusing of unsaturated flow (fingers, weeps)).

Flow focusing factors are estimated with the use of a high-resolution fracture continuum numerical flow model, called the flow focusing model, that captures the intermediate-scale heterogeneity. This two-dimensional model is 100 m wide and extends from the bottom of the PTn unit to the repository horizon, a distance of 150 m at a typical location within the repository domain. The grid spacing is 0.25 m and 0.5 m in the horizontal and vertical directions, respectively. The model explicitly includes the hydrologic properties of the model layers from the top of the TSw unit to the repository horizon (BSC 2004a, Section 6.8.1). In contrast to the site-scale unsaturated zone flow model, in which the rock properties within geologic units are considered uniform, the flow focusing model represents the intermediate-scale heterogeneity of the fractured rock, which is treated as a stochastic heterogeneous continuum with variable permeability. Both uniform and nonuniform percolation fluxes were applied at the top boundary of the heterogeneous domain to investigate uncertainty in flow focusing due to top boundary flux distribution. The resulting percolation flux distribution at the bottom boundary is analyzed to obtain flow focusing factors (BSC 2004a, Section 6.8.2; SNL 2007a, Section 6.6.5.2).

Simulations were conducted for several flow scenarios, with varying percolation flux rates of 1, 5, 25, 100, and 500 mm/yr; different infiltration patterns (uniform, locally concentrated, and permeability dependent); and different realizations, as well as correlation lengths of the heterogeneous fracture permeability field. A distribution of flow focusing factors is readily generalized from the cross-sectional flux calculation by normalizing the flux values to the average infiltration rate imposed at the top boundary. Factors larger than 1 correspond to increased percolation fluxes, and factors smaller than 1 correspond to decreased percolation fluxes compared to the average percolation. For example, Figure 2.3.3-22a shows the distribution of flow focusing factors across the bottom of the model area, with 5 mm/yr uniform percolation imposed at the top and a spatial correlation of 1 m for fracture permeability. The profile demonstrates a significant variability, with flow focusing values ranging from about zero to more than six. Analysis of additional cross sections between the top and bottom boundary are statistically similar (BSC 2004a, Section 6.8.2), indicating that the basic flow focusing characteristics (Figure 2.3.3-5) develop within tens of meters from the top of the model and remain similar within a unit over extended vertical distances (SNL 2007a, Section 6.6.5.2). The frequency distribution over the entire model domain is shown in Figure 2.3.3-22b (BSC 2004a, Figure 6-25b). The infiltration cases, covering a range from 1 to 500 mm/yr, are statistically similar. This means that flow focusing factors, as modeled, are independent of the percolation flux (i.e., the distribution of flow focusing factors is not correlated to the distribution of percolation fluxes). The majority of the normalized flux values (focusing factors) ranges from zero to about two. The maximum percolation flux that occurs in the model domain is generally about five to six times higher than the infiltration flux prescribed at the upper boundary. The minimum percolation flux is almost zero (SNL 2007a, Section 6.6.5.2).

Based on these modeling results, a single frequency distribution of flow focusing factors is developed for use in the simulation of emplacement drift seepage. A regression analysis of the resulting flow focusing factors is shown in Figure 2.3.3-23, and provides a probability distribution function to be used in defining the local percolation flux relevant for seepage. This distribution conserves mass, so the amount of downward water flow remains unchanged when flow focusing factors are used as multipliers to the site-scale percolation fluxes. As shown in Figure 2.3.3-23, the infiltration distribution and fracture permeability (distribution and correlation length 1, 2, and 3 m, referred to as field 1, field 2, and field 3) have little effect on flow focusing (BSC 2004a, Section 6.8.2).

In summary, the local percolation flux sampled during the probabilistic TSPA seepage calculations is interpolated for a given location, climate state, and infiltration scenario from percolation flux distributions provided by the site-scale unsaturated zone flow model, multiplied by a flow focusing factor sampled from the cumulative distribution function shown in Figure 2.3.3-22b. The interpolated fluxes at selected repository locations are consistent with and provided by the multiscale thermal-hydrologic model (SNL 2008b). The local percolation flux defines one axis of the three-parameter seepage lookup table calculated by the seepage model for performance assessment for use in the TSPA seepage calculations. Flow channeling introduced by small-scale heterogeneity (i.e., smaller than the drift scale) is captured by the small-scale heterogeneity considered in the seepage model for performance assessment (Section 2.3.3.2.3.4) (SNL 2007a, Section 6.4.2).

2.3.3.2.3.6   Parameter and Model Uncertainty

The first part of this section explains the derivation of probability distributions for the three seepage-relevant parameters evaluated by the seepage model for performance assessment: (1) the capillary strength parameter; (2) the reference permeability, and (3) the local percolation flux (Sections 2.3.3.2.3.6.1, 2.3.3.2.3.6.2, and 2.3.3.2.3.6.3, respectively). Separate probability distributions are developed for spatial variability and for uncertainty. These parameters are defined in the context of the conceptual framework of the seepage model for performance assessment (SNL 2007a, Section 6.4.2), as follows: (1) the capillary strength is the calibrated effective parameter, as estimated by the seepage calibration model; (2) the permeability represents the mean value of the small-scale stochastic permeability fields in the drift-scale model domain; and (3) the percolation flux is the local flux arriving at the upper boundary of the seepage model for performance assessment (SNL 2007a, Section 6.6.5). The spatial variability distributions of these parameters refer to the intermediate-scale distribution within the repository units that is used for the calculation of repository-wide seepage rates in the TSPA (SNL 2007a, Section 6.6). The second part of this section describes how the different sources of model uncertainty are incorporated in the seepage prediction framework (Section 2.3.3.2.3.6.4).

2.3.3.2.3.6.1   Variability and Uncertainty of Capillary Strength

The capillary strength parameter is one of the key parameters affecting the capillary diversion at the emplacement drift crown (BSC 2004b, Section 6.3.3.2; SNL 2007a, Section 6.6.2). The larger this parameter, the stronger the capillary force holding water in the fractures, thus preventing it from seeping into emplacement drifts. The capillary strength parameter is estimated by matching seepage-rate data from liquid release tests (Section 2.3.3.2.2.1.1) using the seepage calibration model (Section 2.3.3.2.3.3). These estimates are uncertain due to uncertainty in the seepage-rate data and uncertainty in the seepage calibration model. The capillary strength parameter is also variable in space because different locations in the repository have different rock property characteristics and different capillary barrier behavior (BSC 2004b, Section 6.6.4). This variability in space is uncertain because of the limited number of testing locations where capillary strength parameters are available. Excavation effects are accounted for in the calibrated capillary strength values, because the liquid-release tests have been conducted in the excavation-disturbed zone near the drifts.

A summary of the calibrated capillary strength values is provided in Table 2.3.3-2. Data from six test intervals in the lower lithophysal zone (Tptpll), and four intervals in the middle nonlithophysal zone (Tptpmn), are analyzed. Multiple inversions with different realizations of the underlying heterogeneous permeability field are performed for test locations in the lower lithophysal zone. Uncertainties in the seepage rate data and in the seepage calibration model are propagated through each individual inversion, and are reflected in the estimation uncertainty of the parameters determined for each realization of the stochastic permeability field (BSC 2004b, Sections 6.6.3 and 6.6.4; SNL 2007a, Section 6.6.2). For each test location, the average and standard error of the capillary strength parameter determined using the set of realizations of the permeability field is calculated, providing an estimate and corresponding estimation uncertainty for a given test location (BSC 2004b, Section 6.6.4; SNL 2007a, Section 6.6.2). These values provide the basis for developing appropriate probability distributions that characterize spatial variability and uncertainty of the seepage-relevant capillary strength parameter for use in the TSPA. The variability of capillary

strength refers to the variation of the effective drift scale parameter within the repository rock units. Figure 2.3.3-7 shows the locations of niches and drift sections where seepage tests have been conducted. The Tptpmn unit test locations (Niches 3 and 4) are separated by a distance of about 1,700 m. The two niches represent areas in the middle nonlithophysal zone with distinct fracture characteristics. The Tptpll unit test locations (Niche 5 and systematic testing boreholes) are in relatively close proximity within a 150 m long section of the ECRB Cross-Drift. Where several boreholes were tested in one niche, the typical distance between test intervals was on the order of a few meters. Thus, the 10 available capillary strength values (Table 2.3.3-2) are not randomly placed over the entire repository area. They are clustered at four selected test locations within two different rock types (BSC 2004b, Section 6.5.1).

To evaluate the spatial variability of capillary strength from the data discussed above, it is important to recall the nature of the parameter in question. If capillary strength solely represented the capillary behavior of the fractured rock, this parameter would be expected to vary considerably between the Tptpmn and Tptpll units, as a result of potential differences in fracture aperture and fracture wall roughness. Thus, the analysis would need to be conducted separately for the two geologic units. However, as noted previously, the ambient seepage models derive and apply capillary strength as an effective process parameter that accounts for a number of additional factors affecting seepage (Section 2.3.3.2.3; BSC 2004b, Section 6.3.3.2). Some of these factors (e.g., drift-wall roughness, film flow along drift wall, artifacts of finite discretization) are largely independent of intermediate- and large-scale variation. Consequently, analysis of statistical measures can be conducted without distinguishing between geologic units. Applying different averaging methods (SNL 2007a, Table 6.6-2) yields consistent estimates of capillary strength values, thereby confirming that a single mean and standard deviation provides representative estimates for the repository host rock. Using all 10 samples of both geologic units to derive the mean, standard deviation, and standard error of the mean is, therefore, appropriate (SNL 2007a, Sections 6.6.2 and 6.6[a]).

Figure 2.3.3-24 (SNL 2007a, Figure 6.6-2) shows the relatively uniform spread among the 10 data points of the capillary strength parameter, thereby demonstrating that a uniform distribution is appropriate for representing spatial variability of this parameter. The lower bound (402 Pa) and upper bound (780 Pa) of this uniform distribution are calculated from the mean and standard deviation, combining data from the 10 tests in both the Tptpmn and Tptpll repository host units (SNL 2007a, Table 6.6-2).

As discussed in *Abstraction of Drift Seepage* (SNL 2007a, Section 6.6.2), the main source of uncertainty in the capillary strength parameters is uncertainty in spatial variability distribution because only a limited number of data points is available. This uncertainty is expressed in the mean and in the range of the distribution. Other sources of uncertainty—such as the measurement uncertainty and conceptual model uncertainty—are considered less important in view of the careful experimental design used for liquid release and air injection testing, and the careful modeling and validation process that supports the seepage conceptual models. The estimation uncertainty of capillary strength is mainly a result of uncertainty in the small-scale fracture permeability distribution at each test location (BSC 2004b, Section 8.2; SNL 2007a, Section 6.6.2.3). This source of estimation uncertainty is directly accounted for in the seepage model for performance assessment (Section 2.3.3.2.3.4), and is passed through the seepage abstraction to the TSPA (Section 2.3.3.2.4).

An empirical method is used to describe the combined uncertainty of the capillary strength parameter, based on estimates of the standard error of the mean of the 10-data-point sample. Uncertainty is accounted for by varying the mean of the uniform probability distribution for spatial variability, with the magnitude of variation sampled from an uncertainty distribution. The uncertainty distribution that represents this stochastic adjustment of the mean is a symmetric triangular distribution with a mean of 0, a minimum of -105 Pa, and a maximum of $+105$ Pa, taking into consideration the standard errors of the mean value (SNL 2007a, Sections 6.6.2 and 6.3[a]). A schematic of the spatial variability and uncertainty in the capillary strength parameter is given in Figure 2.3.3-25 (SNL 2007a, Figure 6.6-3), showing the triangular-shaped uncertainty distribution, which assigns a probability to the mean of the uniform-shaped spatial variability distribution. In other words, the capillary strength parameter is to be sampled from a uniform distribution on the interval $[402\text{ Pa} + X, 780\text{ Pa} + X]$, where X is sampled from a triangular distribution having mode 0, lower bound -105 Pa, and upper bound $+105$ Pa. Thus, the most likely spatial variability distribution is the one where $X = 0$ (i.e., the uniform distribution with a minimum value of 402 Pa and a maximum value of 780 Pa). Least likely are the two bounding cases, where the triangular distribution at -105 Pa or $+105$ Pa indicates a zero probability. Considering the combined effect of spatial variability and uncertainty, the range of capillary strength parameter values to be used in the TSPA extends from 297 to 885 Pa, with the most likely value at 591 Pa (SNL 2007a, Section 6.6.2). The spatial variability and uncertainty distributions developed for the Tptpmn and Tptpll units are also suitable for the Tptpul and Tptpln units, respectively, because of similarity in the rock types (SNL 2007a, Section 6.6.4).

An alternative statistical method was applied in *Abstraction of Drift Seepage* (SNL 2007a, Section 6.6[a]) to support the distributions described above (and used in the TSPA drift seepage submodel). A maximum likelihood estimation was conducted to characterize the spatial variability and related uncertainty of the 10-data-point sample of capillary strength values. The resulting parameter range estimated by this analysis is 355 Pa to 825 Pa, which is slightly smaller than the range previously obtained. The consistency between the two approaches is very good, considering that the range determined by the maximum likelihood estimation describes only spatial variability and related uncertainty, while the larger range used in the TSPA drift seepage submodel includes additional sources of uncertainty.

2.3.3.2.3.6.2   Variability and Uncertainty of Fracture Permeability

The second key parameter affecting the diversion of water around drifts is the tangential fracture permeability in the boundary layer near the emplacement drift wall (BSC 2004b, Section 6.3.3.2; SNL 2007a, Section 6.6.3). As this parameter increases, water flow around the drift is more likely, and seepage is less likely. In a consistent manner, both the seepage calibration model and the seepage model for performance assessment apply a stochastic continuum conceptualization for fracture permeability in the drift vicinity. The small-scale variability of the continuum fracture permeability at a resolution of about 1 ft is implicitly accounted for in these models, using lognormal probability distributions based on air injection measurements that were performed on the same scale (SNL 2007a, Section 6.6.3). While the standard deviation of these small-scale fracture permeability distributions can be treated as a constant for abstraction purposes (as determined by sensitivity analyses showing its relative insignificance for reasonable ranges of standard deviation), the mean values of the distributions may vary significantly over the repository rock units. For the

TSPA, distributions covering the intermediate-scale variability and the uncertainty of these mean values of small-scale fracture permeability are developed (SNL 2007a, Section 6.6.3).

The most appropriate information on small-scale fracture permeability stems from the air injection testing conducted in the boreholes located above the niches. Using the pressure response as input, the air-permeability value of the tested interval is calculated by an analytical solution. Tests were performed using the same testing methodology and identical packer setup before and after niche excavation, thereby providing insight into the permeability changes induced by stress release due to drift excavation. Note that the fracture permeability needed for seepage calculations is the value that is representative of the excavation-disturbed zone, rather than the undisturbed formation (BSC 2004f, Section 6.1.2.2).

The mean values and the standard deviations of the small-scale permeability data are calculated (SNL 2007a, Table 6.6-3) with the standard deviations reflecting spatial variability on a 1 ft test interval scale. This small-scale variability of permeability is explicitly accounted for in the seepage model for performance assessment. The mean permeability and its potential intermediate-scale variation within the repository units are quantified and provided to the TSPA (SNL 2007a, Section 6.6.3.2).

The two main host rock units (Tptpll and Tptpmn) have different fracture permeability ranges. Analyses of intermediate-scale variability are therefore conducted separately for the two units. To obtain a sample size sufficient for a statistical analysis of permeability in the two units, permeability values from the following sources are combined after appropriate adjustments are made: (1) preexcavation and postexcavation mean permeabilities from niche studies (BSC 2004f, Section 6.1); (2) permeabilities from air injection tests in surface-based boreholes (LeCain 1995); and (3) permeabilities from numerous boreholes drilled as part of the Single Heater Test and Drift Scale Test (SNL 2007d, Sections 6.2 and 6.3). With the exception of postexcavation permeability values, which are representative of the seepage-relevant excavation-disturbed zone and on the appropriate scale, the measured permeability values are adjusted to account for excavation effects, for scale effects resulting from different lengths of the injection intervals, or both (SNL 2007a, Section 6.6.3.2). Excavation effects are accounted for based on the measured pre- and post-excavation data and the simulation results from the thermal-hydrologic-mechanical model (BSC 2004a, Section 6.3.2). The permeability data used, the adjustments made, and the results of the statistical analysis of the combined data set are described in detail in *Abstraction of Drift Seepage* (SNL 2007a, Section 6.6.3).

For the middle nonlithophysal unit (Tptpmn), the log-permeability (permeability units of square meters) is described by normal distribution with a mean of -12.2 and a standard deviation of 0.34 (SNL 2007a, Section 6.6.3.2.1). For the lower lithophysal unit (Tptpll), the log-permeability is described by a normal distribution with a mean of -11.5 and a standard deviation of 0.47 (SNL 2007a, Section 6.6.3.2.2). These distributions represent spatial variability in the drift-scale, disturbed-zone permeability value across the repository horizon.

Uncertainty in this seepage relevant parameter stems from (1) uncertainty in the derived air permeability values (which is a combination of the uncertainty in the measured flow-rate and pressure data and uncertainty regarding their analysis); and (2) uncertainty in the characterization

of its spatial variability. The first source is insignificant in comparison to the second (SNL 2007a, Section 6.6.3.3), and is thus not explicitly represented in the TSPA seepage calculations.

The main uncertainty source for fracture permeability is related to spatial variability, which is evaluated using values from the limited number of testing locations in the Tptpmn and Tptpll units. Uncertainty in the spatial variability of log-permeability is empirically accounted for by varying the mean of the distribution for spatial variability within appropriate ranges. A triangular uncertainty distribution is applied with a mean of zero and the upper and lower bounds related to the standard errors, which describe the potential uncertainty in the estimated mean of a sample (SNL 2007a, Section 6.6.3.3). A schematic of the spatial variability and uncertainty distributions for log permeability in the lower lithophysal unit is given in Figure 2.3.3-26. The triangular distribution representing uncertainty in log permeability in the Tptpll unit has a range of ±0.92; the corresponding distribution for the Tptpmn unit has a range of ±0.68 (SNL 2007a, Section 6.6.3.3). 99% of the log permeability values sampled from the combined uncertainty and variability distribution shown in Figure 2.3.3-26 lie within the range from −12.9 to −10.0, as shown in Figure 2.3.3-27. The permeability distributions developed for the Tptpmn and Tptpll units are also suitable for the Tptpln and Tptpul units, respectively, because of similarity in the rock types (SNL 2007a, Section 6.6.4).

2.3.3.2.3.6.3   Variability and Uncertainty of Local Percolation Flux

The local percolation flux at the repository horizon is the third key parameter affecting seepage into emplacement drifts (BSC 2004b, Section 6.3.3.1; SNL 2007a, Section 6.6.5). The larger this parameter, the greater the potential for seepage to occur and the larger the amount of water that can seep into emplacement drifts. The large-scale spatial and temporal variability of percolation fluxes in the unsaturated zone are captured by the percolation flux distributions generated by the site-scale unsaturated zone flow model (Section 2.3.2). As is discussed in Section 2.3.3.2.3.5, the multiscale thermal-hydrologic model uses these distributions to calculate downward fluxes for repository locations used in in-drift thermal-hydrologic calculations. These interpolated downward fluxes are then multiplied by the flow focusing factor to account for intermediate-scale flow redistributions, as explained in Section 2.3.3.2.3.5 (SNL 2007a, Section 6.6.5). The final results are then used as inputs to the TSPA drift seepage submodel to propagate percolation flux variability and uncertainty for the probabilistic seepage calculation.

There are several sources of uncertainty related to the large-scale percolation flux estimates provided by the unsaturated zone flow model. Uncertainty related to the future climates and net infiltration during the first 10,000 years after emplacement is accounted for using a range of alternative infiltration maps for each of the climate states: present day, monsoon, and glacial-transition (Sections 2.3.1 and 2.3.2). These infiltration maps, used as upper boundary conditions for the unsaturated zone flow model, lead to alternative percolation flux distributions. For a given climate state, the relative importance of a selected infiltration map is represented by a weighting factor (Section 2.3.2.3.5.1). The weighting factors are determined through comparison with measured data from the unsaturated zone (e.g., distributions of temperature and chloride), using a generalized likelihood uncertainty estimation method. Four maps were selected, representing the range of present-day infiltration at Yucca Mountain, giving four percolation flux distributions associated with weighting factors of 62%, 16%, 16%, and 6% (Section 2.3.2.4.1.2.4.5; Table 2.3.2-27). These same weighting factors are also used for the monsoon and glacial transition

climates. During the post-10,000-year time period, uncertainty in deep percolation is accounted for based on the proposed revision to 10 CFR 63.342(c), where a log-uniform distribution is prescribed for average percolation through the repository footprint ranging from 13 to 63 mm/yr. Four alternative percolation flux maps have been developed to provide upper boundary conditions that simulate this range of average fluxes at the repository. These are also associated with weighting factors of 62%, 16%, 16%, and 6%.

Uncertainty related to simulation of flow processes in the unsaturated zone has been addressed by calibration and validation of the model to a wide variety and large amount of data from different sources (SNL 2007b, Sections 6 and 7). For the scope of evaluating seepage, the most important sources of uncertainty are the flow diversion capacity of the PTn and the impact of spatial variability within stratigraphic units (SNL 2007a, Sections 6.6.5.1 and 6.6.5.3). The impact of the PTn flow diversion was addressed in Section 6.8.2 of *Abstraction of Drift Seepage* (SNL 2007a), where seepage rates were estimated using results of an alternative flow model for the PTn (Section 2.3.2.4.2.1). It was shown that the alternative flow model does not significantly impact the seepage estimates. The effect of intermediate scale spatial variability, which is not accounted for in the unsaturated zone model results, is explicitly incorporated in the TSPA drift seepage submodel using the flow focusing concept. It is recognized that the flow focusing factors used in the seepage abstraction model may be overestimating the variability of percolation flux, because a fine grid resolution was used for the numerical study (SNL 2007a, Section 6.6.5.3). The resulting percolation flux distributions used for seepage evaluation cover the spatial variability of this parameter and all related uncertainties.

2.3.3.2.3.6.4   Model Uncertainty

The uncertainty inherent in the ambient seepage results is a result of uncertainty in the key input parameters to the model, as well as uncertainty that arises from the modeling methodology (conceptual model) independent of the model input.

Uncertainty in the key input parameters for ambient seepage is accounted for in the TSPA drift seepage submodel by feeding appropriate probability distributions into the seepage lookup tables derived from the seepage model for performance assessment. The probabilities assigned to these key parameters distinguish between spatial variability and uncertainty using separate distributions. Spatial variability and uncertainty distributions for the capillary strength parameter and the local permeability have been derived by statistical analysis of the sparsely distributed data available from underground testing and surface-based boreholes (Sections 2.3.3.2.3.6.1 and 2.3.3.2.3.6.2). Spatial variability distributions for the local percolation flux are provided from site-scale simulations with the site-scale unsaturated zone flow model (Section 2.3.3.2.3.6.3). As discussed in Sections 2.3.1 and 2.3.2, alternative flux distributions have been developed that account for uncertainty in future climate, net infiltration, and deep percolation. For seepage purposes, the site-scale fluxes are then adjusted to account for intermediate-scale heterogeneity, using a spatial distribution of flow focusing factors.

The conceptual model used in the seepage model for performance assessment is adopted from the conceptual framework of the seepage calibration analyses, conducted with the seepage calibration model. The calibrated seepage calibration model with the appropriate effective parameters is capable of reproducing and predicting observed seepage data from liquid-release tests

(Section 2.3.3.2.3.3). The seepage model for performance assessment, which is conceptually consistent with the seepage calibration model, is thus likely to provide reasonable predictions of seepage into intact emplacement drifts. Alternative conceptual models corroborate the findings of the seepage calibration and prediction models (Section 2.3.3.2.3.7 below). Accordingly, the uncertainty about the conceptual model used in the seepage predictions for intact drifts is small compared to uncertainty in the model input parameters (as explained above). Prediction results from the seepage model for performance assessment are uncertain, however, because the exact structure of local heterogeneity in the drift vicinity is unknown. This estimation uncertainty is described by the range of seepage results available from multiple realizations of the stochastic permeability fields used in the seepage model. The lookup tables available for intact and collapsed drifts thus not only provide the mean seepage over all realizations, but also the spread in the seepage results expressed by the standard deviation. As pointed out in Section 2.3.3.2.4.3, the TSPA drift seepage submodel samples from both the mean seepage values as well as the standard deviations to account for estimation uncertainty (SNL 2007a, Section 6.5.1.2).

Additional sources of uncertainty need to be considered in the seepage assessment of degraded or collapsed drifts after seismic activity. First, there is considerable variability and uncertainty in the drift degradation results that provide input to the TSPA drift seepage submodel. This source of uncertainty is accounted for by using the rockfall regression curves developed in *Seismic Consequence Abstraction* (SNL 2007e, Sections 6.7.1.2 and 6.7.2.3) for categorizing drift degradation with respect to seepage (Section 2.3.3.2.4). These regression curves provide the mean rockfall volume for a seismic event of given magnitude, as well as the variation of volumes on account of drift degradation variability and uncertainty. There is also increased uncertainty about the seepage prediction results for degraded drifts, because liquid release tests have only been performed for mostly intact openings. This source of uncertainty is accounted for as follows (SNL 2007a, Sections 6.5.1.5 and 6.2.4[a]). For drifts that have moderately degraded but not collapsed (for example, after local wedge-type rockfall in nonlithophysal rock), the ambient seepage rates from the seepage model performance assessment lookup table are increased by 20% to account for increased estimation uncertainty in the prediction. The choice of a 20% increase is based on a seepage sensitivity calculation with larger estimation uncertainties described in *Abstraction of Drift Seepage* (SNL 2007a, Section 6.5.1.5). For fully collapsed drifts in lithophysal rock, uncertainty is accounted for by the conservatism involved in using worst case profiles, and by assuming that all seepage from the surrounding rock into the rubble filled opening can potentially contact the drip shield or the waste package, independent of the actual seepage location (SNL 2007a, Section 6.2.4[a]). For strongly degraded drifts in nonlithophysal rock, uncertainty is accounted for by the conservatism in using the local percolation flux at the drift as the upper-bound value for seepage (SNL 2007a, Section 6.2.3.1[a]).

2.3.3.2.3.7   Alternative Conceptual Models of Ambient Seepage

The following alternative conceptual models were considered for evaluating ambient seepage:

- A discrete-fracture network model (BSC 2004b, Section 6.4.1)

- An analytical solution for seepage assuming a homogeneous porous medium (BSC 2004a, Section 6.9.1)

- An evaluation of ponding probability (BSC 2004b, Section 6.4.2)

- Observations of calcite and opal in lithophysal cavities (BSC 2004b, Section 6.4.3)

- A simplified analysis using liquid-release test data (BSC 2004b, Section 6.4.4).

In addition, an alternative conceptualization of flow focusing that could affect ambient seepage calculations was also evaluated (BSC 2004a, Section 6.9.2).

As discussed below, most of these alternatives were excluded because they would potentially underestimate seepage.

2.3.3.2.3.7.1   Discrete-Fracture Network Model

A discrete-fracture network model is an alternative conceptual model to the heterogeneous continuum model used for the two ambient seepage models (BSC 2004b, Section 6.4.1). In a discrete-fracture network model, individual fractures are discretized into appropriately small computational gridblocks. The flow equations solved within and between gridblocks are identical to those solved by a continuum model. A high-resolution discrete-fracture network model is capable of generating channelized flow and discrete seepage events. As discussed in Section 2.3.3.2.3.2, in-plane flow diversion is the key mechanism enabling capillary diversion around drifts; both the base-case continuum model and a three-dimensional discrete-fracture network model can simulate in-plane flow diversion (BSC 2004b, Section 6.4.1). However, a discrete-fracture network model requires detailed data on fracture-network geometry and unsaturated hydrologic properties on the scale of individual fractures, along with conceptual models and simplifying assumptions regarding unsaturated flow within fractures and across fracture intersections. The scarcity of this information leads to substantial uncertainty, which can partly be overcome by calibrating the model against hydrogeologic data using an approach very similar to that used for continuum models (Section 2.3.3.2.3.3). Results from a simplified calibrated fracture continuum model were compared to those of a discrete-fracture network model, yielding consistent results (Finsterle 2000). Given the consistency of results, the simplicity of the continuum conceptual model is considered an advantage over the complexity of the discrete-fracture network model.

2.3.3.2.3.7.2   Homogeneous Porous Medium Model

Ambient seepage into an underground opening excavated from a homogeneous porous medium can be calculated using an analytical solution derived by Philip et al. (1989). However, in a natural, fractured-porous medium, seepage is controlled by heterogeneity-induced channeling and local ponding effects (Sections 2.3.3.2.1.3 and 2.3.3.2.3.7.3). These conditions cause seepage to occur at significantly lower percolation fluxes than if the medium is homogeneous. Therefore, the homogeneous model would predict unrealistically low, less conservative seepage rates (BSC 2004a, Section 6.9.1).

2.3.3.2.3.7.3   Seepage Governed by Ponding Probability

As an alternative conceptual model to the ambient seepage models, seepage can be related to the local ponding probability that is derived from the variability of the permeability field (BSC 2004b,

Section 6.4.2). This alternative approach assumes that, in strongly heterogeneous formations, seepage is predominantly affected by pressure variations governed by local heterogeneity, rather than the presence and geometry of the capillary barrier. This behavior is different from the behavior in a homogeneous system where the geometry of the capillary barrier has a strong impact on seepage (Philip et al. 1989). Strong, medium- to small-scale heterogeneities tend to increase seepage because they increase channeling and local ponding. This effect is also included in the base-case ambient seepage models through the estimation of effective, seepage relevant parameters determined for multiple realizations of the small scale heterogeneous permeability field (BSC 2004b, Section 6.4.2). While the ponding approach (BSC 2004b, Section 6.4.2) provides guidance on extrapolating seepage predictions to other units or drift geometries, this approach requires a calibration step similar to that performed for the seepage calibration model and offers no clear advantage over the selected modeling approach. Nevertheless, the concept that ponding probability affects seepage is consistent with and corroborates the two ambient seepage models, which produce random seepage locations as a result of local ponding in a stochastic permeability field (BSC 2004b, Section 6.4.2).

2.3.3.2.3.7.4   Inferring Seepage from Precipitates in Lithophysal Cavities

Observations of calcite and opal in lithophysal cavities have been evaluated to estimate water accumulation rates into these small openings (BSC 2004d, Section 7.7.5). Calcite precipitates from downward-percolating meteoric water because of (1) evaporation; (2) CO_2 outgassing as a result of the geothermal gradient; and (3) interaction with a gas phase containing less CO_2 than the gas with which the water was last equilibrated. Considering these calcite-precipitation mechanisms, and assuming water enters the cavities as seepage, the calcite-deposition data were used along with certain water-to-calcite ratios to estimate seepage rates into lithophysal cavities. The analysis of calcite and opal precipitation data shows that (1) not all lithophysal cavities encountered seepage; and (2) seepage flux derived from mineral deposits is a small fraction of estimated percolation flux (Marshall et al. 2003, Section 5; BSC 2004b, Section 6.4.3). Both conclusions corroborate the concept of a capillary barrier reducing seepage below the value of the percolation flux (BSC 2004b, Section 6.4.3).

The advantage of using geochemical information to infer seepage is the fact that calcite and opal were deposited over a long period of time, and therefore record natural percolation conditions. The disadvantages of this approach are that (1) seepage is inferred in an indirect manner, requiring a geochemical model with associated assumptions; (2) the calcite deposited on lithophysal cavity floors may not originate from seepage, because there is a lack of evidence of dripping from cavity ceilings (absence of stalactites or stalagmites), even where fractures containing coatings intersect lithophysae ceilings; (3) the data reflect seepage into small cavities, instead of into a large opening; (4) seepage into lithophysal cavities does not include potential impacts from the excavation-disturbed zone around the emplacement drift; and (5) the historic record and the approach are not easily translated into seepage predictions under changed conditions (BSC 2004b, Section 6.4.3).

The seepage rates estimated from calcite-deposition data are significantly lower than those predicted by the TSPA using data derived from the seepage model for performance assessment. Therefore, inferring seepage from secondary mineral depositions in lithophysal cavities was not selected to quantitatively estimate seepage into emplacement drifts (BSC 2004b, Section 6.4.3).

2.3.3.2.3.7.5   Inferring Seepage Threshold Directly from Liquid-Release Tests

The seepage threshold has been directly estimated from the liquid-release test data based on a number of assumptions with regard to a cross-sectional area of flux between the borehole and the niche ceiling, evaporation, and steady-state flow field (BSC 2004b, Section 6.4.4). Once the seepage threshold was estimated, a capillary strength parameter was derived assuming seepage into a cylindrical cavity excavated from a homogeneous porous medium. The seepage model for performance assessment that is discussed in Section 2.3.3.2.3.4.1 calculates a lower seepage threshold and potentially more seepage than that inferred directly from liquid-release tests; this model is, therefore, a more conservative approach (BSC 2004b, Section 6.4.4).

2.3.3.2.3.7.6   Alternative Flow Focusing Model

The flow focusing factor generated by the flow focusing model (Section 2.3.3.2.3.5) was determined for a gridblock width of 0.25 m. An alternative flow focusing model was developed in which the resulting flow focusing is averaged over 5-m-long sections (which approximates the emplacement drift diameter) at the bottom boundary (BSC 2004a, Section 6.9.2). The resulting distribution of flow focusing factors for 15 simulations was analyzed using the approach described in Section 2.3.3.2.3.5. Other parameters are identical to the flow focusing model selected for use (BSC 2004a, Section 6.9.2). The results show that 5 m averaged flow focusing factors range from 0.2 to 2.4 for the 15 simulations, indicating that it is less focused than the flow focusing obtained from a grid width of 0.25 m. Seepage calculations conducted in Abstraction of Drift Seepage (SNL 2007a, Sections 6.8.1 and 6.8.2) demonstrate that the flow focusing model selected for use in TSPA provides a more conservative estimate of flow focusing parameters with respect to seepage (SNL 2007a, Section 6.6.5.2.3).

2.3.3.2.3.8   Summary of Ambient Seepage Modeling

The modeling for determining seepage-relevant parameters and simulating seepage under ambient conditions is summarized as follows:

- The testing conducted within the drifts and niches (Section 2.3.3.2.2) provides the conceptual basis and sufficient data for the development, calibration, and validation of the ambient seepage models (BSC 2004b, Section 6.5).

- The estimation of effective seepage-relevant, model-related parameters on the scale of interest is an appropriate methodology, given that the framework of the seepage model for performance assessment is consistent with the seepage calibration model (BSC 2004b, Section 6.3; BSC 2004a, Section 6.3).

- The seepage model for performance assessment is used to calculate ambient seepage into intact and degraded emplacement drifts for combinations of the three key parameters (permeability, capillary strength, and local percolation flux), and for multiple realizations of the heterogeneous permeability field (BSC 2004a, Section 6.6). The seepage rates and their uncertainties resulting from these simulations are summarized in lookup tables that will be passed through the seepage abstraction for probabilistic sampling in the TSPA seepage calculations.

- Spatial variability of seepage-relevant parameters is examined using the available data. This variability is reflected in the probability distributions of the key seepage-relevant parameters used in the TSPA (SNL 2007a, Section 6.6).

- Uncertainties in calibration data are appropriately propagated through the seepage calibration model (BSC 2004b, Section 8.2). Conceptual model uncertainty and uncertainty in spatial variability are reflected in the probability distributions of the key seepage-relevant parameters used in the TSPA (SNL 2007a, Section 6.6).

- Uncertainty in the calculated seepage rate as a result of uncertainty in the small-scale properties has been quantified and is propagated to the TSPA drift seepage submodel component (SNL 2007a, Sections 6.6 and 6.8).

2.3.3.2.4   Ambient Component of Drift Seepage Abstraction
[NUREG-1804, Section 2.2.1.3.3: AC 4(1) to (4), AC 5]

The purpose of the ambient component of the drift seepage abstraction is to provide the necessary methodology, tools, parameter distributions, lookup tables, and simplifications to the TSPA, so that the ambient seepage calculations can be performed by the TSPA drift seepage submodel. Ambient seepage describes the evolution of seepage over most of the time period important for the performance assessment, except for the early postclosure stages when thermal perturbation is strong (Section 2.3.3.3). To develop an appropriate abstraction model for the TSPA, the drift seepage abstraction described in *Abstraction of Drift Seepage* (SNL 2007a) has assembled relevant input from various sources, and then synthesized and simplified this input into a coherent framework. Ambient seepage is calculated in the TSPA using a probabilistic approach that provides repository-wide seepage rates and their distributions, while accounting for the spatial and temporal variability and inherent uncertainty of seepage-relevant properties and processes. Various factors are important for predicting ambient seepage. The methodology of incorporating each of these factors, as described below, is directly based on the data and process-model discussion provided in the previous sections. As a result, the abstraction results (and thus the results of the TSPA drift seepage submodel) are consistent with the respective process model results—or, they provide appropriate upper bounds where they differ (SNL 2007a, Section 7). Confidence in the ambient seepage abstraction is also provided by the seepage calculations for the ESF South Ramp seepage event (Section 2.3.3.4.3), as well as by natural analogues for seepage processes (Section 2.3.3.5).

According to the drift seepage abstraction, the ambient seepage results derived from the seepage model for performance assessment provide the basis for the quantitative evaluation of seepage as a function of three key hydrologic properties (Section 2.3.3.2.3.4). These results are passed to the TSPA in the form of seepage lookup tables, so that a large number of realizations can be examined in probabilistic calculations. The key hydrologic parameters entering the lookup tables are the capillary strength and permeability in the drift vicinity, as well as the local percolation flux. For a given set of these parameters, the seepage rate and related estimation uncertainty are determined by linear interpolation between lookup table values (see below). Of importance in this process are the probabilistic distributions of the key hydrologic parameters that feed into the lookup tables. Appropriate distributions for these parameters have been developed that account for relevant processes, and describe their temporal and spatial variability and uncertainty (Section 2.3.3.2.3.6). Transient effects on ambient seepage are incorporated by using different percolation flux

distributions for the future climate stages. Transient changes in the other hydrologic properties—for example, from mechanical and chemical effects in response to thermal perturbation or drift degradation—need not be considered in the seepage calculation (Sections 2.3.3.2.1.4 and 2.3.3.3.3.4). The effects of rock bolts on the drift ceiling need not be explicitly addressed in the ambient seepage abstraction (Section 2.3.3.2.3.4.1). Ambient seepage, however, does depend on the considered scenario class. As mentioned before, different lookup tables have been developed to account for drift degradation in response to single or multiple seismic events. How the TSPA submodel chooses the appropriate seepage scenario for given degradation conditions is explained in Section 2.3.3.2.4.2. This section also describes the simple method for calculating seepage into magma-filled drifts after igneous intrusion (see below).

The general calculation procedure for ambient seepage as outlined above is the same for the pre-10,000-year period and the post-10,000-year period. Changes in the long-term climate are accounted for by using the appropriate percolation flux fields for the post-10,000-year climate (Section 2.3.3.2.3.5). The abstraction methodology also accounts for the fact that the probability of disruptive events occurring at Yucca Mountain increases with time, so that more and more drifts are expected to be severely degraded or fully collapsed (Section 2.3.3.4.2).

The most significant information passed from the drift seepage abstraction to the TSPA drift seepage submodel is discussed in more detail in the following sections.

2.3.3.2.4.1   Probability Distributions for Seepage-Relevant Parameters

The probability distributions for two of the three key parameters affecting seepage (i.e., capillary strength and permeability) are described in Section 2.3.3.2.3.6. For each location examined during each probabilistic TSPA realization, stochastic values for capillary strength and permeability are sampled from these distributions (SNL 2007a, Section 6.6). The capillary strength distributions are based on the values calibrated by the seepage calibration model, using seepage-rate data from liquid-release tests conducted in different locations along the ESF and ECRB Cross-Drift. The permeability distributions are mostly based on small-scale air permeability measurements conducted in boreholes drilled in close proximity above ESF niches. The effect of excavation on these properties is included in both parameter distributions. Probability distributions are provided separately for spatial variability and uncertainty, and, in case of fracture permeability, separately for the main repository units Tptpll and Tptpmn. As discussed in *Abstraction of Drift Seepage* (SNL 2007a, Section 6.6.4), the probability distributions for the Tptpll and Tptpmn can also be used for the Tptpul and Tptpln, where data from seepage experiments and small-scale air injection tests are not available.

As described in Section 2.3.3.2.3.5, the third key parameter affecting seepage—the local percolation flux arriving at repository drifts—is based on the large-scale percolation fluxes simulated by the site-scale unsaturated zone flow model (Section 2.3.2). These large-scale percolation fluxes are (1) spatially variable as a result of infiltration and rock properties variability; (2) time dependent due to changes in climate; and (3) have a probabilistic component due to the stochastic sampling from different infiltration scenarios (Section 2.3.3.2.3.6.3). To incorporate intermediate-scale heterogeneity, the large-scale percolation fluxes interpolated for a given repository location are multiplied by a stochastic sampled value taken from the distribution of flow focusing factors described in Section 2.3.3.2.3.5. While the large-scale distribution of percolation

fluxes is developed by the site-scale unsaturated zone flow model, the actual interpolated flux values at given repository locations are provided to the TSPA by the multiscale thermal-hydrologic model (SNL 2008b), to ensure consistency between seepage calculations and in-drift thermal-hydrologic calculations.

For each TSPA realization, the process described above provides a set of parameters for which seepage is evaluated. The respective probability distributions for capillary strength, permeability, percolation flux, and flow focusing factors are not correlated in the TSPA. These uncorrelated distributions mean that the stochastic variables used to sample from the respective distributions are generated independently (SNL 2007a, Sections 6.6 and 6.7).

2.3.3.2.4.2   Ambient Seepage for Different Scenario Classes

Conditions in the unsaturated zone and within the repository depend on location and may change with time. They are also impacted by the effects of disruptive events; specifically, seismic events (Section 2.3.4) and igneous intrusions (Section 2.3.11). As part of the drift seepage abstraction, a methodology was developed to represent emplacement drift seepage for disruptive event scenarios (SNL 2007a, Sections 6.5, 6.7, and 6.2[a]). There is no specific methodology for early failure events (early failure of drip shields or waste packages), because the seepage conditions are not affected by these changes in the EBS (SNL 2008a, Section 6.3.3.1.2).

2.3.3.2.4.2.1   Ambient Seepage for the Nominal Scenario

The drift seepage abstraction for the nominal scenario applies to all emplacement drift segments that are (1) below the boiling temperature of water (Section 2.3.3.3); (2) not affected by a seismic event; and (3) not affected by an igneous event. In this case, seepage rates and uncertainties are calculated from the seepage lookup table for intact drifts described in Section 2.3.3.2.3.4 (SNL 2007a, Section 6.4.2; BSC 2004a). To account for increased estimation uncertainty due to moderate drift shape changes—for example from isolated rockfall unrelated to seismic events—the calculated seepage rates for intact drifts are increased by 20% based on a probabilistic sensitivity calculation (SNL 2007a, Section 6.5.1.5).

2.3.3.2.4.2.2   Ambient Seepage for Seismic Scenarios

Emplacement drifts may partially or completely collapse as a result of seismic events (Section 2.3.4). The degree of drift degradation depends on the geologic unit and the rock properties, as well as on the magnitude and occurrence probability of seismic events.

Drifts in Nonlithophysal Rock—In nonlithophysal rock units, the damage to drifts from seismic events will be mostly limited to local gravitational drop of rock blocks (wedge type rockfall), even for large seismic events (Section 2.3.3.2.1.4). As long as the number of local breakouts from rockfall is small, such cases are handled in the same manner as discussed above for the nominal scenario, where the seepage rates obtained from the intact-drift lookup table are increased by 20% to account for estimation uncertainty due to moderate drift shape changes (Section 2.3.3.2.3.4.2). If, on the other hand, seismic events cause significant degradation with local breakouts at several locations and multiple topographic lows at the roof, the predictions from the intact-drift lookup table cannot be used because the capillary barrier capability can be significantly diminished

(Figure 2.3.3-28). In this case, the seepage rates are set equal to an upper-bound value given by the local percolation flux arriving at the drift (i.e., the seepage percentage is set to 100%). As explained in Section 2.3.3.2.4.1, the local percolation flux is based on the large-scale percolation fluxes simulated by the site-scale unsaturated zone flow model, multiplied by a stochastic sampled value taken from the distribution of flow focusing factors.

As described in *Abstraction of Drift Seepage* (SNL 2007a, Section 6.2.3[a]), the drift seepage conditions at any given time are categorized by assessing the rockfall volume that has accumulated in response to the multiple seismic events considered to occur up to this point in time. The rockfall volume, in turn, is linked to the magnitude of a seismic event by rocktype-specific regression functions given in *Seismic Consequence Abstraction* (SNL 2007e, Section 6.7.2.3), while the rockfall volume from multiple seismic events is calculated as the sum of the rockfall volumes from individual events. (This procedure is consistent with Section 2.3.4, where the cumulative rockfall volume is used to evaluate the potential mechanical damage to the drip shield or the waste package.) The rock-type specific regression functions describe the mean rockfall volume, as well as the possible variation of rockfall volumes caused by the spread between different drift degradation realizations. Based on the visual inspection of simulated drift shapes (BSC 2004e), a threshold rockfall volume of 0.5 m^3 per meter drift length is defined for nonlithophysal rocks (SNL 2007a, Section 6.2.3[a]). If the cumulative volume in a given drift section at a given time is smaller than this threshold, seepage is handled in the TSPA in the same manner as discussed above for the nominal scenario. If this threshold is exceeded, seepage is set equal to the local percolation flux arriving at the drift.

Details on the procedure for determining the threshold rockfall volume of 0.5 m³/m drift length are given in *Abstraction of Drift Seepage* (SNL 2007a, Section 6.2.3[a]); a brief explanation is given below. Results from a three-dimensional discontinuum analysis of seismically-induced rockfall in 25-m-long drift sections were used to plot footprints of the fallen rocks (BSC 2004e, Section 6.3). (See three-dimensional visualizations for selected cases in *Drift Degradation Analysis* (BSC 2004e, Figures 6-89 and 6-90)). More than 60 geomechanical simulation cases (representing different seismic events and different rock strength categories) were evaluated, with focus on the abundance of topographic lows created by the fallen rock blocks. The different cases were grouped into four classes of rockfall severity, ranging from cases with isolated rockfall and no impact on seepage (Severity Class 1) to cases with numerous topographic lows and potentially strong impact on seepage (Severity Class 4). The severity classes were defined as follows:

- **Class 1: Few dispersed small rock blocks have dislodged**—Rockfall masses are so dispersed that no topographic lows form. The intact-drift seepage model results are applicable.

- **Class 2: Few large or several small blocks have dislodged away from crown**—Some localized concentration of rockfall exists. However, if some topographic lows form, these are mainly on the sides. Therefore, the intact-drift seepage model results can be used.

- **Class 3: Few large or several small blocks have dislodged along the crown**—Some topographic lows form near the crown of the drift. Therefore, the intact-drift seepage model results may not be applicable in parts of the drift.

- **Class 4: Several large and many medium/small blocks have dislodged along the crown**—Significant rockfall has occurred and numerous topographic lows exist in most parts of the crown. Therefore, the intact-drift seepage model results are not applicable for most parts of the drift.

Figure 2.3.3-29 shows examples of drift footprints representative of the four categories. As illustrated, the drift footprint in Class 4 (Figure 2.3.3-29 (4)) shows significant rockfall and numerous topographic lows in most parts of the drift crown; the predictions from the intact-drift lookup table are clearly not applicable here. In contrast, the impact of rockfall on seepage is minimal for Classes 1 and 2 (Figure 2.3.3-29 (1) and (2)) because there are only a few localized rockfall occurrences, and the intact-drift seepage model results can be applied. Cases with Severity Class 3 show intermediate rockfall suggesting that the intact-drift model results may not be applicable in parts of the drift (Figure 2.3.3-29 (3)).

To allow determining severity of rockfall based on rockfall volume, a correlation between the severity class and the simulated volume of rockfall was developed using results from all geomechanical rockfall simulation cases (SNL 2007a, Section 6.2.3[a]). In Table 2.3.3-3, the mean, median, as well as the 5th and 95th percentiles of rockfall volumes (per unit drift length) are given for the four classes. The threshold value of 0.5 m^3/m was chosen based on the rockfall statistics for Severity Class 4, using the lower bound (5th percentile) rockfall volume of all simulation cases in this class to determine whether the intact-drift seepage results can be used in a given case or not (SNL 2007a, Section 6.2.3.1[a]). This threshold value ensures that the more severe of the cases in Class 3 (i.e., those with rockfall volume slightly larger than the mean of this class) are considered to have too many topographic lows to allow the use of the intact-drift seepage model.

Drifts in Lithophysal Rock—In lithophysal rock units, seismic events with large PGVs will lead to complete collapse of emplacement drifts, with rubble rock material filling the enlarged opening. For other seismic events with smaller PGVs, the extent of drift damage in lithophysal rocks is expected to be less significant, ranging from partial drift collapse for low strength rock to minor damage for all other rock-strength categories. A series of smaller seismic events over time, on the other hand, may lead to complete collapse even if individual events are not strong enough to cause severe damage.

Two different drift seepage conditions are considered for drifts in lithophysal rocks. All cases with minor damage and moderate drift shape changes are handled in the same manner as discussed above for the nominal scenario (SNL 2007a, Section 6.5.1.5). The seepage rates obtained from the intact-drift lookup table are increased by 20% to account for estimation uncertainty due to moderate drift degradation. In all other cases, seepage is calculated using the lookup table for complete drift collapse, or using both look-up tables, as explained in more detail below. While seepage into collapsed drifts is expected to be higher than seepage into intact drifts, most of the percolation flux is diverted around the tunnel openings in both cases (Section 2.3.3.2.3.4.2).

In a process similar to the nonlithophysal rocks, the drift seepage conditions at any given time are categorized by assessing the rockfall volume that has accumulated in response to a series of seismic events. As above, the rockfall volumes corresponding to a given seismic event, as well as their variability and uncertainty range, can be determined by rock-type specific regression functions (SNL 2007e, Section 6.7.1.2), and rockfall volumes from individual events can be added up to account for the seismic history. Threshold volumes are again defined based on the visual inspection of simulated drift shapes. Drifts are considered intact or moderately degraded in the seepage calculation if the cumulative volume is smaller than 5 m^3 per meter drift length (i.e., in this case, seepage is handled in the TSPA in the same manner as discussed above for the nominal scenario) (SNL 2007a, Section 6.2.2.1[a]). Drifts are considered fully collapsed if the cumulative rockfall volume is larger than 60 m^3 per meter drift length (SNL 2007a, Section 6.2.2.1[a]). In intermediate cases with partial collapse, seepage is determined from a linear interpolation between the results obtained for the nominal scenario and those obtained for fully collapsed drifts, using the cumulative rockfall volume as the interpolation parameter (SNL 2007a, Section 6.2.2.1[a]). This interpolation procedure affects not only the seepage rates, but also the seepage fraction, because overall a different number of drift segments will arrive at seepage conditions.

Details on the procedure of determining the above threshold volumes and the interpolation approach are given in *Abstraction of Drift Seepage* (SNL 2007a, Section 6.2.2[a]); a brief explanation is given below. For three levels of horizontal PGVs, namely 0.4 m/s, 1.05 m/s, and 2.44 m/s, a total number of 15 different realizations (cases) were considered in the drift degradation simulations for lithophysal rock (SNL 2007e, Table 6-28). The 15 cases have the same horizontal PGV, but differ with respect to other seismic characteristics, such as the vertical PGV. A list of these ground motion characteristics is given in Tables X-1 through X-5 of *Drift Degradation Analysis* (BSC 2004e). The 15 cases also use different rock mass categories to represent the variability of geotechnical rock mass quality throughout the repository, ranging from Category 1 (poor quality) to Category 5 (high quality) (SNL 2007e, Section 6.7.1.1). Results from the different drift degradation simulations are listed in Table 2.3.3-4, where the observed rockfall volume for each case is given per drift length, and in Figures 2.3.3-30 through 2.3.3-32, where the corresponding drift profiles are depicted. Overall, the rockfall volumes in lithophysal units (where partial or full collapse is quite common for large PGV levels and low-quality rock) are larger than in nonlithophysal units (with wedge-type rockfall rather than full collapse).

As discussed in SNL (2007a, Section 6.2.2[a]), visual inspection of the 15 profiles developed for the 0.4-m/s PGV seismic event suggests that all drifts remain essentially intact and very similar to their original shape (Figure 2.3.3-30). These drift shapes can be represented in TSPA using the seepage lookup table for intact drifts. Rockfall volumes are typically a few cubic meters per meter drift length or less. The one exception is Case 11 (low-quality rock and relatively strong ground motion), where over 7 m^3/m rockfall is predicted, generating a wider drift with an asymmetric roof. Furthermore, all profiles obtained for the severe 2.44-m/s PGV seismic event result in complete drift collapse, with large rubble-filled openings and circular to parabolic shape (Figure 2.3.3-32). These drift shapes need to be represented in TSPA using the seepage lookup table for collapsed drifts. Rockfall volumes range from about 60 m^3/m to more than 110 m^3/m.

At the intermediate 1.05-m/s PGV level, the degradation results show a range from minor collapse (no relevant changes in drift width and shape) to partial collapse (larger width and relevant drift shape changes) (Figure 2.3.3-31). From visual inspection, the intact-drift lookup table can be used

for the cases with minor collapse (such as Cases 1, 3, 5, 6, 8, 9, 12, 13). All other realizations, such as Cases 2, 4, 7, 10, 11, 14, and 15, are intermediate cases, for which seepage results would be larger than those calculated from the intact-drift lookup table, but smaller than those calculated from the collapsed drift lookup table. Since no seepage simulations are available for such moderately degraded drifts, these cases need to be categorized as either intact or fully collapsed, or an interpolation needs to be conducted between seepage results for intact and collapsed drifts. Categorization as intact would mean underestimating seepage, which is nonconservative with respect to dose. Categorization as fully collapsed would mean overestimating seepage, which is conservative with respect to dose, but not necessarily realistic. Therefore, linear interpolation between the seepage results for intact and collapsed drifts is the method used in the TSPA drift seepage submodel.

Comparison of the drift shapes in Figures 2.3.3-30 through 2.3.3-32 with the rockfall volumes in Table 2.3.3-4 suggests a good correlation between the magnitude of rockfall and the drift degradation impact on seepage. It is thus reasonable to use the rockfall volume as the key parameter for the categorization of drifts and the selection of seepage lookup tables in TSPA. The above defined rockfall threshold volumes were determined based on this correlation. All rockfall volumes smaller than 5 m^3/m correspond to minor degradation, in which case drifts can be considered intact for the seepage calculation. All rockfall volumes larger than 60 m^3/m correspond to complete drift collapse, in which case drifts can be considered fully collapsed for the seepage calculation. All rockfall volumes between 5 and 60 m^3/m correspond to intermediate cases with partial collapse, where seepage is to be determined from linear interpolation.

2.3.3.2.4.2.3   Seepage for an Intruded Drift (Igneous Scenario)

If a dike intersects an emplacement drift during an igneous event, magma will fill the drift and solidify as it cools (Section 2.3.11) (Table 2.3.3-1, FEP 1.2.04.03.0A, Igneous Intrusion into Repository). Once the interface at the drift wall drops below 100°C, liquid water will be able to enter the drift and travel through the cooled magma (Section 2.3.11.1). Given the uncertainties in modeling seepage under these conditions, the drift seepage abstraction conservatively sets the seepage flux for an intruded drift equal to the local percolation flux. This treatment assumes undisturbed flow fields in the vicinity and through the intruded drift after the drifts return to temperatures below the boiling point of water (i.e., no capillary barrier at the interface between the cooled magma and the surrounding tuff, and no difference in hydrologic properties) (Section 2.3.11.1).

2.3.3.2.4.2.4   Seepage During Preclosure Period

Seepage in ventilated drifts in units below the PTn unit is not expected. As discussed in Section 2.3.3.2.2.3.2, the South Ramp seepage event is the first unambiguous evidence of seepage under ambient conditions (SNL 2007a, Section 7.1.1[a]). However, the location of this event is not overlain by bedded or nonwelded tuffs such as the PTn. No unambiguous evidence of dripping from natural percolation water has ever been observed in the ventilated sections of the ESF and the ECRB Cross-Drift below the PTn. Therefore, in the TSPA, seepage is not considered to occur during the preclosure period while forced ventilation is in operation in the emplacement drifts (Section 2.3.3.2.2.2.2).

2.3.3.2.4.3   Ambient Seepage Lookup Tables

Lookup tables of ambient seepage rates are passed to the TSPA drift seepage submodel for both intact and fully collapsed drifts. These lookup tables are based on the systematic seepage simulations performed with the seepage model for performance assessment, which produces precalculated seepage rates and associated uncertainty for these two cases over a large parameter range (BSC 2004a, Sections 6.6.1 and 6.6.3). To ensure that the parameter range encompasses the parameter variation in the TSPA drift seepage submodel, the local percolation flux values have been increased further by calculations conducted in *Abstraction of Drift Seepage* (SNL 2007a, Section 6.1[a]). Both lookup tables provide values for mean seepage and the associated standard deviation on account of estimation uncertainty (Section 2.3.3.2.3.6.4). The seepage rate evaluated by the TSPA for a given scenario and parameter set is taken to be the mean seepage rate (interpolated from the respective lookup table), perturbed by a stochastic value that is sampled from the uncertainty distribution provided by the corresponding standard deviation (SNL 2007a, Section 6.5.1). As mentioned above, this final value is increased by 20% in all cases where the intact-drift lookup table is used.

2.3.3.3   Thermal Seepage
            [NUREG-1804, Section 2.2.1.3.3.3: AC 1(1) to (5), (7) to (9), AC 2(1) to (3), AC 3(1) to (4), AC 4(1) to (4), AC 5; Section 2.2.1.3.6.3: AC 1(6)]

Thermal seepage refers to seepage into drifts during the time period when flow and transport processes in the near-field rock are perturbed by the heat emanating from the waste. Thermal seepage processes have been analyzed using the thermal-hydrologic seepage model (BSC 2005a). This model predicts the thermally-driven coupled processes in the drift vicinity—including moisture redistribution from boiling and condensation of pore water—and evaluates the combined effect of two different processes that can prevent seepage at elevated conditions: (1) flow diversion as a result of capillary forces, which is effective at all temperature ranges; and (2) flow diversion as a result of pore water vaporization, which is effective only if boiling temperatures prevail in the rock. As described below, the thermal-hydrologic seepage model is applied to selected simulation cases varying a range of parameters important for thermal seepage (e.g., thermal-operating mode, local percolation flux, and seepage-relevant rock properties). For implementation in the TSPA, the transient thermal seepage results (as obtained from the model) are then compared to ambient seepage simulations for the same set of conditions and properties, but without the heat input, with the goal of qualitatively describing the evolution of thermal seepage in comparison to the ambient seepage rates.

Section 2.3.3.3.1 (below) provides a conceptual description of the thermal-hydrologic processes governing flow and seepage after repository closure. This discussion builds on the understanding of ambient hydrologic processes in the fractured TSw units surrounding the emplacement drifts (Section 2.3.3.2), and describes the added thermal-hydrologic effects due to heat from radioactive decay. The data and data uncertainty section (Section 2.3.3.3.2) presents in situ thermal tests, especially the Drift Scale Test, used to obtain site-specific data and their associated uncertainties. The model and model uncertainty section discusses the thermal-hydrologic seepage model as well as results, uncertainties, and model support activities (Section 2.3.3.3.3). The thermal component of the drift seepage abstraction is presented in Section 2.3.3.3.4.

2.3.3.3.1   Conceptual Description of Thermal-Hydrologic Processes
[NUREG-1804, Section 2.2.1.3.3.3: AC 1(1) to (5), (7) to (9)]

The heat generated by the decay of the radioactive waste results in rock temperatures elevated from ambient for a few thousand years after emplacement (Section 2.3.5). During the first few hundred years after closure, these temperatures will be high enough to cause boiling conditions in the drift vicinity, giving rise to local water redistribution and altered flow paths (BSC 2005a, Sections 6.1 and 6.2). Thermal expansion of the rock matrix induces thermal stresses and associated changes in flow properties near emplacement drifts (thermal-hydrologic-mechanical effects) (BSC 2004g, Sections 6.1 and 6.2). Thermally driven effects also cause dissolution and precipitation of minerals, which may affect flow properties (thermal-hydrologic-chemical effects) (SNL 2007f). Thermal-hydrologic-mechanical and thermal-hydrologic-chemical processes and their effects on seepage are discussed in Section 2.3.3.3.3.4 (Excluded FEPs 2.1.09.12.0A, Rind (chemically altered zone) forms in the near field; 2.2.01.02.0A, Thermally-induced stress changes in the near field; and 2.2.10.04.0A, Thermo-mechanical stresses alter characteristics of fractures near repository, in Section 2.2, Table 2.2-5).

The major thermal-hydrologic processes occurring around an emplacement drift are shown in Figure 2.3.3-33 for an idealized, circular drift. As shown in this figure, heating of the rock causes pore water in the rock matrix to boil and vaporize. The vapor moves away from the boiling location through the permeable fracture network, driven primarily by the pressure increase caused by boiling. Vapor will either flow into the open drifts or will flow away from the drifts, and further into the near-field rock. Vapor that remains in the near-field rock will condense in the rock fractures once it reaches cooler regions away from the drift. The condensate can then drain either toward the heat source (from above) or away from the drift into the zone below the heat source. Condensed water can also imbibe from fractures into the matrix, leading to increased liquid saturation in the rock matrix. A dryout zone develops around the drift, separated from the zone of condensation by a nearly isothermal zone maintained nominally at the boiling temperature of water (Table 2.3.3-1, FEPs 2.2.07.10.0A, Condensation zone forms around drifts; and 2.2.10.12.0A, Geosphere dryout due to waste heat). This nearly isothermal zone is characterized by a collection of the following processes that are referred to as a heat pipe signature: continuous boiling, vapor transport, condensation, and migration of water back toward the heat source resulting from capillary forces or gravity drainage (BSC 2005a, Sections 6.1 and 6.2; Pruess et al. 1990) (Table 2.3.3-1, FEP 2.2.10.10.0A, Two-phase buoyant flow/heat pipes). At later stages, with the heat output of the waste continuously decreasing, rock temperatures drop below boiling, the dryout zone resaturates, and the conditions in the drift vicinity slowly return to a long-term ambient status (Table 2.3.3-1, FEPs 2.1.08.11.0A, Repository resaturation due to waste cooling; and 2.2.07.11.0A, Resaturation of geosphere dryout zone).

The heating of near-field rock to the boiling temperature of water and the resulting flow perturbation affects the potential for seepage. Condensed water forms a zone of sightly elevated water saturation in the fractures above the dryout zone. Water from this zone may be mobilized to flow rapidly down towards the drift. However, seepage would only be possible if both the vaporization barrier in the boiling zone and the capillary barrier at the drift ceiling would be breached. Results from the thermal-hydrologic seepage model demonstrate that this scenario is not expected (Section 2.3.3.3.3.1).

As mentioned above, part of the vapor produced from boiling of pore water will flow into the open drifts, where it is subject to natural-convection transport along the drift axis and possible condensation on drift walls. These processes are included in the TSPA drift-wall condensation submodel that is described in Section 2.3.5.4.2, and are based on the prediction of condensation rates provided by the *In-Drift Natural Convection and Condensation* model (SNL 2007g).

Emplacement drifts may collapse as a result of low-probability seismic events (Section 2.3.4). The thermal conditions in a collapsed emplacement drift are different from those in an intact emplacement drift, because the properties of the rubble are different from those of the intact host rock in an open, air-filled drift. The extent to which these differences impact seepage under thermally elevated conditions is governed by the time at which significant drift collapse occurs. The abstraction of seepage for drift collapse cases during the thermal period of repository performance is described in Section 2.3.3.3.4, based on thermal-hydrologic modeling of rubble-filled collapsed drifts (SNL 2007a, Sections 6.4.3.4 and 6.5.3).

The impact of repository heat on the hydrologic, chemical, and mechanical conditions was examined using heater experiments, which included the Large Block Test, the Single Heater Test, and the Drift Scale Test. A short description of these tests is presented in Section 2.3.3.3.2.

2.3.3.3.2 Data and Data Uncertainty
[NUREG-1804, Section 2.2.1.3.3.3: AC 2(1) to (3), AC 3(1) to (4)]

This section describes the data from field tests and laboratory experiments that support the development of process models for thermal seepage and other coupled processes. Uncertainties in these data are also discussed. A primary data source for providing relevant rock properties, as well as measured data on the thermal-hydrologic response of the rock, are the three in situ field thermal tests that have been conducted at Yucca Mountain: the Large Block Test, the Single Heater Test, and the Drift Scale Test. The Large Block Test was conducted in a block of fractured rock excavated from an outcrop of the Tptpmn unit at the ground surface just southeast of Yucca Mountain. Both the Single Heater Test and the Drift Scale Test were performed underground within the Tptpmn subunit at the repository level (SNL 2007d, Section 6). While the Single Heater Test incorporated relatively small heated rock volume, with a 5-m long heater placed into a horizontal borehole in a side alcove of the ESF, the Drift Scale Test was much larger in size, with an approximately 50-m long drift segment heated by 9 floor-canister heaters as well as 50 borehole heaters. Of the three heater tests, the Drift Scale Test is the best suited for model validation against measured data, because of the wealth of measured data available from this test, and because its geometric setup and scale are most similar to the design of the emplacement drifts. The Drift Scale Test is therefore the main test used for model support, as discussed below. In addition to the thermal tests, which provided data only on the Tptpmn unit, thermal rock properties have been measured in the laboratory using cores taken from surface-based boreholes.

The Large Block Test and the Single Heater Test were used to evaluate thermal-hydrologic modeling concepts and to plan the more detailed and long-duration Drift Scale Test. For example, the measured response of the Large Block Test to a transient water influx event—caused by strong rainfall onto the outcrop—was compared against the simulated response (Mukhopadhyay and Tsang 2002) using a process model similar to the thermal-hydrologic seepage model, thereby providing confidence that processes controlling thermal-hydrologic seepage are adequately

accounted for in the thermal-hydrologic seepage model (Mukhopadhyay and Tsang 2002; SNL 2007d, Section 6.1). Comparison of measured data and model results for the Single Heater Test also showed good agreement (Tsang and Birkholzer 1999).

The Drift Scale Test provides the bulk of the data used to evaluate the evolution of temperature, liquid saturation, and the thermally induced liquid refluxing, all of which potentially affect seepage into drifts. Although surface and underground thermal tests were all conducted in the Tptpmn unit, experience in coupled processes testing and modeling of subsurface systems shows that the results provide the basis for coupled processes modeling of other repository horizon units, provided that appropriate thermal properties are assigned to each unit (BSC 2005a, Section 7.1.3).

The purpose of the Drift Scale Test was to evaluate the coupled thermal, hydrologic, chemical, and mechanical processes that result from heating within emplacement drifts at an intermediate scale. The Drift Scale Test was conducted in Alcove 5, which is approximately 50 m in length and 5 m in diameter. Alcove 5 was excavated off the main ESF drift (Figure 2.3.3-34) within the Tptpmn unit (SNL 2007d, Section 6.3; BSC 2005a, Section 7.2). Nine electrical floor-canister heaters were placed in this drift section to simulate radioactive-waste-bearing containers. Electrical heaters were also placed in a series of horizontal boreholes (wing heaters) that were drilled perpendicularly outward from the central axis to both sides of the drift. These heaters were emplaced to simulate the effect of adjacent emplacement drifts. The Drift Scale Test heaters were activated on December 3, 1997. The temperature was continuously monitored during the heating, and neutron logs, electrical resistivity tomography, and cross-hole ground-penetrating radar tomography were performed to track changes in matrix liquid saturation. Several air injection tests were conducted in hydrology boreholes to track changes in fracture permeability and fracture liquid saturation (SNL 2007d, Section 6.3.2.4; BSC 2005a, Section 7.2.2). Monitoring and testing were also conducted to support investigation of thermal-hydrologic-chemical and thermal-hydrologic-mechanical processes (Section 2.3.5). After just over 4 years, on January 14, 2002, the heaters were switched off, and, since that time, the test area has been slowly cooling. Figure 2.3.3-34 shows a schematic view of the test layout with the main heater tunnel, the wing heaters, and the array of observation boreholes monitoring temperature, as well as chemical, mechanical, and hydrologic variables. Data on the evolution of temperature, liquid saturation, and permeability (SNL 2007d, Sections 6.3.1 and 6.3.2; CRWMS M&O 1998) are used to support the development of the thermal-hydrologic seepage model, as discussed in Section 2.3.3.3.3.2.

The impact of uncertainty and variability in these data, from both in situ tests as well as from core measurements, has been evaluated by conducting comprehensive sensitivity analyses with the thermal-hydrologic seepage model (BSC 2005a, Section 8). Uncertain and spatially variable model input parameters are the rock properties and the model boundary conditions, which have been varied in wide ranges to represent the potential parameter variation in the field. Sensitivity to all parameters relevant for thermal seepage was explicitly studied by (1) modeling two host rock units with different thermal and hydrologic properties (Tptpmn and Tptpll); (2) varying the fracture capillary strength parameter; (3) analyzing percolation scenarios with different flux multiplication factors; (4) changing host rock thermal conductivities and fracture permeabilities; and (5) simulating several different thermal loads. In all these cases, covering a wide range of property values and conditions, the main conclusions regarding thermal seepage were similar—in that no seepage (flow of liquid water into drifts) is predicted to occur during the period when temperatures in the rock are above the boiling temperature of water—and that thermal seepage is always less in magnitude

compared to the respective long-term ambient values (Section 2.3.3.3.3). As explained below, the thermal component of the drift seepage abstraction is a qualitative element that uses these main conclusions about the magnitude and evolution of thermal seepage. Since these conclusions are valid over the required range of conditions and parameter values used in the TSPA, uncertainty and variability in these data are intrinsically accounted for.

2.3.3.3.3   Model and Model Uncertainty
[NUREG-1804, Section 2.2.1.3.3.3: AC 3(1) to (4), AC 4(1) to (4), AC 5; Section 2.2.1.3.6.3: AC 1(6)]

The main process model for predicting the effect of heat on seepage is the thermal-hydrologic seepage model that is explained below (BSC 2005a). While incorporating some specific data and methods adopted from the modeling framework that was developed for ambient seepage, this model uses a conceptual approach for thermal-hydrologic processes that is consistent with the drift-scale models that describe coupled thermal-hydrologic-chemical (SNL 2007f; SNL 2007h) and thermal-hydrologic-mechanical (BSC 2004g) processes (Section 2.3.3.3.3). The basic model approach is also consistent with the multiscale thermal-hydrologic model (SNL 2008b), which describes mountain-scale and drift-scale temperature effects on in-drift thermal-hydrologic conditions for use in the TSPA. This latter model is discussed in Section 2.3.5. In contrast to the thermal-hydrologic seepage model, the multiscale thermal-hydrologic model was not specifically designed to capture seepage processes; therefore, the modeling framework developed for ambient seepage was not explicitly incorporated into the multiscale thermal-hydrologic model (which would require, for example, representing the small-scale heterogeneity in fracture permeability or using the calibrated effective fracture capillary-strength parameters).

2.3.3.3.3.1   Thermal-Hydrologic Seepage Model

The thermal-hydrologic seepage model evaluates coupled thermal-hydrologic processes and their impact on seepage (BSC 2005a, Section 6.2). This drift-scale model combines the two processes that prevent seepage into drifts at elevated temperatures: (1) capillary diversion, which is effective over the entire temperature range expected at Yucca Mountain; and (2) vaporization due to heat, which is effective while temperature is elevated above the boiling point of water. Besides incorporating the conceptual framework for ambient seepage, the thermal-hydrologic seepage model accounts for mass and energy transport processes, including the movement of both gaseous and liquid phases, transport of latent and sensible heat, phase transition between liquid and vapor, and vapor pressure lowering. The fractured rock is treated as a dual-permeability domain, accounting for the fractures and the rock matrix as two separate, overlapping continua. Similar to the ambient seepage models, a stochastic continuum model is implemented for fractures near the drift to consider the small-scale variability of permeability that accounts for flow channeling. The capillary strength parameter close to the drift wall was derived from the seepage calibration model by calibrating against ambient seepage rate data (Section 2.3.3.2.3.3) (BSC 2004b, Section 6.6.3; BSC 2005a, Section 6.2.1).

A key question relating to thermal seepage during the period above boiling temperature of water is whether water percolating down the fractures will boil off in the rock region above the drifts, or may penetrate all the way to the drift walls and, possibly, seep into the open cavities. Prediction of this behavior requires an understanding of small-scale flow channeling, because rapid preferential flow

is more likely to penetrate into the superheated rock zone. In addition to explicitly representing the small-scale heterogeneity in fracture permeability, the active fracture concept (BSC 2004c, Section 6.3.7) is applied in the thermal seepage predictions to account for the fact that unsaturated flow is restricted to a limited number of (active) fractures, and that flow within a fracture is likely to occur in individual fingers rather than in the entire fracture plane. A comparison study indicated that the thermal seepage rates simulated using the active fracture concept were slightly higher than those obtained with a standard dual permeability model (BSC 2005a, Sections 6.2.2.2 and 6.2.4.2). Another specific model choice was made with respect to the heat that can be conducted between the matrix rock and the fractures. When flow in the fractures occurs in individual fingers, the interface area available for heat flow from the matrix to the liquid water is much less than the full geometric contact area between fractures and matrix (Birkholzer and Zhang 2006). This effect is accounted for in the thermal-hydrologic seepage model by a significant reduction in the effectiveness of heat transfer from the matrix to the liquid flow in the fractures (BSC 2005a, Section 6.2.1.1.2).

Thermal seepage simulations were conducted for the two main repository host units (Tptpmn and Tptpll), and for a wide range of conditions and rock properties covering the expected variability and uncertainty in seepage-relevant factors. For example, four different thermal loads were analyzed to account for temperature variability arising from heat-output variation among waste packages, emplacement-time differences among repository sections, three-dimensional edge effects, and variation in thermal properties (SNL 2008b). The maximum rock temperatures in these cases ranged from as high as 150°C to a case that remains below boiling conditions at all times. Other factors in sensitivity studies were permeability, capillary strength, thermal conductivity, conceptual models for fracture–matrix interaction, and the local percolation flux arriving at emplacement drifts.

As explained in Section 2.3.3.2.3.5, the local percolation fluxes can vary considerably in space and will be affected by future climate changes. The thermal-hydrologic seepage model accounts for this spatial and temporal variation with appropriate flux boundary conditions at the top of the model domain. Consistent with the future climate analyses for the Yucca Mountain (Section 2.3.1), the model considers three long-term climate states during the period of thermal perturbation: the present-day climate, the monsoon climate, and the glacial transition climate. One flux scenario was simulated using percolation fluxes of 6, 16, and 25 mm/yr, respectively, for these three periods (BSC 2005a, Section 6.2.1), which is about twice as high as the average fluxes given for the most likely infiltration scenario (Section 2.3.2.4.1.2.4.2). Additional flux scenarios have been studied to cover the possible upper range of local percolation fluxes within the repository units. These scenarios were defined by multiplying the boundary fluxes of the first case, using constant flow focusing factors of 5, 10, or 20. These large factors were chosen because the relevant cases for ambient and thermal seepage to occur are cases where the percolation flux is comparably high.

The transient simulations with the thermal-hydrologic seepage model were conducted in a two-dimensional cross section extending from the ground surface to the water table (Figure 2.3.3-35). Because of the two-dimensionality, the emplacement drift in the center of the domain needed to be treated as a closed system without axial flow and transport components. The model therefore does not address the effect of natural-convection vapor transport along the drift. It was shown in related studies (Section 2.3.5.4.2; SNL 2008b, Section 7.5; Birkholzer et al. 2006) that natural convection causes the transport of vapor-rich gases from the heated emplacement sections towards the cooler drift end sections, where the vapor condenses and drains off into

underlying rock formations. As a result, a considerable fraction of the moisture in the formation is effectively removed from the heated rock mass through evaporation into and transport along the open drifts. The two-dimensional thermal seepage model, in contrast, predicts that the majority of the vapor produced from boiling/evaporation of formation water remains in the fractured rock, which is a conservative treatment with respect to thermal seepage (Birkholzer et al. 2006).

The thermal-hydrologic seepage model simulates the flow and transport processes near the drift during repository heating and cooling, and explicitly calculates transient seepage rates into the drift under elevated temperature conditions for a simulation period of 4,000 years after waste emplacement. This is the period when the main flow perturbations are expected as a result of repository heat (SNL 2007a, Section 6.4.3.3). After this period, thermal-hydrologic effects on calculated seepage are small and can be approximated by ambient seepage models (SNL 2007a, Section 6.5.2). The simulation results from the thermal-hydrologic seepage model that are relevant to drift seepage abstraction are discussed below.

Thermal-hydrologic conditions are strongly driven by the thermal load placed into the emplacement drifts, and by the local percolation flux. For the case with an average thermal load (representative of a drift in the center of the repository), the heat generated from the waste packages results in maximum rock temperatures at the emplacement drift wall between 120°C and 140°C, depending on the hydrogeologic unit and the amount of percolation considered. In this case, the period during which rock temperature is above the boiling point of water is about 1,000 years for the base-case flux scenario. The rock temperature at the end of the 4,000 year thermal period decreased to about 65°C. Greater percolation flux leads to cooler temperatures and a shorter boiling period with stronger heat pipe processes (liquid–vapor counterflow in the boiling-temperature zone). These calculated results from the thermal-hydrologic seepage model are consistent with the thermal-hydrologic results obtained with the two-dimensional thermal-hydrologic submodels used in the multiscale thermal-hydrologic model that is described in Section 2.3.5 (SNL 2008b, Sections 6.2.2, 6.2.3, and 6.2.4; SNL 2007a, Section 6.4.3).

Seepage under thermal conditions is possible only when two conditions are met simultaneously: (1) water arrives at the drift wall; and (2) the water potential at the drift wall exceeds a given threshold value that depends on capillary forces. The modeling results consistently demonstrate that the thermal perturbation of the flow field, causing increased downward flux from the condensation zone toward the drifts, is strongest during the first few hundred years after closure, corresponding to the time period when rock temperature is highest and the vaporization is most effective in limiting seepage. Even for high percolation fluxes into the model domain and strong flow channeling as a result of fracture heterogeneity, water cannot penetrate far into the superheated rock during the time that rock temperature is above the boiling point of water. Seepage will not occur when the drift crown temperature exceeds the boiling point of water. Much of the mobilized water is diverted around the dryout zone and drains away from the drift, as shown in Figure 2.3.3-36a. At the time when temperature has returned to below-boiling conditions (Figure 2.3.3-36b), fractures start to rewet at the drift wall. However, while the vaporization has become less effective, capillary diversion continues to form a barrier against water seepage into the drift (BSC 2005a, Sections 6.2.2, 6.2.3, and 6.2.4; SNL 2007a, Section 6.4.3).

Transient seepage rates were explicitly calculated by the thermal-hydrologic seepage model to directly quantify the potential for seepage during the thermally perturbed time period. These

transient seepage rates were compared with seepage results from ambient (steady-state) simulations. In other words, seepage results considering the combined effectiveness of the vaporization and the capillary barrier were compared with seepage results considering only the capillary barrier contribution. Results illustrating the evolution of thermal seepage for one realization and a flow focusing factor of 10 are given in Figure 2.3.3-37. To illustrate the transient seepage behavior, a simulation case with a large percolation flux is selected so that seepage is observed (BSC 2005a, Section 6.2.2.2). The results show that capillary diversion alone effectively prevents seepage (even without including the effects of heat) during the first 600 years after waste emplacement, as both ambient and thermal seepage are zero during this period. Since a large superheated zone has developed, two processes prevent seepage simultaneously and independently. These two processes are the vaporization of pore water and the flow diversion due to capillary forces. Later, as rock temperature decreases and the model boundary conditions change to monsoonal climate with higher infiltration and, correspondingly, higher percolation (at 600 years), the saturation in the rock surrounding the drift starts to increase. Seepage begins to occur a few hundred years after the rock temperatures have dropped below boiling conditions, with the delay caused by the relatively slow rewetting of the fractures. Initially, thermal seepage is considerably smaller than the respective ambient seepage value. With the assumed stepwise increase in infiltration at 2,000 years from emplacement (at the change to a glacial-transition climate) and the corresponding stepwise increase in percolation, the thermal seepage percentage increases, but still remains smaller than ambient seepage. At the end of the 4,000-year thermal period, the seepage percentage for thermal seepage is at about 17%, which is only slightly smaller than the long-term ambient value of 19.5% for a 250 mm/yr percolation flux (SNL 2007a, Sections 6.4.3 and 6.5.2).

As mentioned above, a wide range of conditions were studied in a sensitivity analysis, consistent with the potential variability in thermal output of different waste packages, spatial variability in percolation flux, and heterogeneous variability in hydrologic properties. Even over this wide range, there are several important observations with respect to thermal seepage that are common to all cases (BSC 2005a, Sections 6.2.4 and 8.1; SNL 2007a, Sections 6.4.3 and 6.5.2):

- Seepage during the 4,000-year thermal period is never observed in simulation runs for which the respective ambient seepage is zero.

- Seepage never occurs when the near-field rock temperature is above the boiling point of water.

- In simulation cases for which seepage occurs after the near-field rock temperature decreases to below the boiling point of water, seepage is initiated at several hundred to a few thousand years after rock temperature returns to below the boiling point of water.

- Thermal seepage rates are always smaller than the respective ambient seepage values. Thus, the ambient seepage values provide an asymptotic upper limit for thermal seepage.

These main qualitative conclusions form the basis for the thermal component of the drift seepage abstraction, as explained in Section 2.3.3.3.4.

2.3.3.3.3.2   Thermal-Hydrologic Seepage Model Support

The thermal-hydrologic seepage model is supported by comparison with related models of in situ heater tests conducted at Yucca Mountain, with particular focus on the Drift Scale Test (BSC 2005a, Section 7). The Drift Scale Test is simulated with a version of the thermal-hydrologic seepage model called the Drift Scale Test thermal-hydrologic model. The thermal-hydrologic seepage model and the Drift Scale Test thermal-hydrologic model use the same conceptual model (and similar thermal-hydrologic properties) to simulate the same thermal-hydrologic processes (BSC 2005a, Sections 7.1.3 and 7.4). To accommodate the test design of the Drift Scale Test, there are of course differences between the two models regarding the model geometry and thermal load. The Drift Scale Test thermal-hydrologic model is a three-dimensional model, which allows for some heat and mass loss through the leaky bulkhead.

Comparison of measured and simulated data in the Drift Scale Test is primarily based on temperature, which can be measured accurately in the field. Measurements from approximately 1,750 thermal sensors in the test were compared to model results as functions of time and space. Because of the vast amount of measured data available, the comparison is illustrated using temperature profiles and temperature history plots for a few representative examples. Additionally, statistical analysis of the comparison was used to evaluate quantitatively the closeness of the model results to the measurements. Good agreement is achieved, both qualitatively and quantitatively (BSC 2005a, Section 7.4, Table 7.4.3.1-1). Figures 2.3.3-38 and 2.3.3-39 show comparisons between measured and simulated temperatures as functions of space and time. The mean difference between measured temperature at the approximately 1,750 sensors and simulated temperatures did not exceed 5°C, or 2% of the maximum change in rock temperature at any time (BSC 2005a, Section 7.4.3.1.3, Table 7.4.3.1-1). The model results also showed good agreement between measured and predicted locations and durations of the two-phase heat-pipe conditions. This agreement provides confidence that the Drift Scale Test thermal-hydrologic model (and, hence, the thermal-hydrologic seepage model) incorporates the relevant thermal-hydrologic processes (BSC 2005a, Section 7.5).

In addition to temperature analyses, thermal-hydrologic processes are also evaluated by tracking the time-varying locations of the drying and condensation front in response to heating. In the Drift Scale Test, this tracking was done using geophysical methods to determine saturation changes in the matrix and air injection tests to determine saturation changes in the fractures (BSC 2005a, Sections 7.4.3.2 and 7.4.3.3). These methods are semi-quantitative but produce images that can be compared with model results. Figure 2.3.3-40 provides an example of the agreement between simulated and measured contours of matrix saturation. The latter is based on ground penetrating radar measurements. The comparison indicates that the model captures the changes in drying and condensation reasonably well. Simulated fracture saturations and air-permeability changes calculated from these saturation changes were compared with measured air-permeability data obtained at different times throughout the heating phase of the test. This comparison showed that the main trends of air-permeability changes were captured by the results of the Drift Scale Test thermal-hydrologic model (BSC 2005a, Section 7.4.3.3). To provide additional confidence, the simulated fracture-saturation results were also compared to the location and timing of water collection from several packed-off borehole intervals (BSC 2005a, Section 7.4.3.3). The location and timing of water collection events correspond with the predicted evolution of high saturation conditions from the Drift Scale Test thermal-hydrologic model. In summary, the described model–

data comparisons provide confidence that the Drift Scale Test thermal-hydrologic model accurately represents the relevant TH processes at the drift scale (BSC 2005a, Section 7.5).

While the Drift Scale Test results—as well as results from the other in situ heater tests at Yucca Mountain—provide valuable data on the strongly perturbed near field thermal-hydrologic conditions in the rock mass, there have been no seepage observations during the test and thus no measured seepage data are available that can be used for direct comparison with the model. The vaporization barrier generated by the heater output appeared to be totally effective in the Drift Scale Test, because of the intense thermal load and the rather small local percolation flux. To gain additional confidence, a simulation model similar to the thermal-hydrologic seepage model was applied to a laboratory heater test conducted by the Center for Nuclear Waste Regulatory Analyses at the Southwest Research Institute in San Antonio (hereafter referred to as the Centers experiment) (Figure 2.3.3-41). In contrast to the in situ heater tests at Yucca Mountain, where natural percolation is relatively small, the Centers experiment was operated using artificial water release from the top of the experimental apparatus, thereby testing the thermal seepage potential for extreme flow conditions. Test results indicated that water rapidly flowing in vertical fractures was able to penetrate the above-boiling rock region and seep into a horizontal cylindrical opening (Green and Prikryl 1998; Green and Prikryl 1999; Green et al. 2003). In other words, thermal seepage was shown to be possible despite above-boiling temperatures in the rock matrix.

Application of the thermal-hydrologic seepage model to the Centers experiment is described in Birkholzer and Zhang (2006). It is demonstrated there that the numerical simulations can reproduce the experimental observation of thermal seepage, provided that the model accounts for channelized flow in fractures and a related reduction in the fracture-matrix heat transfer. This result provides confidence that the conceptual model, as discussed in Section 2.3.3.3.3.1, and which features a significant reduction in the heat transfer from the matrix to the liquid flow in the fractures, is adequate. Birkholzer and Zhang (2006) also concluded that the Centers experiment was operated at conditions that are very favorable for thermal seepage, and that these conditions are not representative of those expected at Yucca Mountain.

The thermal-hydrologic seepage model calculations are also supported by comparison with an alternative conceptual model of water flow in the superheated rock environment. In this alternative model, the thermally perturbed downward flux from the condensation zone toward the superheated rock zone was conceptualized to form episodic preferential-flow events (finger flow) (BSC 2005a, Section 6.3 and Figure 6.3-1a). The effectiveness of vaporization was then tested for conditions where downward flux in small fingers is fast and large in magnitude compared to average flow. A semianalytical solution (Birkholzer 2003) was used to simulate this process of episodic finger flow in a superheated fracture. Using the analytical solution, the maximum penetration distance into the superheated rock was determined for specific episodic flow events and thermal conditions, and the amount of water arriving at the drift crown was calculated. It was shown that finger flow is not likely to penetrate through the superheated rock during the first several hundred years of heating, when rock temperature is high and boiling conditions exist in a sufficiently large region above the drifts. Only later, when the boiling zone is small and the impact of vaporization is limited, can channelized water arrive at the drift crown (where the water potential does not exceed the threshold for seepage because capillary diversion is effective). The results of the alternative conceptual model show that refluxing of condensate water above the drifts does not result in seepage when the drift crown is

above 100°C, because of the combined effects of vaporization and capillary diversion (BSC 2005a, Section 6.3.4).

2.3.3.3.3.3   Model Uncertainty

The main sources of model uncertainty, with respect to the thermal-hydrologic seepage model, are uncertainty in model input parameters and uncertainty in the conceptual model. As discussed above, uncertainty with respect to the conceptual model has been addressed by comparison of in situ and laboratory heater tests, as well as by comparison with an alternative conceptual model. These activities build confidence in the validity of the conceptual model for thermal seepage. The rock properties and the model boundary conditions are uncertain, and spatially variable, model input parameters. Sensitivity to parameters relevant for thermal seepage was explicitly studied, using the thermal-hydrologic seepage model, by (1) assessing seepage in two host rock units with different thermal and hydrologic properties; (2) varying the seepage relevant fracture capillary strength parameter; (3) analyzing infiltration scenarios with different flux multiplication factors; (4) changing host rock thermal conductivities and fracture permeabilities; and (5) simulating several different thermal loads (Section 2.3.3.3.3.1). In all these cases, which cover a wide range of property values and conditions, the main conclusions regarding thermal seepage were similar—in that no seepage (flow of liquid water into drifts) is predicted to occur during the period of above-boiling temperatures in the rock—and that thermal seepage is always less in magnitude compared to the respective long-term ambient values. This confirms that these main conclusions hold for all relevant repository conditions considered in TSPA.

2.3.3.3.3.4   Coupled Mechanical and Chemical Processes and Impact on Seepage

Rock properties relevant for seepage are affected by thermal-hydrologic-mechanical and thermal-hydrologic-chemical effects. Thermally-induced stresses change fracture apertures, leading to permeability and porosity changes, which are combined with changes in fracture capillary strength. Thermal-hydrologic-chemical processes, such as mineral precipitation and dissolution in fractures and matrix, also have the potential for modifying the permeability, porosity, and capillary strength of the system. Drift-scale models with conceptual approaches similar to the thermal-hydrologic seepage model have been utilized to evaluate the impact of such processes and property changes on seepage. These models are the thermal-hydrologic-mechanical seepage model (BSC 2004g), and the thermal-hydrologic-chemical seepage model (SNL 2007f). On the basis of these modeling studies, changes in drift-scale hydrologic properties induced by thermal effects are concluded to have no significant impact on seepage (Excluded FEPs 2.1.09.12.0A, Rind (chemically altered zone) forms in the near field; 2.2.01.02.0A, Thermally-induced stress changes in the near field; and 2.2.10.04.0A, Thermo-mechanical stresses alter characteristics of fractures near repository, in Section 2.2, Table 2.2-5). Therefore, results from these two models are not utilized in the seepage calculations conducted in the TSPA drift seepage submodel. Specific details are provided in Section 2.3.5, as well as in *Abstraction of Drift Seepage* (SNL 2007a, Sections 6.4.4, 6.5.1.4, and 6.5[a]).

2.3.3.3.4   Thermal Component of Drift Seepage Abstraction
[NUREG-1804, Section 2.2.1.3.3.3: AC 5]

The thermal component of the seepage abstraction provides the methodology that is used in the TSPA drift seepage submodel for calculating seepage during the time period of thermal perturbation. Results from complex drift-scale simulations are simplified for further use in the TSPA, making sure that variability and uncertainty in data and processes are adequately accounted for. The simplified abstraction procedure for thermal seepage is based on the consistent qualitative trends that were observed in various simulation scenarios conducted by the thermal-hydrologic seepage model.

In intact or moderately degraded drifts, seepage under thermal conditions, as estimated by the thermal-hydrologic seepage model and other coupled processes models discussed in Sections 2.3.3.3.3 and 2.3.5, is shown to be zero whenever temperatures in the rock are above the boiling point of water, and is never higher than ambient seepage during the cooldown period (i.e., there is no enhanced seepage as a result of thermal perturbation). Based on these results, which have been consistently observed over a wide range of sensitivity cases, the thermal seepage for intact or moderately degraded drifts is set to zero for the period in which rock temperatures in the drift vicinity are above the boiling point of water (SNL 2007a, Section 6.5.2.1). The threshold drift wall temperature that defines the duration of this boiling period is set to 100°C, which is a few degrees greater than the boiling point of water at the repository elevation, thereby ensuring that no heat-pipe activity is occurring at the drift wall and also accommodating some uncertainty in modeling results (SNL 2007a, Section 6.5.2.1). For the remaining time during cooldown, the rate of thermal seepage is conservatively set equal to the ambient seepage rates, which do not include the potential benefits from thermal perturbation in reducing seepage, as shown in Figure 2.3.3-42.

The abstraction method for thermal seepage is thus a qualitative method that describes the transient evolution of seepage relative to the ambient seepage rates. The advantage of this approach is that the lookup tables for ambient seepage, which comprise precalculated seepage results over the entire parameter range sampled in the TSPA (Section 2.3.3.2.4.3), can be consistently used for the thermal and the post-thermal period. For TSPA implementation of the thermal seepage abstraction, detailed information is required about the duration of the boiling period as a function of location in the repository. This information is provided by the multiscale thermal-hydrologic model (Section 2.3.5.4.1). If the rock temperatures at the drift wall are above 100°C, the ambient seepage rate determined for the considered TSPA parameter case and location is set to zero.

For collapsed drifts (seismic scenario class), the thermal seepage rates are set (starting at the time of collapse) equal to the ambient seepage rate derived from the lookup table for collapsed drifts (Section 2.3.3.2.4.3). No modification is made to incorporate thermal effects in this bounding approach (SNL 2007a, Section 6.5.3). As mentioned earlier, seepage into collapsed drifts is defined as the flow of water from the largely intact rock into the rubble-filled drift opening. Simulations were conducted with the thermal-hydrologic seepage model to analyze the conditions within and around a collapsed drift, and to determine the impact on the seepage abstraction (BSC 2005a, Section 6.4.3.4). Results from this model suggest that the temperatures in the intact rock will often not reach boiling conditions. This is because (1) the drift size above the heat-producing waste canisters has increased after the collapse; and (2) thermal conduction within the rubble material is less effective than thermal radiation within an open drift, thereby giving rise to a much stronger

in-drift temperature gradient. Since there is generally no vaporization barrier in the intact rock, water seepage from the fractured formation into the rubble-filled drift is limited only by the capillary-induced flow diversion, as described and accounted for in the ambient seepage prediction. However, depending on the temperature conditions near the waste packages, the seeping water may boil off within the rubble material. This fate of water inside the rubble-filled opening is described in Sections 2.3.4 and 2.3.5 (SNL 2007e).

How to categorize emplacement drifts with respect to the drift degradation and seepage conditions in the case of seismic events is explained in Section 2.3.3.2.4.2. In the case of igneous intrusion (Section 2.3.11), the drift seepage abstraction sets the seepage flux for an intruded drift equal to the local percolation flux, independent of the thermal conditions in the drift and the near-field rock prior to the igneous intrusion event (Section 2.3.3.2.4.2.3). As mentioned above, early failure events do not require a change in the abstraction methodology for seepage (Section 2.3.3.2.4.2).

2.3.3.4   Total System Performance Assessment Implementation of Drift Seepage
[NUREG-1804, Section 2.2.1.3.3.3: AC 5(1), (2)]

2.3.3.4.1   General Approach

The TSPA drift seepage submodel calculates the seepage rate (amount of seepage per time for each waste package) as a function of time and repository location for the nominal and disruptive event scenarios. The probabilistic procedure for calculating seepage in the TSPA is conducted according to the ambient and thermal components of the drift seepage abstraction that is described in Sections 2.3.3.2.4 and 2.3.3.3.4. These abstraction components provide the necessary specifications, tools, parameter distributions, lookup tables, and simplifications, based on evaluation of various data and process model sources.

2.3.3.4.1.1   Nominal and Seismic Scenarios

The seepage calculation for the nominal and seismic scenarios in the TSPA is performed using a probabilistic approach that accounts for the spatial and temporal variability and the inherent uncertainty of seepage-relevant properties and processes. The resulting information takes the form of repository-wide probability distributions for seepage rates at given points in time. The TSPA procedure for calculating seepage can be organized into two main steps, as illustrated in Figure 2.3.3-43 for the nominal scenario. Table 2.3.3-5 describes the inputs required by the TSPA drift seepage submodel (SNL 2007a, Sections 6.5.1 and 6[a]).

Step 1 consists of determining the long-term ambient seepage rates, using seepage lookup tables derived from the seepage model for performance assessment (Section 2.3.3.2.4). Probabilistic distributions have been defined describing the spatial variability and uncertainty of the key hydrologic parameters (capillary strength, permeability, local percolation flux) that feed into these lookup tables. The general calculation procedure for ambient seepage (as outlined above) is the same for the pre-10,000-year period and the post-10,000-year period. Transient effects on ambient seepage are incorporated (1) by using different percolation flux distributions for the future climate stages during the pre-10,000-year and the post-10,000-year periods; and (2) by incorporating drift shape changes caused by seismic activity and their impacts on seepage.

Step 2 involves adjusting the ambient seepage rate for thermal effects, if necessary. The abstraction method for thermal effects on seepage is a qualitative method that describes the transient evolution of seepage relative to the ambient seepage rates (Section 2.3.3.3.4). The advantage of this approach is that the lookup tables for ambient seepage, which comprise precalculated seepage results over the entire parameter range sampled in the TSPA, can be consistently used for the thermal and the post-thermal period.

Depending on the drift degradation conditions at the considered time step, ambient seepage needs to be calculated from the lookup table for intact drifts, or from the lookup table for collapsed drifts, or it needs to be set equal to the local percolation flux arriving at the considered drift (Section 2.3.3.2.4.2.2). Thus, before initiating Step 1 (below), the TSPA drift seepage submodel needs to evaluate the degree of drift degradation and its impact on seepage, which in turn depend on the geologic unit and the rock properties, as well as on the magnitude and occurrence probability of seismic events. In a procedure that accounts for the different geomechanical behavior in lithophysal and nonlithophysal units, drifts are categorized as mostly intact or strongly degraded by assessing the rockfall volume that has accumulated in a given drift location as a result of the seismic events that occurred during the considered time period (SNL 2008a, Section 6.6.1.3.2). This information is provided by rock-type specific regression functions that link the magnitude of seismic events to rockfall volume (Section 2.3.4). In case there have been no seismic events (e.g., in the nominal scenario or at early stages when no seismic event has occurred), the rockfall volume is set to zero.

For a given cumulative rockfall volume V, the following seepage procedure is applied: in nonlithophysal units, the lookup table for intact (or moderately degraded) drifts is used for the seepage calculation if V is smaller than a threshold value of 0.5 m^3 per meter drift length (i.e., drifts are mostly intact). Otherwise, seepage is set to the local percolation flux arriving at the drift (i.e., drifts are strongly degraded, with many topographic lows at the ceiling, so that the intact-drift lookup table cannot be used). In lithophysal units, the lookup table for intact (or moderately degraded) drifts is used for the seepage calculation if the cumulative volume is smaller than a threshold value of 5 m^3 per meter drift length (i.e., drifts are mostly intact). The lookup table for collapsed drifts is used for the seepage calculation if the cumulative rockfall volume is larger than a threshold value of 60 m^3 per meter drift length (i.e., drifts are fully collapsed). In intermediate degradation cases, seepage is interpolated between the results obtained for intact and collapsed drifts, using the rockfall volume as the interpolation parameter (SNL 2007a, Section 6.2[a]). The rockfall threshold values have been determined based on the visual inspection of various simulated drift shapes provided in *Drift Degradation Analysis* (BSC 2004e, Appendix R). Once the drift degradation category is determined, Steps 1 and 2 can be conducted as described below.

- **Step 1: Determine Ambient Seepage**

  – The first task is to sample appropriate values for the seepage-relevant parameters (permeability and capillary-strength), which feed into the seepage rate lookup tables (see Step 1A in Figure 2.3.3-43). The probabilities assigned to the permeability and the capillary-strength parameter distinguish explicitly between spatial variability and uncertainty, using separate probability distributions (Section 2.3.3.2.3.6). Spatial variability of permeability is described by a lognormal probability distribution, while spatial variability of the capillary-strength parameter is expressed by a uniform distribution. The uncertainty of both parameters is represented by triangular

distributions (using a log value for permeability) with a mean of zero and a range value defining the uncertainty of the respective parameter. The TSPA drift seepage submodel conducts stochastic sampling of the spatial variability distributions at each one of several thousand waste package locations (*r*) in the repository area to derive values of permeability and capillary strength. (These locations are consistent with those considered in the multiscale thermal-hydrologic model for in-drift thermal-hydrologic calculations; see Section 2.3.5.) A schematic illustration of this procedure for the capillary-strength parameter is given in Figure 2.3.3-44. Within each realization (*R*), the sampled values of permeability and capillary strength are adjusted to account for uncertainty using stochastic sampling of the log-triangular (permeability) and triangular (capillary strength) uncertainty distributions (Section 2.3.3.2.4.1).

– The next task is to sample appropriate values for the local percolation flux. First, one of the four alternative unsaturated-zone percolation flux distributions available for each climate state needs to be selected (Sections 2.3.1 and 2.3.2). For each realization (*R*), the TSPA chooses one distribution in a random process that accounts for the relative probability of each percolation flux scenario (see Step 1A in Figure 2.3.3-43) (Section 2.3.3.2.3.6.3). For each location *r*, the appropriate climate stage, and the chosen flux distribution, the percolation flux value is provided by the TSPA EBS thermal-hydrologic environment submodel, based on a spatial interpolation of site-scale percolation fluxes. This interpolation is conducted by the multiscale thermal-hydrologic model (Section 2.3.5). Then, a multiplication factor is sampled from the flow-focusing factor distribution. The product of the interpolated site-scale percolation flux and the sampled flow-focusing factor is the local percolation flux for seepage (Section 2.3.3.2.3.5). Flow focusing factors increase the site-scale fluxes in some areas, and reduce them in other areas, while the total amount of downward water flow over all sampled values remains unchanged (SNL 2007a, Section 6.6.5.2.2).

– For drifts categorized as intact or moderately degraded, the mean seepage rate for a given realization and location is extracted from the intact drift lookup table, using the corresponding parameter set determined above (Section 2.3.3.2.4.2.1). The standard deviation, which is different for each parameter set, and which represents the estimation uncertainty in seepage results, is also obtained (SNL 2007a, Section 6.7.1.1) (see Step 1B in Figure 2.3.3-43). The extracted mean seepage rate is then adjusted by applying a uniform probability density function, the range of which depends on the standard deviation. The value sampled from this distribution is added to the mean seepage rate in order to obtain the ambient seepage rate (SNL 2007a, Section 6.7.1.1) (see Step 1C in Figure 2.3.3-43). The ambient seepage rate is increased by 20% to account for increased estimation uncertainty in the prediction (SNL 2007a, Section 6.7.1.2).

– For drifts in lithophysal units categorized as fully collapsed, the mean seepage rate and standard deviation for a given realization and location are extracted from the collapsed-drift lookup table, using the corresponding parameter (Section 2.3.3.2.4.2.2). The mean seepage rate is then adjusted for estimation uncertainty by applying a uniform probability density function, the range of which is defined by the standard deviation (Section 2.3.3.2.3.6.4). In intermediate drift degradation cases representing

partial collapse (with rockfall volume between 5 m^3 and 60 m^3 per meter drift length), two seepage rates are calculated using both the intact and collapsed drift lookup tables. The resulting rate is then interpolated between these two values, using the rockfall volume as the interpolation parameter (Section 2.3.3.2.4.2.2). This interpolation procedure affects not only the seepage rates, but also the seepage fraction, because overall a different number of drift segments will arrive at seepage conditions.

– For strongly degraded drifts in nonlithophysal units, the seepage rate is simply set equal to the local percolation flux (including flow focusing) and the seepage fraction is set equal to one, as determined above (Section 2.3.3.2.4.2.2).

• **Step 2: Adjust Ambient Seepage for Thermal Effects**

– For drifts categorized as intact or moderately degraded, seepage rates are set to zero during the time period that the drift wall temperature is above 100°C (Section 2.3.3.3.4). If the temperature is below 100°C, the ambient rate determined in Step 2 is used without further adjustment (see Step 2 in Figure 2.3.3-43).

– For fully collapsed drifts, there is no adjustment for thermal effects (Section 2.3.3.3.4). In other words, seepage from the intact rock into the rubble-filled opening is set equal to the ambient seepage rate for a collapsed drift, independent of thermal considerations.

The seepage fraction is calculated in addition to the repository-wide distribution of seepage rates for the realization and the time considered. As mentioned before, the seepage fraction is defined as the number of drift segments with seepage over the entire repository, divided by the total number of drift segments (SNL 2007a, Section 6.5).

2.3.3.4.1.2   Igneous Scenario

For drifts intruded by magma, the seepage rate is set equal to the local percolation flux incident on the drift, starting at the time that the magma has cooled to temperatures below boiling (Section 2.3.11.1). This conservative approach is used because of the uncertainties in modeling in-drift conditions after an igneous event (SNL 2007a, Section 6.5.1.7).

2.3.3.4.1.3   Early Failure Scenario

No changes in the seepage calculations are required for the early failure scenario (early failure of drip shields or waste packages), because the seepage conditions are not affected by these changes in the EBS.

2.3.3.4.2   Example Calculation for Nominal and Seismic Scenarios

In order to demonstrate the capabilities of the Upper Natural Barrier, and to evaluate sensitivities in the abstraction process, a simplified probabilistic calculation of seepage is conducted for a variety of cases following the methodology described in Sections 2.3.3.2.4, 2.3.3.3.4, and 2.3.3.4.1. Results from this calculation are not utilized in the TSPA, although these results provide a quantitative

picture of expected seepage behavior. The TSPA drift seepage submodel performs a more comprehensive probabilistic seepage calculation within a Monte Carlo simulation procedure to provide the seepage results used in the TSPA.

The simplified probabilistic seepage calculation is conducted for the Tptpll unit, which comprises about 80% of the emplacement area. (Because the seepage abstraction is identical for lithophysal repository units, this calculation is also representative of the Tptpul. Together, the Tptpll and the Tptpul comprise about 85% of the emplacement area.) Probabilistic seepage results are calculated separately for the intact drift case, and the collapsed drift case, using a random procedure with a sample size of 10,000 stochastic cases. The spatial variability and uncertainty distributions developed for the Tptpll unit are simultaneously sampled in one calculational loop. In each stochastic seepage case, uncorrelated random numbers are generated to sample from spatial variability distributions (for capillary strength, permeability, percolation flux, and flow focusing factors, as described in Section 2.3.3.2.3.6), and from uncertainty distributions (for capillary strength, permeability, and seepage uncertainty, as described in Section 2.3.3.2.3.6) (SNL 2007a, Section 6.8). The impact of thermal perturbation is not explicitly accounted for in this simplified probabilistic seepage calculation (i.e., the ambient seepage rates are not adjusted for the impact of boiling on seepage). This is of course different in the TSPA drift seepage, where the ambient seepage rates for intact drifts are set to zero if the drift wall temperature is above 100°C (Section 2.3.3.4.1).

For each random parameter set, mean seepage rates and related standard deviations are interpolated from the appropriate seepage lookup tables for intact or collapsed drifts (Section 2.3.3.2.3.4), and the mean seepage rates are adjusted for seepage uncertainty. Separate calculations are conducted for the three climate states during the first 10,000-years after emplacement (the present-day, monsoon, and glacial-transition climates), as well as for the post-10,000-year climate, each with four alternative spatial variability distributions for percolation flux to account for climate and infiltration uncertainty. Seepage results for the intact drift cases include the 20% increase on account of estimation uncertainty (Section 2.3.3.2.4.2.1).

As explained in Section 2.3.2, four alternative unsaturated flow fields for the pre-10,000-year climates have been derived by the unsaturated zone flow model using the 10th, 30th, 50th, and 90th percentile of a suite of 40 Monte-Carlo derived infiltration scenarios. Comparison with measured data from the unsaturated zone (e.g., distributions of temperature and chloride concentrations) determined weighting factors that define the relative occurrence probability of these four alternative flow fields (SNL 2007b, Section 6.8). The weighting factors derived from this comparison are 62% for the flow field derived using the 10th percentile infiltration map, 16% for the flow field derived using the 30th percentile infiltration map, 16% for the flow field derived using the 50th percentile infiltration map, and 6% for the flow field derived using the 90th percentile infiltration map. Thus, while these four flow fields are based on the 10th, 30th, 50th, and 90th percentile infiltration scenarios, they are associated with relative occurrence probabilities (or weighting factors in the TSPA calculation) of, respectively, 62%, 16%, 16%, and 6%.

The flow fields for the post-10,000-year period are based on the stipulated distribution of average percolation flux to the repository horizon in the U.S. Nuclear Regulatory Commission (NRC) proposed rule (10 CFR 63.342(c)), prescribing a log-uniform distribution ranging from 13 mm/yr to 64 mm/yr. Four alternative unsaturated zone flow fields were generated within this specified

range (SNL 2007b, Section 6.1.4). These four flow fields are as follows: (1) the first flow field has a 62% probability, and an average percolation flux through the repository footprint of 21.29 mm/yr; (2) the second flow field has a 16% probability and an average percolation flux through the repository footprint of 39.52 mm/yr; (3) the third flow field has a 16% probability, and an average percolation flux through the repository footprint of 51.05 mm/yr; and (4) the fourth flow field has a 6% probability, and an average percolation flux through the repository footprint of 61.03 mm/yr (SNL 2007b, Tables 6.1-3 and 6.8-1).

Figures 2.3.3-27, 2.3.3-45, and 2.3.3-46 present some example results from the simplified probabilistic calculation for ambient seepage into intact drifts located in the Tptpll unit. In this case, the calculations use the percolation flux distribution derived from the 10th percentile infiltration scenario for the pre-10,000-year period and from the first flow field for the post-10,000-year period. As pointed out above, these percolation flux distributions are the most likely of all four distributions, with a relative probability of 62%. Figure 2.3.3-45 provides histograms of the calculated seepage rates in kilograms per year per waste package location, showing the samples with nonzero seepage. The number of seepage occurrences clearly increases with the future climate changes. The seepage rates vary from small values below 0.1 kg/yr per waste package drift section up to almost 10,000 kg/yr per location (SNL 2007a, Section 6.4[a]). Figure 2.3.3-46 provides histograms of the calculated seepage percentages for each climate state, again showing only the samples with nonzero seepage. (As explained before, the seepage percentage is defined as the seepage rate divided by the mean percolation flux arriving over the footprint of the considered drift segment.) The seepage percentages also show considerable variability covering the entire range from 0% up to 100%. Most probable, however, are the small seepage percentages; only a few samples reach 80% seepage and more.

Figure 2.3.3-27 provides histograms of the distributions of seepage-relevant parameters sampled in the probabilistic seepage calculation. For permeability and capillary strength, the histograms represent the combined effect of spatial variability and uncertainty sampling, using the separate distributions described in Section 2.3.3.2.3.6. For percolation flux, the histograms represent the combined effect of spatial variability in the percolation flux distribution plus flow focusing. The fraction of all sampled parameter values that resulted in seepage is plotted in a light-yellow color. Seepage is less likely for parameter combinations with larger permeability, larger capillary strength, and smaller percolation flux. This is consistent with the understanding of seepage processes (Section 2.3.3.2.1.2). As the mean tangential permeability along the drift perimeter increases, more water is diverted around the drift opening without dripping. As the capillary strength of the fractured rock increases, more water is retained in the formation without dripping. Finally, as less water arrives at the drift crown, it is more likely that the seepage threshold is not exceeded.

Figures 2.3.3-47 through 2.3.3-49 summarize results of the simplified probabilistic calculation for intact drifts in the Tptpll unit, providing (1) the mean seepage rate (i.e., mean over 10,000 stochastic cases of the seepage rate in kilograms per year per drift segment containing one waste package); (2) The mean seepage percentage (i.e., mean seepage rate divided by mean percolation flux across reference area, with reference area given by footprint of considered drift segments); and (3) the mean seepage fraction during the present-day, monsoon, and glacial-transition climates. The four alternative unsaturated zone flow fields, which correspond to the 10th, 30th, 50th, and 90th percentile infiltration scenarios, arrive at four different sets of seepage results. For the flow field based on the 10th percentile infiltration scenario, the most likely flow field with a relative

probability of 62%, seepage is expected to occur at about 8% of the waste package locations during the first 600 years after emplacement, without considering thermal effects, which would further reduce or eliminate seepage (Figure 2.3.3-49). This percentage rises to about 13% during the monsoon climate, and to about 17% during the glacial-transition climate. On average over all waste packages, the amount of seeping water per drift segment containing one waste package is 1.2, 4.6, and 14.4 kg/yr for the three climate states, respectively (Figure 2.3.3-47). These amounts translate to mean seepage percentages of 1.1%, 2.2%, and 4.7% (Figure 2.3.3-48). Thus, for the present-day climate and the most likely of the four flow fields, on average about 99% of the percolation flux would be diverted around drifts in the Tptpll unit. For the wetter climate states of the monsoonal and the glacial-transition climate states, the percentage of diverted flux would be approximately 98% and 95%, respectively (SNL 2007a, Section 6.4[a] and Table 6-5[a]).

Figures 2.3.3-47 through 2.3.3-49 also present results for the other three unsaturated zone flow fields provided for each climate state; namely, those corresponding to the 30th, the 50th, and the 90th percentile infiltration scenarios (SNL 2007a, Section 6.4[a] and Table 6-5[a]). As expected from the higher percolation fluxes, the 30th percentile infiltration scenario results in more seepage. Here, the seepage fraction varies from 16.7% for the present-day climate, to 22.8% during the monsoon period, to 29.5% during the glacial-transition climate. The respective mean seepage percentages are 3.0%, 4.9%, and 8.0%. Most seepage is seen for the 90th percentile infiltration scenario, with the seepage fraction as high as 52.6% during the monsoon climate. The mean seepage percentage during this climate state is 19.5%. Thus, even for the least likely of the four unsaturated zone flow fields, with a relative probability of 6% and comparably strong downward percolation, the diversion capacity of the unsaturated rock is about 81% overall. However, more than half of all waste packages are expected to experience some amount of seepage in this case (SNL 2007a, Section 6.4[a] and Table 6-5[a]). Overall, the observed seepage percentages demonstrate the important barrier capability of the unsaturated flow processes in the fractured rock at and above the repository horizon.

Figures 2.3.3-47 through 2.3.3-49 furthermore show seepage results for the post-10,000-year climate state. There are four alternative unsaturated zone flow fields for this period (Flow Fields 1 through 4, with different relative probabilities of 62%, 16%, 16%, and 6%, respectively), which represent the stipulated distribution of average percolation flux given in the NRC proposed rule for the post-10,000-year climate (Section 2.3.2.4.1.2.4.2). In general, the expected seepage for the post-10,000-year period is higher than the seepage expected during the first 10,000 years after emplacement. This is because the NRC-mandated percolation fluxes for the post-10,000-year period are generally higher than during the first 10,000 years after emplacement (when comparing the flow fields with the same relative occurrence probability, such as the 10th percentile scenarios for the pre-10,000-year period with Flow Field 1 for the post-10,000-year period) (Tables 2.3.2-14 and 2.3.2-15). The one exception is the 90th percentile infiltration scenario for the monsoon climate, which features both the highest average percolation fluxes as well as the most seepage. As pointed out before, it can be expected that many drifts in the lower lithophysal units collapse as a result of seismic ground motion during the post-10,000-year period (Sections 2.3 and 2.4). Thus, the more likely seepage results for this time period are those for collapsed drifts presented below.

Summary statistics for seepage in collapsed drifts are depicted in Figures 2.3.3-50 through 2.3.3-52, for the climate states and alternative unsaturated zone flow fields discussed above. Evaluation of seepage into collapsed drifts requires use of the collapsed-drift lookup table, but uses the same

probability distributions for permeability and capillary strength as in the intact cases. The resulting values for seepage rates, percentages, and fractions have increased considerably compared to the intact-drift values, thus indicating the significance of drift collapse. For the post-10,000-year period, where the collapsed-drift case is more likely because of the increasing probability of strong seismic events, the mean seepage rates range from about 183 to about 945 kg per year, per waste package and the seepage fraction ranges from about 53% to about 70%. In other words, seepage would be expected in the majority of waste package locations. However, the mean seepage percentage is between about 16% and about 29%, meaning—that even in these cases—most of the percolation flux would still be diverted around the collapsed opening.

2.3.3.4.3 Seepage Calculations for ESF South Ramp Seepage Event

During the period between October 2004 and February 2005, unusually heavy precipitation occurred in the Yucca Mountain area. On February 28, 2005, Yucca Mountain Project personnel working in the South Ramp of the ESF observed—in select areas—wet spots on the main drift's crown, ribs, and invert. This field observation is considered the first unambiguous evidence of seepage under ambient conditions. See Section 2.3.3.2.2.3.2 for more details on the field observations, and for a discussion of the several factors specific to the South Ramp location and geology that have contributed to the occurrence of seepage.

A seepage abstraction validation study was conducted to examine whether the approach employed to calculate seepage into waste emplacement drifts yields results that are consistent with the observed seepage in the ESF South Ramp (SNL 2007a, Section 7.1[a]). It is important to realize that this validation study was not an attempt to predict, reproduce, or analyze the South Ramp seepage data in a detailed quantitative manner. Such an effort would require the development of a specific model and a specific characterization and analysis approach best suited for capturing the hydrogeologic conditions in the South Ramp as they prevailed before, and during, the period of the seepage observations. Instead, the seepage abstraction conceptual framework outlined in Section 2.3.3.4.1—developed for the estimation of long-term seepage into waste emplacement drifts in the Topopah Spring unit—was used with minimal adjustments to examine whether the results of the probabilistic approach employed in the TSPA (which considers uncertainty and spatial variability in fracture permeability, capillary strength, and local percolation flux) would provide reasonable seepage estimates, even if applied to the different conditions in the South Ramp. (Section 2.3.3.2.2.3.2) If so, confidence can be gained that the TSPA approach captures the processes relevant for the prediction of natural seepage into large underground openings.

Details on the seepage abstraction validation study and its results are given in *Abstraction of Drift Seepage* (SNL 2007a, Section 7.1[a]). The following main steps were conducted, in a procedure that closely follows the abstraction approach developed for seepage calculations in the TSPA:

- Develop a heterogeneous fracture-continuum model of a 5-m-long section of the ESF.

- Evaluate seepage for a range of parameter values. The three seepage-relevant parameters varied are (1) reference fracture permeability; (2) van Genuchten capillary strength parameter; and (3) average percolation flux at top model boundary.

- Develop a lookup table of seepage as a function of the three seepage-relevant parameters.

- Determine probability distributions for the three seepage-relevant parameters.

- Randomly sample from the probability distributions and determine related seepage flux.

- Determine the seepage fraction (percentage of realizations with nonzero seepage).

- Compare modeling results to qualitative information from seepage observations in the ESF South Ramp.

Good qualitative agreement was observed between the model results and observations, in terms of seepage fraction and seepage flux (SNL 2007a, Section 7.1[a]). Assuming reasonable probability distributions for fracture-continuum permeability, capillary strength, and local percolation flux, it was estimated that seepage would occur along about 37% of the ESF South Ramp section where the PTn unit is not present, compared with the observation that about 13% of this section of the ESF South Ramp exhibited wet spots in February 2005. Thus, the seepage simulations yielded results that are higher than but generally consistent with observations made in the South Ramp. Specifically, the model predicted that some (but not all) locations along the ESF South Ramp will encounter seepage, which is in qualitative agreement with the actual observations.

In summary, the seepage abstraction approach used to estimate long-term ambient seepage into waste emplacement drifts in the Topopah Spring unit has been minimally adapted to be able to estimate short-term, transient seepage into the ESF South Ramp located in the Tiva Canyon unit. These preliminary results indicate that the seepage predictions made with the models and approach used in the TSPA are reasonable, even when applied to a different hydrogeologic unit and different hydrologic conditions.

2.3.3.5   Analogue Observations
[NUREG-1804, Section 2.2.1.3.3.3: AC 5(1)]

Natural and man-made analogues provide evidence that supports the concept of water exclusion from underground openings as simulated in the suite of seepage models. Seepage exclusion in underground openings (drifts) is consistent with processes that occur in caves, lava tubes, rock shelters, and surface structures. Additional discussion of the use of natural analogues to support models for unsaturated zone flow is discussed in Section 2.3.2 (BSC 2004h, Section 8.2).

Analogues show that infiltrating water in the unsaturated zone is diverted around underground openings, and does not become seepage even for areas with greater precipitation rates than present-day rates at Yucca Mountain (BSC 2004h, Section 15.7.5). For example, observations of the hydrologic behavior of ancient man-made tunnels and natural caves provide information about water seepage into the natural and mined openings in an unsaturated zone over thousands of years. The archaeological and historical records in natural analogue sites provide qualitative information on the degradation of materials that is relevant to the performance of the repository (e.g., the preservation of materials in Egyptian pyramids and tombs that are over 5,000 years old points to absence of seepage). For example, unsaturated zone caves smaller than emplacement drifts contain ancient paintings preserved for more than 30,000 years, and contain a mummified human body that is more than 9,400 years old (DOE 2002, p. 2-33). These observations of natural caves and ancient

man-made tunnels and pyramids support the concept that a deep geologic repository in the unsaturated zone would keep waste dry and isolated (BSC 2004h, Section 8).

The qualitative evidence for water exclusion and flow diversion is substantiated by quantitative seepage measurements and observations in caves. These studies show that seepage is considerably smaller than percolation flux, thereby corroborating the seepage testing and modeling results at Yucca Mountain. For cases in which some seepage is observed, at least some of the water that enters underground openings does not drip but rather flows down the walls (and as such does not meet the definition of seepage used for performance assessment). In the instances in which dripping has been noted in settings that are analogous to Yucca Mountain, the drips are attributed to asperities in the surface of the roof and ceiling of the opening. These observations are consistent with the representation of seepage in the TSPA (BSC 2004h, Sections 8 and 15.7.5).

One such setting with various similarities to Yucca Mountain is the Nopal I uranium mine in Peña Blanca, Chihuahua, Mexico, which is currently being investigated as a natural analogue for Yucca Mountain performance assessment. Similarities between Peña Blanca and Yucca Mountain include the rock type, fracturing, and climate, making the Peña Blanca site an excellent analogue for investigating flow and radionuclide transport. One ongoing component of the study at Nopal I is an evaluation of radionuclide transport through the unsaturated zone via a seepage study of the +00 m adit at the Nopal I uranium mine (Levy et al. 2005; Ghezzehei et al. 2006). Seasonal rainfall on the exposed bedrock along the +10 m surface infiltrates into the fractured rhyolitic ash-flow tuff, and seeps into the +00 adit located 8 m below. At present, seepage data in the adit are being collected to investigate the spatial and temporal variability in seepage. The data collected so far indicate that the seepage within the adit is highly heterogeneous, and that, with the exception of a few zones with fast flow paths, there is a significant reduction in seepage compared to the amount of water infiltration at the surface (Dobson et al. 2008).

Similarly, calcite deposition in lithophysal cavities present in the host rock at Yucca Mountain provides natural analogue evidence of capillary diversion, which corroborates the concept of reduced or complete exclusion of seepage into underground openings in the unsaturated zone, compared to the natural percolation flux. There is little or no evidence of water dripping from cavity ceilings and accumulating in isolated masses on the floors of open cavities (Paces et al. 2001; Whelan et al. 2002, Section 4.1). In addition, calculated seepage rates from observations of naturally occurring calcite and opal precipitation in lithophysal cavities at Yucca Mountain (Marshall et al. 2003; BSC 2004d, Section 7.7.5) are much smaller than the seepage calculated by the seepage model for the TSPA and the estimated percolation flux.

Additional information on natural analogues for the unsaturated zone that are applicable to seepage is discussed in Section 2.3.2.

2.3.3.6   Conclusions

The seepage-related models described in this section incorporate the FEPs that contribute to the capability of the Upper Natural Barrier to limit seepage into emplacement drifts. A complete list of FEPs addressed in this section is given in Table 2.3.3-1. As demonstrated in Section 2.3.3.4.2, seepage is prevented or substantially reduced compared to the percolation flux arriving at a given repository location, as a result of diversion of water around the drifts.

The FEPs associated with parameters and parameter characteristics that have been determined to be important to barrier capability, with respect to water seeping into drifts, have been introduced in Section 2.3.3.1. These are the following (Section 2.1, Table 2.1-2):

- Flow diversion around repository drifts
- Water influx at the repository
- Rock properties of host rock and other units
- Fractures and Fracture flow in the unsaturated zone
- Unsaturated groundwater flow in the geosphere.

The reduction in seepage, compared to the percolation flux, is mainly a result of capillary pressures holding water in the formation and diverting it around the cavity, thereby preventing it from entering the cavity (such as an emplacement drift). The effectiveness of capillary diversion depends mostly on the local percolation flux and the near-field properties of the fractured rock.

When rock temperatures rise above the boiling point of water near the drift, as a result of heat generated by radioactive decay, vaporization of percolating water prevents seepage, thereby also contributing to barrier capability. However, the period of above-boiling temperatures lasts only for the first few hundred to a few thousand years after closure, which is a small fraction of the period of geologic stability. Therefore, while included in the seepage calculation conducted in the TSPA, the FEPs related to flow diversion caused by boiling and dryout (e.g., Geosphere dryout due to waste heat) have been determined to be less significant to barrier capability.

An integrated conceptual framework has been developed that models the seepage-relevant processes near the emplacement drifts for a range of relevant repository scenarios and conditions. The framework, as defined by the drift seepage abstraction, is implemented in the TSPA drift seepage submodel for the calculation of time-dependent repository-wide seepage rates and seepage fractions. The seepage calculation in the TSPA is based on and consistent with theoretical analyses, numerical modeling studies, laboratory and field experiments, as well as natural analogues, which all show that seepage into underground openings excavated in unsaturated formations is smaller than the percolation flux at the given location.

Uncertainties and Conservatisms Associated with the Capability of the Upper Natural Barrier Related to Seepage—Uncertainties associated with unsaturated flow and seepage at ambient and thermally perturbed conditions result from both the uncertainty and variability in the data and parameters used to represent the characteristics of the natural system, and from the simplifications and uncertainties in the models used to simulate important processes. The uncertainties associated with data and parameters that are important to barrier capability are described in Sections 2.3.3.2.3.6.1, 2.3.3.2.3.6.2, and 2.3.3.2.3.6.3 for ambient seepage, and in Section 2.3.3.3.2 for thermal seepage. The uncertainties associated with the seepage process models are described in 2.3.3.2.3.6.4 for ambient seepage, and Section 2.3.3.3.3.3 for thermal seepage. Uncertainties related to the seepage assessment of degraded drifts are described in Sections 2.3.3.2.3.6.4 and 2.3.3.2.4.

Relevant sources of data and model uncertainty are accounted for in the drift seepage abstraction, and are propagated to the TSPA drift seepage submodel. For example, ambient seepage is a function of three key hydrologic properties: (1) the capillary-strength parameter; (2) permeability; and

(3) local percolation flux that are spatially variable and uncertain. Spatial variability and uncertainty distributions for the capillary-strength parameter and the local permeability have been derived based on the liquid-release and air-permeability data available at various locations in the ESF and ECRB Cross-Drift (Sections 2.3.3.2.3.6.1 and 2.3.3.2.3.6.2). Spatial variability distributions for the local percolation flux are developed using site-scale simulations with the site-scale unsaturated zone flow model, while sampling from four alternative unsaturated zone flow fields accounts for uncertainty (Section 2.3.3.2.3.6.3). Flow focusing factors represent the effect of intermediate-scale heterogeneity. The resulting distributions cover the spatial variability and uncertainty inherent in these parameters (Section 2.3.3.2.3.6.3).

Model uncertainty in the ambient seepage predictions is incorporated in the TSPA seepage calculation by sampling the mean seepage rates as well as the spread in the seepage results stemming from estimation uncertainty (Section 2.3.3.2.3.6.4). Uncertainty in seepage results for degraded drifts is caused by (1) the variability and uncertainty in the degraded drift shapes and conditions; and (2) the increased uncertainty in the seepage simulation results. The former is implemented in the TSPA drift seepage submodel sampling of the uncertain rockfall volumes, in response to seismic events, and respective drift degradation from regression curves provided by the TSPA model for the seismic scenario class that is described in Section 2.3.4 (Section 2.3.3.2.4.2.2), whereas the latter is accounted for using upper-bound estimates in the seepage simulations (e.g., by selecting worst-case drift profiles representing the conditions after collapse).

Seepage during the thermal period is calculated in the TSPA by a simplified representation of the transient behavior. This simplification, which is based on the consistent trends observed in various sensitivity scenarios conducted by the thermal-hydrologic seepage model, uses upper-bound estimates for thermal seepage that account for both variability and uncertainty in data and models. Seepage is set to zero for all drifts with wall temperatures above 100°C. For the remaining time during cooldown, seepage is set equal to the respective ambient seepage rates calculated for the given set of parameters and conditions (Sections 2.3.3.3.3.3 and 2.3.3.3.4).

Summary of Consistency Between TSPA Model Abstractions and Process Models—The ambient and thermal seepage process models provide the seepage rates that feed into the drift seepage abstraction. The ambient seepage rates are directly used in the TSPA drift seepage submodel by interpolation from seepage lookup tables. The thermal seepage rates are simplified using an upper-bound approach. Process model results providing information on seepage-relevant parameters and factors are either directly used without further modification (such as the unsaturated zone flow fields or the flow focusing factors), or have been abstracted to develop reasonable simplifications (such as the selected drift profiles for degraded drifts). In summary, the TSPA drift seepage submodel is consistent with supporting process models.

Summary of Key Output Parameters Provided to TSPA—The outputs from the drift seepage abstraction to the TSPA drift seepage submodel are shown in Figure 2.3.3-1. They include the seepage calculation methodology for nominal, seismic, igneous and early-failure scenarios; variability and uncertainty distributions for seepage-relevant parameters; flow-focusing factors; and seepage lookup tables containing mean seepage flow rates and their uncertainty for both intact and collapsed drifts.

2.3.3.7   General References

Altman, W.D.; Donnelly, J.P.; and Kennedy, J.E. 1988. *Qualification of Existing Data for High-Level Nuclear Waste Repositories: Generic Technical Position*. NUREG-1298. Washington, D.C.: U.S. Nuclear Regulatory Commission. TIC: 200652.

Birkholzer, J. 2003. "Penetration of Liquid Fingers into Superheated Fractured Rock." *Water Resources Research, 39* (4), 9-1 through 9-21. Washington, D.C.: American Geophysical Union. TIC: 254362.

Birkholzer, J.T.; Webb, S.W.; Halecky, N.; Peterson, P.F.; and Bodvarsson, G.S. 2006. "Evaluating the Moisture Conditions in the Fractured Rock at Yucca Mountain—The Impact of Natural Convection in Heated Emplacement Drifts." *Vadose Zone Journal, 5*, 1172–1193. Madison, Wisconsin: Soil Science Society of America. TIC: 259701.

Birkholzer, J.T. and Zhang, Y. 2006. "The Impact of Fracture-Matrix Interaction on Thermal-Hydrological Conditions in Heated Fractured Rock." *Vadose Zone Journal, 5*, 657–672. Madison, Wisconsin: Soil Science Society of America.TIC: 259700.

BSC (Bechtel SAIC Company) 2004a. *Seepage Model for PA Including Drift Collapse*. MDL-NBS-HS-000002 REV 03. Las Vegas, Nevada: Bechtel SAIC Company. ACC: DOC.20040922.0008.

BSC 2004b. *Seepage Calibration Model and Seepage Testing Data*. MDL-NBS-HS-000004 REV 03. Las Vegas, Nevada: Bechtel SAIC Company. ACC: DOC.20040922.0003.

BSC 2004c. *Conceptual Model and Numerical Approaches for Unsaturated Zone Flow and Transport*. MDL-NBS-HS-000005 REV 01. Las Vegas, Nevada: Bechtel SAIC Company. ACC: DOC.20040922.0006.

BSC 2004d. *Yucca Mountain Site Description*. TDR-CRW-GS-000001 REV 02 ICN 01. Two volumes. Las Vegas, Nevada: Bechtel SAIC Company. ACC: DOC.20040504.0008.

BSC 2004e. *Drift Degradation Analysis*. ANL-EBS-MD-000027 REV 03. Las Vegas, Nevada: Bechtel SAIC Company. ACC: DOC.20040915.0010.

BSC 2004f. *In Situ Field Testing of Processes*. ANL-NBS-HS-000005 REV 03. Las Vegas, Nevada: Bechtel SAIC Company. ACC: DOC.20041109.0001.

BSC 2004g. *Drift Scale THM Model*. MDL-NBS-HS-000017 REV 01. Las Vegas, Nevada: Bechtel SAIC Company. ACC: DOC.20041012.0001.

BSC 2004h. *Natural Analogue Synthesis Report*. TDR-NBS-GS-000027 REV 01. Las Vegas, Nevada: Bechtel SAIC Company. ACC: DOC.20040524.0008.

BSC 2005a. *Drift-Scale Coupled Process (DST and TH Seepage) Models*. MDL-NBS-HS-000015 REV 02. Las Vegas, Nevada: Bechtel SAIC Company. ACC: DOC.20050114.0004.

BSC 2005b. *White Paper: South Ramp Water Seepage During February–May 2005*. Las Vegas, Nevada: Bechtel SAIC Company. ACC: MOL.20050711.0174.

BSC 2006. *Analysis of Alcove 8–Niche 3 Flow and Transport Tests*. ANL-NBS-HS-000056 REV 00. Las Vegas, Nevada: Bechtel SAIC Company. ACC: DOC.20060901.0003.

CRWMS M&O (Civilian Radioactive Waste Management System Management and Operating Contractor) 1997. *Unsaturated Zone Flow Model Expert Elicitation Project*. Las Vegas, Nevada: Civilian Radioactive Waste Management System Management and Operating Contractor. ACC: MOL.19971009.0582.

CRWMS M&O 1998. *Drift Scale Test As-Built Report*. BAB000000-01717-5700-00003 REV 01. Las Vegas, Nevada: Civilian Radioactive Waste Management System Management and Operating Contractor. ACC: MOL.19990107.0223.

Dobson, P.; Cook, P.; Ghezzehei, T.; Rodriquez, J.; and de la Garza, R. 2008. *Heterogeneous Seepage at the Nopal I Uranium Mine, Chihuahua, Mexico.* Berkeley, California: Lawrence Berkeley National Laboratory. ACC: LLR.20080225.0081.

DOE (U.S. Department of Energy) 2002. *Yucca Mountain Science and Engineering Report.* DOE/RW-0539, Rev. 1. Washington, D.C.: U.S. Department of Energy, Office of Civilian Radioactive Waste Management. ACC: MOL.20020404.0042.

Finsterle, S. 2000. "Using the Continuum Approach to Model Unsaturated Flow in Fractured Rock." *Water Resources Research, 36* (8), 2055–2066. Washington, D.C.: American Geophysical Union. TIC: 248769.

Ghezzehei, T.A.; Dobson, P.F.; Rodriguez, J.A.; and Cook, P.J. 2006. "Infiltration and Seepage through Fractured Welded Tuff." *Proceedings of the 11th International High-Level Radioactive Waste Management Conference (IHLRWM), April 30-May 4, 2006, Las Vegas, Nevada,* 105–110. La Grange Park, Illinois: American Nuclear Society. TIC: 258345.

Green, R.; Painter, S.; Fratesi, B.; Manepally, C.; and Walter, G. 2003. *Status Report for Multiphase Flow Simulation*. San Antonio, Texas: Center for Nuclear Waste Regulatory Analyses. ACC: LLR.20070927.0115.

Green, R.T. and Prikryl, J.D. 1998. "Penetration of the Boiling Isotherm by Flow Down a Fracture." *Proceedings of the Third International Conference on Multiphase Flow, ICMF'98, Lyon, France, June 8-12, 1998*, 1-7. Halle (Saale), Germany: Martin-Luther-University Halle-Wittenberg. TIC: 260046.

Green, R.T. and Prikryl, J.D. 1999. "Formation of a Dry-Out Zone Around a Heat Source in a Fractured Porous Medium." *Proceedings of the Second International Symposium on Two-Phase Flow Modelling and Experimentation Pisa, Italy, 23–26 May, 1999*. Celata, G.P., Di Marco, P., and Shah, R.K., eds. *III*, III-1849–III-1856. Pisa, Italy: Edizioni ETS. TIC: 259792.

LeCain, G.D. 1995. *Pneumatic Testing in 45-Degree-Inclined Boreholes in Ash-Flow Tuff near Superior, Arizona.* Water-Resources Investigations Report 95-4073. Denver, Colorado: U.S. Geological Survey. ACC: MOL.19960715.0083.

Levy, S.S.; Dobson, P.F.; Fayek, M.; Goodell, P.; Ku, R.; and Murrell, M.T. 2005. "Peña Blanca Natural Analogue." *Office of Science and Technology and International OSTI&I: Annual Report 2005.* DOE/RW-0581, 169–170. Washington, D.C.: U.S. Department of Energy, Office of Science and Technology and International. ACC: HQO.20060322.0021.

Marshall, B.D.; Neymark, L.A.; and Peterman, Z.E. 2003. "Estimation of Past Seepage Volumes from Calcite Distribution in the Topopah Spring Tuff, Yucca Mountain, Nevada." *Journal of Contaminant Hydrology, 62–63*, 237–247. New York, New York: Elsevier. TIC: 254210.

Mongano, G.S.; Singleton, W.L.; Moyer, T.C.; Beason, S.C.; Eatman, G.L.W.; Albin, A.L.; and Lung, R.C. 1999. *Geology of the ECRB Cross Drift–Exploratory Studies Facility, Yucca Mountain Project, Yucca Mountain, Nevada*. Deliverable SPG42GM3. Denver, Colorado: U.S. Geological Survey. ACC: MOL.20000324.0614.

Mukhopadhyay, S. and Tsang, Y.W. 2002. "Understanding the Anomalous Temperature Data from the Large Block Test at Yucca Mountain, Nevada." *Water Resources Research, 38* (10), 28-1 through 28-12. Washington, D.C.: American Geophysical Union. TIC: 253867.

Paces, J.B.; Neymark, L.A.; Marshall, B.D.; Whelan, J.F.; and Peterman, Z.E. 2001. *Ages and Origins of Calcite and Opal in the Exploratory Studies Facility Tunnel, Yucca Mountain, Nevada*. Water-Resources Investigations Report 01-4049. Denver, Colorado: U.S. Geological Survey. TIC: 251284.

Philip, J.R.; Knight, J.H.; and Waechter, R.T. 1989. "Unsaturated Seepage and Subterranean Holes: Conspectus, and Exclusion Problem for Circular Cylindrical Cavities." *Water Resources Research, 25* (1), 16–28. Washington, D.C.: American Geophysical Union. TIC: 239117.

Pruess, K.; Wang, J.S.Y.; and Tsang, Y.W. 1990. "On Thermohydrologic Conditions Near High-Level Nuclear Wastes Emplaced in Partially Saturated Fractured Tuff, 2. Effective Continuum Approximation." *Water Resources Research, 26* (6), 1249–1261. Washington, D.C.: American Geophysical Union. TIC: 224854.

Richards, L.A. 1931. "Capillary Conduction of Liquids Through Porous Mediums." *Physics, 1*, 318–333. New York, New York: American Physical Society. TIC: 225383.

Salve, R. 2005. "Observations of Preferential Flow During a Liquid Release Experiment in Fractured Welded Tuffs." *Water Resources Research, 41,* 1–14. Washington, D.C.: American Geophysical Union. TIC: 258071.

SNL (Sandia National Laboratories) 2007a. *Abstraction of Drift Seepage.* MDL-NBS-HS-000019 REV 01, ADD 01. Las Vegas, Nevada: Sandia National Laboratories. ACC: DOC.20070807.0001.

SNL 2007b. *UZ Flow Models and Submodels*. MDL-NBS-HS-000006 REV 03 ADD 01. Las Vegas, Nevada: Sandia National Laboratories. ACC: DOC.20080108.0003.

SNL 2007c. *Total System Performance Assessment Data Input Package for Requirements Analysis for Transportation Aging and Disposal Canister and Related Waste Package Physical Attributes Basis for Performance Assessment*. TDR-TDIP-ES-000006 REV 00. Las Vegas, Nevada: Sandia National Laboratories. ACC: DOC.20070918.0005.

SNL 2007d. *Thermal Testing Measurements Report*. TDR-MGR-HS-000002 REV 01. Las Vegas, Nevada: Sandia National Laboratories. ACC: DOC.20070307.0010.

SNL 2007e. *Seismic Consequence Abstraction*. MDL-WIS-PA-000003 REV 03. Las Vegas, Nevada: Sandia National Laboratories. ACC: DOC.20070928.0011.

SNL 2007f. *THC Sensitivity Study of Heterogeneous Permeability and Capillarity Effects*. ANL-NBS-HS-000047 REV 01. Las Vegas, Nevada: Sandia National Laboratories. ACC: DOC.20070807.0006.

SNL 2007g. *In-Drift Natural Convection and Condensation*. MDL-EBS-MD-000001 REV 00 ADD 01. Las Vegas, Nevada: Sandia National Laboratories. ACC: DOC.20070907.0004.

SNL 2007h. *Drift-Scale THC Seepage Model*. MDL-NBS-HS-000001 REV 05. Las Vegas, Nevada: Sandia National Laboratories. ACC: DOC.20071010.000.

SNL 2008a. *Total System Performance Assessment Model/Analysis for the License Application*. MDL-WIS-PA-000005 REV 00 ADD 01. Las Vegas, Nevada: Sandia National Laboratories. ACC: DOC.20080312.0001.

SNL 2008b. *Multiscale Thermohydrologic Model*. ANL-EBS-MD-000049 REV 03 ADD 02. Las Vegas, Nevada: Sandia National Laboratories. ACC: DOC.20080201.0003.

Tsang, Y.W. and Birkholzer, J.T. 1999. "Predictions and Observations of the Thermal-Hydrological Conditions in the Single Heater Test." *Journal of Contaminant Hydrology, 38* (1–3), 385–425. New York, New York: Elsevier. TIC: 244160.

van Genuchten, M.T. 1980. "A Closed-Form Equation for Predicting the Hydraulic Conductivity of Unsaturated Soils." *Soil Science Society of America Journal, 44* (5), 892–898. Madison, Wisconsin: Soil Science Society of America. TIC: 217327.

Wang, J.S.Y. and Elsworth, D. 1999. "Permeability Changes Induced by Excavation in Fractured Tuff." *Rock Mechanics for Industry, Proceedings of the 37th U.S. Rock Mechanics Symposium, Vail, Colorado, USA, 6–9 June 1999*, Amadei, B.; Kranz, R.L.; Scott, G.A.; and Smeallie, P.H., eds. *2*, 751–757. Brookfield, Vermont: A.A. Balkema. TIC: 245246.

Wang, J.S.Y.; Trautz, R.C.; Cook, P.J.; Finsterle, S.; James, A.L.; and Birkholzer, J. 1999. "Field Tests and Model Analyses of Seepage into Drift." *Journal of Contaminant Hydrology, 38*, (1-3), 323-347. New York, New York: Elsevier. TIC: 244160.

Whelan, J.F.; Paces, J.B.; and Peterman, Z.E. 2002. "Physical and Stable-Isotope Evidence for Formation of Secondary Calcite and Silica in the Unsaturated Zone, Yucca Mountain, Nevada." *Applied Geochemistry, 17* (6), 735–750. New York, New York: Elsevier. TIC: 253462.

Zhou, Q.; Salve, R.; Liu, H.-H.; Wang, J.S.Y.; and Hudson, D. 2006. "Analysis of a Mesoscale Infiltration and Water Seepage Test in Unsaturated Fractured Rock: Spatial Variabilities and Discrete Fracture Patterns." *Journal of Contaminant Hydrology, 87,* 96–122. New York, New York: Elsevier. TIC: 258803.

Ziegler, J.D. 2005. Report of Unexpected Geologic Condition, South Ramp of the Exploratory Studies Facility between Stations 75+00 and 76+00. Letter from J.D. Ziegler (DOE/ORD) to J.D. Parrott (NRC), March 23, 2005, 0324055103, MFR: OLA&S:DHC-0848, with enclosure. ACC: MOL.20050406.0362.

INTENTIONALLY LEFT BLANK

Table 2.3.3-1. Features, Events, and Processes Addressed in Section 2.3.3

FEP Number and FEP Name	FEP Description	Summary of Technical Basis and Approach for FEP Inclusion
1.1.02.02.0A Preclosure ventilation	The duration of preclosure ventilation acts together with waste package spacing (as per design) to control the extent of the boiling front (zone of reduced water content).	The effects of preclosure ventilation on seepage are accounted for through the calculation of time-dependent thermal conditions in the drift, which affect drift-wall temperature and, thus, the duration of thermal seepage. The ventilation model provides the basis for estimating the fraction of heat removed during the 50-year preclosure period following emplacement. The seepage model for performance assessment and the coupled processes seepage models conservatively do not explicitly account for rock drying in the drift vicinity as a result of evaporation driven by preclosure ventilation (Sections 2.3.3.2.1.2 and 2.3.3.2.4.2.4).
1.2.02.01.0A Fractures	Groundwater flow in the Yucca Mountain region and transport of any released radionuclides may take place along fractures. The rate of flow and the extent of transport in fractures are influenced by characteristics such as orientation, aperture, asperity, fracture length, connectivity, and the nature of any linings or infills.	The seepage calibration model and seepage model for performance assessment are stochastic fracture continuum models. On the drift scale (relevant for seepage), the fracture network is considered a continuum (Section 2.3.3.2.3.2); its characteristics are determined from air injection tests (Section 2.3.3.2.2.1.2) and through model calibration (Section 2.3.3.2.3.3). The models used to estimate percolation flux and coupled processes relevant for seepage are based on a dual-permeability approach, which incorporates fracture and matrix properties averaged for different hydrogeologic units (Sections 2.3.3.2.1.3, 2.3.3.2.3.6, 2.3.3.2.4.1, and 2.3.3.3.3).
1.2.02.02.0A Faults	Numerous faults of various sizes have been noted in the Yucca Mountain region, and specifically in the repository area. Faults may represent an alteration of the rock permeability and continuity of the rock mass, an alteration or short circuiting of the flow paths and flow distributions close to the repository, and/or unexpected pathways through the repository.	Faults as potential conduits for fluid flow are explicitly accounted for in the site-scale unsaturated flow zone model providing the large-scale percolation flux distributions that feeds into the drift seepage abstraction. Thus, the potentially large fluxes expected in fault zones are included in the seepage predictions, and are propagated through the seepage abstraction to the TSPA (Sections 2.3.3.2.2.1, 2.3.3.2.3, 2.3.3.2.4, and 2.3.3.4).
1.2.03.02.0D Seismic induced drift collapse alters in drift thermohydrology	Seismic activity could produce jointed rock motion and/or changes in rock stress, leading to enhanced drift collapse and/or rubble infill throughout part or all of the drifts. Drift collapse could impact flow pathways and condensation within the EBS, mechanisms for water contact with EBS components, and thermal properties within the EBS.	The changes in drift shape as a result of seismic activity and their impact on seepage are explicitly accounted for in the TSPA drift seepage submodel. Drifts are categorized with respect to seismically-induced degradation at each time step considered in the TSPA. Seepage is then determined, depending on the category. For example, ambient seepage into a collapsed drift is calculated using a seepage lookup table specifically developed for such conditions by the seepage model for performance assessment (Sections 2.3.3.2.3.4.2, 2.3.3.2.4.2.2, 2.3.3.3.4, and 2.3.3.4).

Table 2.3.3-1. Features, Events, and Processes Addressed in Section 2.3.3 (Continued)

FEP Number and FEP Name	FEP Description	Summary of Technical Basis and Approach for FEP Inclusion
1.2.04.03.0A Igneous intrusion into repository	Magma from an igneous intrusion may flow into the drifts and extend over a large portion of the repository site, forming a sill, dike, or dike swarm, depending on the stress conditions. This intrusion could involve multiple drifts. The sill could be limited to the drifts, or a continuous sill could form along the plane of the repository, bridging between adjacent drifts.	The strong changes in the drift conditions caused by igneous intrusion, and their impact on seepage, are incorporated in the TSPA drift seepage submodel using a conservative abstraction. Given the uncertainties in predicting seepage processes under such conditions, seepage is set to the local percolation flux arriving at the intruded drift (i.e., no barrier capability is considered there (Sections 2.3.3.2.1.2, 2.3.3.2.4.2, and 2.3.3.3.4).
1.3.01.00.0A Climate change	Climate change may affect the long-term performance of the repository. This includes the effects of long-term change in global climate (e.g., glacial–interglacial cycles) and shorter-term change in regional and local climate. Climate is typically characterized by temporal variations in precipitation and temperature.	The impact of global climate change on seepage is included in TSPA through the calculation of percolation fluxes as a function of climatic conditions. The climate analysis is used to determine the expected climatic conditions that affect net infiltration and, ultimately, the percolation flux at the repository horizon. The unsaturated zone flow fields calculated for different global climate states are sampled in TSPA to obtain the local percolation flux, which is used to evaluate drift seepage. Short-term changes in regional and local climate (e.g., temporal variations in precipitation) are not explicitly accounted for in the seepage calculation, as these short-term fluctuations are considerably damped at the repository horizon. However, related uncertainties and variabilities in the local percolation flux are included in the TSPA drift seepage submodel of the TSPA (Sections 2.3.3.2.1.3, 2.3.3.2.3.5, 2.3.3.2.3.6.3, 2.3.3.2.4, 2.3.3.3.3, and 2.3.3.4).
1.4.01.01.0A Climate modification increases recharge	Climate modification causes an increase in recharge in the Yucca Mountain region. Increased recharge might lead to increased flux through the repository, perched water, or water table rise.	The effects of climate changes on seepage are included explicitly in the TSPA through the unsaturated zone flow fields used to evaluate the seepage-relevant local percolation flux. Flow fields are evaluated for three distinct climate states during the pre-10,000-year period (present-day, monsoon, and glacial transition) and one climate state representing the post-10,000-year period. Uncertainty in each climate state and the resulting net infiltration is accounted for through the use of four alternative unsaturated zone flow fields, which represent different infiltration scenarios (Sections 2.3.3.2.1.3, 2.3.3.2.3.5, 2.3.3.2.3.6.3, 2.3.3.2.4, 2.3.3.3.3, 2.3.3.3.4, and 2.3.3.4).

Table 2.3.3-1. Features, Events, and Processes Addressed in Section 2.3.3 (Continued)

FEP Number and FEP Name	FEP Description	Summary of Technical Basis and Approach for FEP Inclusion
2.1.08.01.0A Water influx at the repository	An increase in the unsaturated water flux at the repository may affect thermal, hydrologic, chemical, and mechanical behavior of the system. Increases in flux could result from climate change, but the cause of the increase is not an essential part of the FEP.	The local percolation flux is one of the key factors affecting drift seepage. Spatial and temporal changes in the local percolation flux are thus included in TSPA. The local percolation flux is explicitly evaluated for different climate states, different infiltration scenarios, and different locations within the repository. Moreover, the local percolation flux is modified to account for random, intermediate-scale flow focusing effects and the impact of small-scale heterogeneity. For both ambient and thermal conditions, the local percolation flux is used to evaluate seepage into waste emplacement drifts, as provided in lookup tables from the seepage model for performance assessment (Sections 2.3.3.2.1.3, 2.3.3.2.3.5, 2.3.3.2.3.6.3, 2.3.3.2.4, 2.3.3.3.3, 2.3.3.3.4, and 2.3.3.4).
2.1.08.02.0A Enhanced influx at the repository	An opening in unsaturated rock may alter the hydraulic potential, affecting local saturation around the opening and redirecting flow. Some of the flow may be directed to the opening, where it is available to seep into the opening.	The impact of an underground opening on the unsaturated flow field (including capillary barrier effect and the related flow diversion around the drifts) and its relevance for seepage is explicitly captured in the seepage calibration model, the seepage model for performance assessment and the thermal-hydrologic seepage model, which provide the basis for the seepage evaluation in TSPA (Sections 2.3.3.2.1.3, 2.3.3.2.2.1, 2.3.3.2.3, 2.3.3.2.4, 2.3.3.3.3, 2.3.3.3.4, and 2.3.3.4).
2.1.08.03.0A Repository dry-out due to waste heat	Repository heat evaporates water from the unsaturated zone rocks near the drifts, as the temperature exceeds the vaporization temperature. This zone of reduced water content (reduced saturation) could migrate outward during the heating phase and then migrate back to the waste package as heat diffuses throughout the mountain and the radioactive heat sources decay. This FEP addresses the effects of dryout within the repository drifts.	This FEP is included in the thermal-hydrologic seepage model (Section 2.3.3.3), which feeds into the drift seepage abstraction and TSPA. The thermal-hydrologic seepage model captures repository dryout during the heating phase and rewetting during the cooling phase. These processes are also captured by other coupled processes models providing direct or indirect input to the TSPA, such as the multiscale thermal-hydrologic model (Section 2.3.5.4.1) and the thermal-hydrologic-chemical seepage model (Section 2.3.5.3).
2.1.08.11.0A Repository resaturation due to waste cooling	Following the peak thermal period, water in the condensation cap may flow downward, resaturating the geosphere dryout zone and flowing into the drifts. This may lead to an increase in water content and/or resaturation in the repository.	The thermal-hydrologic seepage model (Section 2.3.3.3), which feeds into the seepage abstraction, explicitly simulates dryout of the repository, followed by resaturation as the waste packages cool. Dryout and resaturation effects are also captured by other coupled processes models providing direct or indirect input to the TSPA, such as the multiscale thermal-hydrologic model (Section 2.3.5.4.1) and the thermal-hydrologic-chemical seepage model (Section 2.3.5.3).

Table 2.3.3-1. Features, Events, and Processes Addressed in Section 2.3.3 (Continued)

FEP Number and FEP Name	FEP Description	Summary of Technical Basis and Approach for FEP Inclusion
2.1.11.01.0A Heat generation in EBS	Temperature in the waste and EBS will vary through time. Heat from radioactive decay will be the primary cause of temperature change, but other factors to be considered in determining the temperature history include the in situ geothermal gradient, thermal properties of the rock, EBS, and waste materials, hydrologic effects, and the possibility of exothermic reactions. Considerations of the heat generated by radioactive decay should take different properties of different waste types, including DOE SNF, into account.	The thermal-hydrologic seepage model (Section 2.3.3.3), which feeds into the seepage abstraction and TSPA, explicitly simulates the temperature buildup in the EBS and the near-field rock. The model uses prescribed heat generation rates consistent with the multi-scale thermal-hydrologic model (Section 2.3.5.4.1), the thermal-hydrologic-chemical seepage model (Section 2.3.5.3), and the in-drift condensation model (Section 2.3.5.4.2). The calculated temperatures are influenced not only by the heat of radionuclide decay, but also by the geothermal gradient from the ground surface to the water table and the thermal-physical properties of the rock and significant EBS features. The thermal effects from having different types of waste forms, including DOE SNF, are represented by four alternative heat generation rates accounting for temperature variability. Exothermic reactions (FEP 2.1.11.03.0A) produce insignificant amounts of heat and are not included in TSPA.
2.2.01.01.0A Mechanical effects of excavation and construction in the near field	Excavation will produce some disturbance of the rocks surrounding the drifts due to stress relief. Stresses associated directly with excavation (e.g., boring and blasting operations) may also cause some changes in rock properties. Properties that may be affected include rock strength, fracture spacing, and block size, and hydrologic properties, such as permeability.	Excavation effects and their impacts on seepage are included in the TSPA through the use of seepage-relevant parameters calibrated for the excavation-disturbed zone around niches and drifts (Sections 2.3.3.2.2.1, 2.3.3.2.3, 2.3.3.2.4, 2.3.3.3.3, 2.3.3.3.4, and 2.3.3.4).
2.2.03.01.0A Stratigraphy	Stratigraphic information is necessary information for the performance assessment. This information should include identification of the relevant rock units, soils, and alluvium and their thickness, lateral extents, and relationships to each other. Major discontinuities should be identified.	Stratigraphic information is used in TSPA to evaluate seepage into waste emplacement drifts located in specific hydrogeologic units. Seepage-relevant parameters (permeability and capillary strength) are evaluated separately for lithophysal and nonlithophysal rock units, and the percolation flux used to determine seepage is taken from the unsaturated zone flow fields, which incorporate stratigraphic information. Seepage is evaluated for specific repository locations, capturing their respective host rock unit (Sections 2.3.3.2.1.1, 2.3.3.2.1.3, 2.3.3.2.2.1, 2.3.3.2.3, 2.3.3.2.4, 2.3.3.3.2, 2.3.3.3.3, 2.3.3.3.4, and 2.3.3.4).

Table 2.3.3-1. Features, Events, and Processes Addressed in Section 2.3.3 (Continued)

FEP Number and FEP Name	FEP Description	Summary of Technical Basis and Approach for FEP Inclusion
2.2.03.02.0A Rock properties of host rock and other units	Physical properties, such as porosity and permeability of the relevant rock units, soils, and alluvium, are necessary for the performance assessment. Possible heterogeneities in these properties should be considered. Questions concerning events and processes that may cause these physical properties to change over time are considered in other FEPs.	Properties affecting seepage are defined for each of the repository rock units, using appropriate probability distributions that describe their repository-wide variability. The impact of heterogeneity on percolation flux is included through the spatial variability incorporated in the unsaturated zone flow fields, plus the additional variability introduced by flow-focusing factors. The impact of small-scale heterogeneity on seepage is explicitly modeled in (1) the seepage calibration model; (2) the seepage model for performance assessment; and (3) the thermal-hydrologic seepage model. These provide the basis for the seepage evaluation in the TSPA. The impact of potential changes in the physical properties as a result of coupled thermal, mechanical, and chemical processes has been evaluated and considered insignificant (see excluded FEPs 2.2.01.02.0A, 2.2.10.04.0A, 2.2.10.04.0B, 2.2.10.05.0A, and 2.2.10.06.0A, as identified in Section 2.2, Table 2.2-5) (Sections 2.3.3.2.1.3, 2.3.3.2.2.2, 2.3.3.2.3, 2.3.3.2.3.3, 2.3.3.2.4, 2.3.3.3.3, 2.3.3.3.3.4, 2.3.3.3.4, and 2.3.3.4).
2.2.07.02.0A Unsaturated groundwater flow in the geosphere	Groundwater flow occurs in unsaturated rocks in most locations above the water table at Yucca Mountain, including at the location of the repository. See related FEPs for discussions of specific issues related to unsaturated flow.	The impact of unsaturated flow at the repository level on seepage is included in TSPA through the use of local percolation fluxes, which are derived from site-scale unsaturated flow fields, intermediate-scale flow focusing factors, and small-scale flow simulations with a heterogeneous fracture permeability field (Sections 2.3.3.2, 2.3.3.3, and 2.3.3.4).
2.2.07.03.0A Capillary rise in the unsaturated zone	Capillary rise involves the drawing up of water, above the water table or above locally saturated zones, in continuous pores of the unsaturated zone until the suction gradient is balanced by the gravitational pull downward.	Capillary forces and their impact on seepage are included in TSPA through the explicit simulation of capillary- and gravity-driven water flow toward, around, and into waste emplacement drifts. Site-specific, seepage-relevant capillary strength parameters have been calculated using the seepage calibration model and data from liquid-release tests (Sections 2.3.3.2.1.2, 2.3.3.2.1.3, 2.3.3.2.2.1, 2.3.3.2.2.2, 2.3.3.2.3, 2.3.3.2.4, 2.3.3.3.3, 2.3.3.3.4, and 2.3.3.4).

Table 2.3.3-1. Features, Events, and Processes Addressed in Section 2.3.3 (Continued)

FEP Number and FEP Name	FEP Description	Summary of Technical Basis and Approach for FEP Inclusion
2.2.07.04.0A Focusing of unsaturated flow (fingers, weeps)	Unsaturated flow can differentiate into zones of greater and lower saturation (fingers) that may persist as preferential flow paths. Heterogeneities in rock properties, including fractures and faults, may contribute to focusing. Focused flow may become locally saturated.	The unsaturated zone flow fields represent the large-scale redistribution of infiltrating water as it percolates through hydrogeologic layers, with matrix, fractures, and faults explicitly taken into account. Intermediate-scale focusing of flow from the site scale to the drift scale is accounted for in the drift seepage abstraction by using a distribution of flow focusing factors, which were determined from high-resolution simulations of flow in a heterogeneous fracture continuum. Preferential flow induced by small-scale heterogeneity is explicitly accounted for in the suite of seepage process models that feed the drift seepage abstraction and TSPA by using multiple, stochastic, heterogeneous fracture permeability fields. Thus, preferential flow is addressed in the seepage lookup tables and in the thermal component of the drift seepage abstraction (Sections 2.3.3.2.1.3, 2.3.3.2.2.1, 2.3.3.2.2.2, 2.3.3.2.3.5, 2.3.3.2.3.6, 2.3.3.2.4, and 2.3.3.4).
2.2.07.08.0A Fracture flow in the unsaturated zone	Fractures or other analogous channels may act as conduits for fluids to move into the subsurface to interact with the repository and as conduits for fluids to leave the vicinity of the repository and be conducted to the saturated zone. Water may flow through only a portion of the fracture network, including flow through a restricted portion of a given fracture plane.	Fractures as potential conduits for fluid flow are explicitly accounted for in the site-scale unsaturated zone flow model providing the large-scale percolation flux distribution and the drift-scale models used to evaluate seepage under ambient and thermal conditions. The fact that water may only flow through a portion of the fracture network is accounted for through the use of (1) the active fracture model (on the mountain scale), (2) flow focusing factors (on the intermediate scale), and (3) explicit simulation of preferential flow (on the drift scale). Thus, fracture flow and its spatial distribution are embedded in the lookup tables for seepage and propagated to TSPA (Sections 2.3.3.2.1.3, 2.3.3.2.2.1, 2.3.3.2.2.2, 2.3.3.2.3, 2.3.3.2.4, 2.3.3.3.3, 2.3.3.3.4, and 2.3.3.4).
2.2.07.09.0A Matrix imbibition in the unsaturated zone	Water flowing in fractures or other channels in the unsaturated zone may be imbibed into the surrounding rock matrix. This may occur during steady flow, episodic flow, or into matrix pores that have been dried out during the thermal period.	Imbibition of water into the matrix is included in the unsaturated zone flow model that provides the percolation flux for the drift-scale seepage process models and TSPA. The ambient seepage models are stochastic fracture continuum models; the impact of the matrix on seepage during both the liquid-release tests used for model calibration and the calculation of steady-state ambient seepage into waste emplacement drifts is considered small enough that it can be lumped into seepage-relevant parameters applied to the fracture continuum. The thermal-hydrologic seepage model and other drift-scale coupled processes models, on the other hand, include the rock matrix because the matrix impacts heat transfer and provides a source for water that evaporates during above-boiling temperature conditions (Sections 2.3.3.2.1.3, 2.3.3.2.2.1, 2.3.3.2.2.2, 2.3.3.2.3, 2.3.3.2.4, 2.3.3.3.3, 2.3.3.3.4, and 2.3.3.4).

Table 2.3.3-1. Features, Events, and Processes Addressed in Section 2.3.3 (Continued)

FEP Number and FEP Name	FEP Description	Summary of Technical Basis and Approach for FEP Inclusion
2.2.07.10.0A Condensation zone forms around drifts	Condensation of the two-phase flow generated by repository heat may form in the rock where the temperature drops below the local vaporization temperature. Waste package emplacement geometry and thermal loading may affect the scale at which condensation caps form (over waste packages, over panels, or over the entire repository) and the extent to which shedding will occur as water flows from the region above one drift to the region above another drift or into the rock between drifts.	The coupled thermal-hydrologic processes of vapor condensation during the thermal period, which potentially leads to water accumulation above the drifts and shedding between drifts, is explicitly simulated with the thermal-hydrologic process seepage model that feeds into the drift seepage abstraction and TSPA (Sections 2.3.3.2.1.2, 2.3.3.2.1.3, 2.3.3.3, and 2.3.3.4). Vapor condensation in the rock is also captured by other coupled processes models providing direct or indirect input to the TSPA, such as the multiscale thermal-hydrologic model (Section 2.3.5.4.1) and the thermal-hydrologic-chemical seepage model (Section 2.3.5.3).
2.2.07.11.0A Resaturation of geosphere dryout zone	Following the peak thermal period, water in the condensation cap may flow downward into the drifts. Influx of cooler water from above, such as might occur from episodic flow, may accelerate return flow from the condensation cap by lowering temperatures below the condensation point. Percolating groundwater will also contribute to resaturation of the dryout zone. Vapor flow, as distinct from liquid flow by capillary processes, may also contribute.	Resaturation of the vaporization zone around drifts and the potential of return flow of condensation water to the drifts are processes explicitly simulated in the thermal-hydrologic seepage model that feeds the drift seepage abstraction and TSPA. The impact of potential episodic flow events penetrating the dryout zone during the thermal period has been addressed using an alternative conceptual model that corroborated the results obtained with the thermal-hydrologic seepage model (Section 2.3.3.3). Resaturation effects are also captured by other coupled processes models providing direct or indirect input to the TSPA, such as the multiscale thermal-hydrologic model (Section 2.3.5.4.1) and the thermal-hydrologic-chemical seepage model (Section 2.3.5.3).
2.2.07.18.0A Film flow into the repository	Water may enter waste emplacement drifts by a film-flow process. This differs from the traditional view of flow in a capillary network where the wetting phase exclusively occupies capillaries with apertures smaller than some level defined by the capillary pressure. A film-flow process could allow water to enter a waste emplacement drift at nonzero capillary pressure. Dripping into the drifts could also occur through collection of the film flow on the local minima of surface roughness features along the crown of the drift.	The impact of film flow through the fracture network leading to potential drop detachment at the drift wall is implicitly accounted for in the seepage-relevant parameters estimated by the seepage calibration model, which is calibrated against seepage-rate data from liquid-release tests. These seepage-rate data include film flow water appearing at and detaching from the drift wall. The seepage-relevant parameters thus include the effect of film flow; these parameters are propagated to the drift seepage abstraction and TSPA (Sections 2.3.3.2.1.3, 2.3.3.2.2.1, 2.3.3.2.2.2, and 2.3.3.2.3).

Table 2.3.3-1. Features, Events, and Processes Addressed in Section 2.3.3 (Continued)

FEP Number and FEP Name	FEP Description	Summary of Technical Basis and Approach for FEP Inclusion
2.2.07.20.0A Flow diversion around repository drifts	Flow in unsaturated rock tends to be diverted by openings, such as waste emplacement drifts, due to the effects of capillary forces. The resulting diversion of flow could have an effect on seepage into the repository. Flow diversion around the drift openings could also lead to the development of a zone of lower flow rates and low saturation beneath the drift, known as the drift shadow.	The impact of flow diversion around underground openings and its relevance for seepage are explicitly captured by the suite of seepage process models that feed into the drift seepage abstraction and TSPA. The seepage calibration model and seepage model for performance assessment simulate water flow driven by capillary forces and gravity, which are the main processes leading to flow diversion around and seepage into waste emplacement drifts. Site-specific, seepage-relevant parameters characterizing the capillary-barrier and flow-diversion effects are estimated from seepage-rate data and are propagated through the drift seepage abstraction to TSPA (Sections 2.3.3.2.1.3, 2.3.3.2.2.1, 2.3.3.2.2.2, 2.3.3.2.3, 2.3.3.2.4, 2.3.3.3.3, 2.3.3.3.4, and 2.3.3.4).
2.2.10.03.0B Natural Geothermal Effects on Flow in the Unsaturated Zone	Infiltration into the subsurface provides a boundary condition for groundwater flow in the unsaturated zone. The amount and location of the infiltration influences the amount of seepage entering the drifts; and the amount and location of recharge influences the height of the water table, the hydraulic gradient, and therefore specific discharge. Different sources of infiltration could change the composition of groundwater passing through the repository. Mixing of these waters with other groundwaters could result in mineral precipitation, dissolution, and altered chemical gradients in the subsurface.	The hydrologic effects of infiltration and recharge are included in the infiltration model (Section 2.3.1). The time dependence of infiltration results is linked to the timing of climate change (Section 2.3.1). This is incorporated in TSPA through the unsaturated zone flow fields used to evaluate the seepage-relevant local percolation flux. Flow fields are evaluated for three distinct climate states during the pre-10,000-year period (present-day, monsoon, and glacial transition) and one climate state representing the post-10,000-year period. Uncertainty in each climate state and the resulting net infiltration is accounted for through the use of four alternative unsaturated zone flow fields, which represent different infiltration scenarios (Sections 2.3.3.2.1.3, 2.3.3.2.3.5, 2.3.3.2.3.6.3, 2.3.3.2.4, 2.3.3.3.3, 2.3.3.3.4, and 2.3.3.4).

Table 2.3.3-1. Features, Events, and Processes Addressed in Section 2.3.3 (Continued)

FEP Number and FEP Name	FEP Description	Summary of Technical Basis and Approach for FEP Inclusion
2.2.10.10.0A Two-phase buoyant flow/heat pipes	Heat from waste can generate two-phase buoyant flow. The vapor phase (water vapor) could escape from the mountain. A heat pipe consists of a system for transferring energy between a hot and a cold region (source and sink, respectively) using the heat of vaporization and movement of the vapor as the transfer mechanism. Two-phase circulation continues until the heat source is too weak to provide the thermal gradients required to drive it. Alteration of the rock adjacent to the drift may include dissolution that maintains the permeability necessary to support the circulation (as inferred for some geothermal systems).	The coupled thermal-hydrologic processes causing heat-pipe effects are explicitly simulated with the thermal-hydrologic seepage model, which feeds into the drift seepage abstraction. The impact of heat-pipe behavior on near-field conditions and seepage is assessed for various simulation cases and accounted for in the thermal seepage abstraction methodology (Sections 2.3.3.2.1.2, 2.3.3.3, and 2.3.3.4). Heat pipe effects are also captured by other coupled processes models providing direct or indirect input to the TSPA, such as the multiscale thermal-hydrologic model (Section 2.3.5.4.1) and the thermal-hydrologic-chemical seepage model (Section 2.3.5.3).
2.2.10.12.0A Geosphere dryout due to waste heat	Repository heat evaporates water from the unsaturated zone rocks near the drifts as the temperature exceeds the vaporization temperature. This zone of reduced water content (reduced saturation) migrates outward during the heating phase (about the first 1,000 years) and then migrates back to the waste packages as heat diffuses throughout the mountain, and the radioactive sources decay. This FEP addresses the effects of dryout within the rocks.	The coupled processes of vaporization, dryout, condensation, and resaturation are explicitly simulated using the thermal-hydrologic seepage model, which feeds into the drift seepage abstraction and TSPA (Section 2.3.3.3). These processes are also captured by other coupled processes models providing direct or indirect input to the TSPA, such as the multiscale thermal-hydrologic model (Section 2.3.5.4.1) and the thermal-hydrologic-chemical seepage model (Section 2.3.5.3).

Table 2.3.3-1. Features, Events, and Processes Addressed in Section 2.3.3 (Continued)

FEP Number and FEP Name	FEP Description	Summary of Technical Basis and Approach for FEP Inclusion
2.3.11.03.0A Infiltration and recharge	Infiltration into the subsurface provides a boundary condition for groundwater flow in the unsaturated zone. The amount and location of the infiltration influences the amount of seepage entering the drifts; and the amount and location of recharge influences the height of the water table, the hydraulic gradient, and therefore specific discharge. Different sources of infiltration could change the composition of groundwater passing through the repository. Mixing of these waters with other groundwaters could result in mineral precipitation, dissolution, and altered chemical gradients in the subsurface.	The hydrologic effects of infiltration and recharge are included in the infiltration model (Section 2.3.1). The time dependence of infiltration results is linked to the timing of climate change (Section 2.3.1). This is incorporated in TSPA through the unsaturated zone flow fields used to evaluate the seepage-relevant local percolation flux. Flow fields are evaluated for three distinct climate states during the pre-10,000-year period (present-day, monsoon, and glacial transition) and one climate state representing the post-10,000-year period. Uncertainty in each climate state and the resulting net infiltration is accounted for through the use of four alternative unsaturated zone flow fields, which represent different infiltration scenarios (Sections 2.3.3.2.1.3, 2.3.3.2.3.5, 2.3.3.2.3.6.3, 2.3.3.2.4, 2.3.3.3.3, 2.3.3.3.4, and 2.3.3.4).

Table 2.3.3-2. Summary Statistics of Estimated Capillary Strength Parameter for Lower Lithophysal and Middle Nonlithophysal Zone

Location		Interval	Number of Inversions[a]	Estimate 1/α (Pa)				
				Mean	Standard Deviation[b]	Standard Error[c]	Minimum	Maximum
Lower lithophysal zone (Tptpll)	SYBT-ECRB-LA#1	Zone 2	17	534.3	56.8	13.8	447.7	674.1
	SYBT-ECRB-LA#2	Zone 2	21	557.1	56.4	12.3	457.1	676.1
	SYBT-ECRB-LA#2	Zone 3	19	534.8	57.8	13.3	443.1	645.7
	SYBT-ECRB-LA#3	Zone 1	23	452.0	54.7	11.4	382.8	616.6
	Niche 5	Borehole 4	30	671.2	223.2	40.8	356.0	1,197.0
	Niche 5	Borehole 5	24	740.5	339.0	69.2	231.1	1,840.7
Middle nonlithophysal zone (Tptpmn)	Niche 3	Upper middle	1	741	—	—	—	—
	Niche 4	Upper left	1	646	—	—	—	—
	Niche 4	Upper middle	1	603	—	—	—	—
	Niche 4	Upper right	1	427	—	—	—	—

NOTE: [a]Each inversion is based on a different realization of the heterogeneous permeability field.
[b]Represents estimation uncertainty on account of small-scale heterogeneity (not available for estimates for the middle nonlithophysal zone).
[c]Standard error of mean.

Source: BSC 2004b, Table 6-8.

Table 2.3.3-3. Correlation between Rockfall Severity Class and Statistics of Rockfall Volume per Unit Drift Length for Nonlithophysal Rock

Severity	Total Rockfall Volume (m³/m)			
	Mean	Median	5th Percentile	95th percentile
1	0.0209	0.0128	0.0047	0.0539
2	0.1683	0.1093	0.0256	0.4198
3	0.4727	0.3547	0.1246	1.0908
4	1.4215	1.1772	0.5060	2.7261

Source: SNL 2007a, Table 6-4[a].

Table 2.3.3-4. Rockfall Volumes for Various Drift Degradation Simulation Cases in Lithophysal Rock

Realization Case	Ground Motion Number	Rock Mass Category Number	Rubble Volume (m³/m) by PGV H1 Level		
			0.4 m/s	1.05 m/s	2.44 m/s
1	4	3	0.06	2.26	104.75
2	8	5	0	7.63	67.92
3	16	4	0	3.22	69.3
4	12	1	2.13	5.62	109.77
5	2	3	0	3.62	84.2
6	8	1	2.46	3.11	109.85
7	14	2	0.06	5.52	76.59
8	4	4	0	3.42	94.52
9	10	2	0.03	0.58	94.28
10	6	3	0	11.84	60.83
11	9	1	7.16	21.95	82.53
12	1	1	2.12	4.35	111.21
13	1	3	0	0.79	103.52
14	7	4	0	28.96	62.22
15	11	4	0	14.38	72.16

Source: SNL 2007a, Table 6-1[a].

Table 2.3.3-5. Inputs Required by the TSPA Drift Seepage Submodel

Input	Attributes	Source
Probability distributions reflecting spatial variability of the capillary strength parameter, permeability, and the flow focusing factor	Used to sample parameter variability for each location, r, corresponding to the several thousand locations identified by the multiscale thermal-hydrologic model	Drift seepage abstraction
Uncertainty distributions for the capillary strength parameter and permeability	Used to sample parameter uncertainty for a particular realization, R. Applied to all locations and time steps	Drift seepage abstraction
Site-scale percolation flux distributions	Used to provide percolation flux at each location, r, corresponding to the several thousand locations identified by the multiscale thermal-hydrologic model Sixteen fluxes per location reflecting four climate states and four infiltration scenarios	TSPA EBS thermal-hydrologic environment submodel (generated by the site-scale unsaturated zone model and interpolated by the multiscale thermal-hydrologic model)
Response surfaces (i.e., lookup tables) of seepage rate as a function of the capillary strength parameter, permeability, and local percolation flux	Used to interpolate the mean seepage rate at each location, r, corresponding to the several thousand locations identified by the multiscale thermal-hydrologic model Used to sample seepage uncertainty for particular realization, R. Separate tables for intact and collapsed drifts	Drift seepage abstraction (generated by the seepage model for performance assessment)
Thermal-hydrologic variables (drift wall temperature)	Used to evaluate thermal seepage conditions at each location in each percolation subregion	TSPA EBS thermal-hydrologic environment submodel (generated by the multiscale thermal-hydrologic model)
Cumulative rockfall volume	Used to categorize drifts with respect to drift degradation, for particular realization, R, and rock unit	Seismic consequence abstraction (provides rock-type specific regression curves that link seismic event to rockfall volume)

Source: SNL 2007a, Section 6.7.
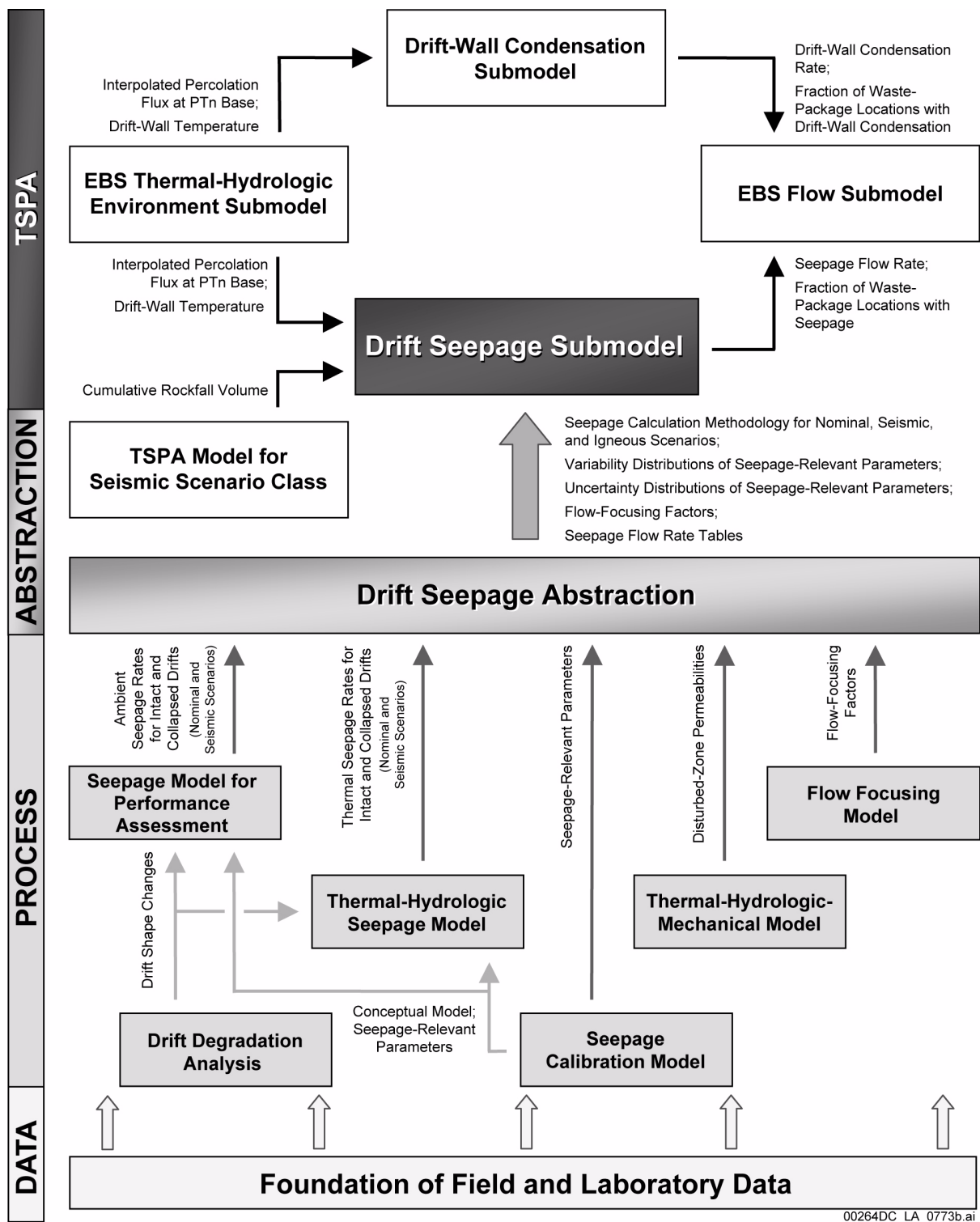
Figure 2.3.3-1.   Information Flow Supporting TSPA Seepage Calculations at the Data, Process,
                   Abstraction, and TSPA Levels

Source: Modified from SNL 2007a, Figure 1-1; SNL 2008a, Figure 6.3.3-2.
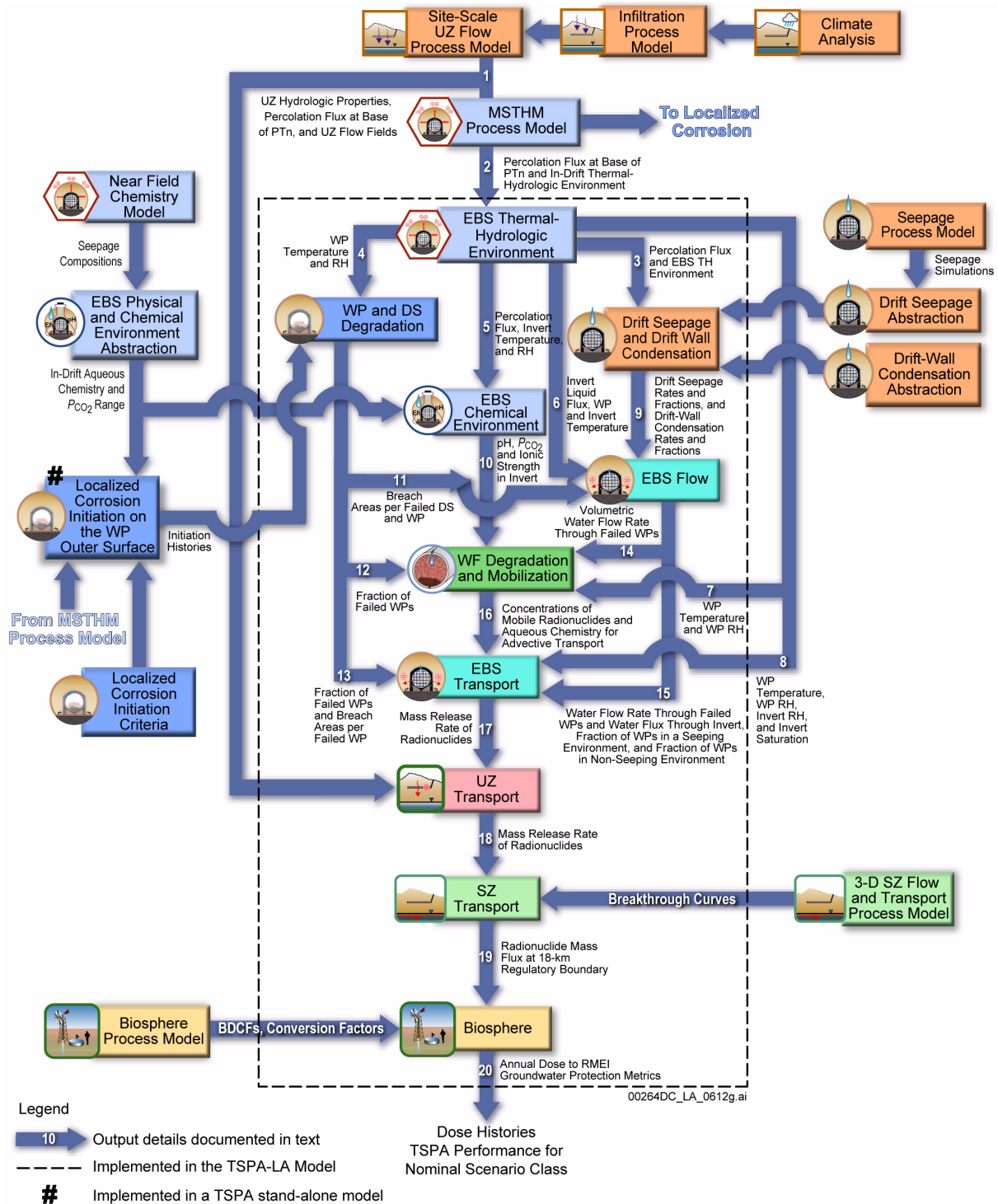
Figure 2.3.3-2.   Information Transfer Among the Principal Model Components of the TSPA Nominal
                    Scenario Class Model

NOTE: For details about outputs and information transfer shown on this figure, see Section 2.4.2.3.2.1.
        BDCF = biosphere dose conversion factor; DS = drip shield; LC = localized corrosion; PA = performance
        assessment; RH = relative humidity; RMEI = reasonably maximally exposed individual; SZ = saturated zone;
        TH = thermal-hydrologic; UZ = unsaturated zone; WF = waste form; WP = waste package.
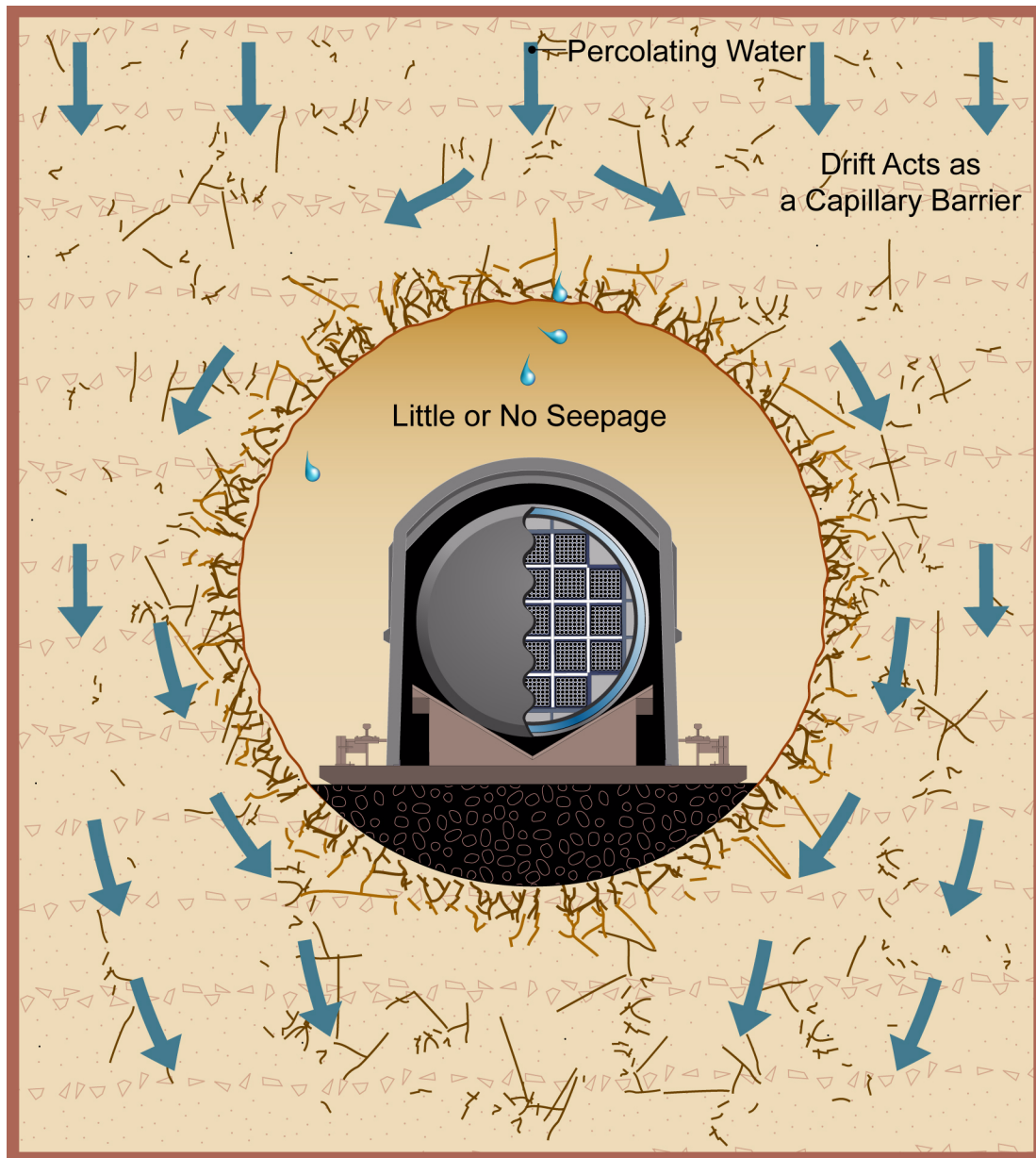
Drawing Not To Scale
00264DC_LA_0198f.ai

Figure 2.3.3-3.   Schematic Showing Reduced Seepage as a Result of Capillary Flow Diversion in the Unsaturated Zone
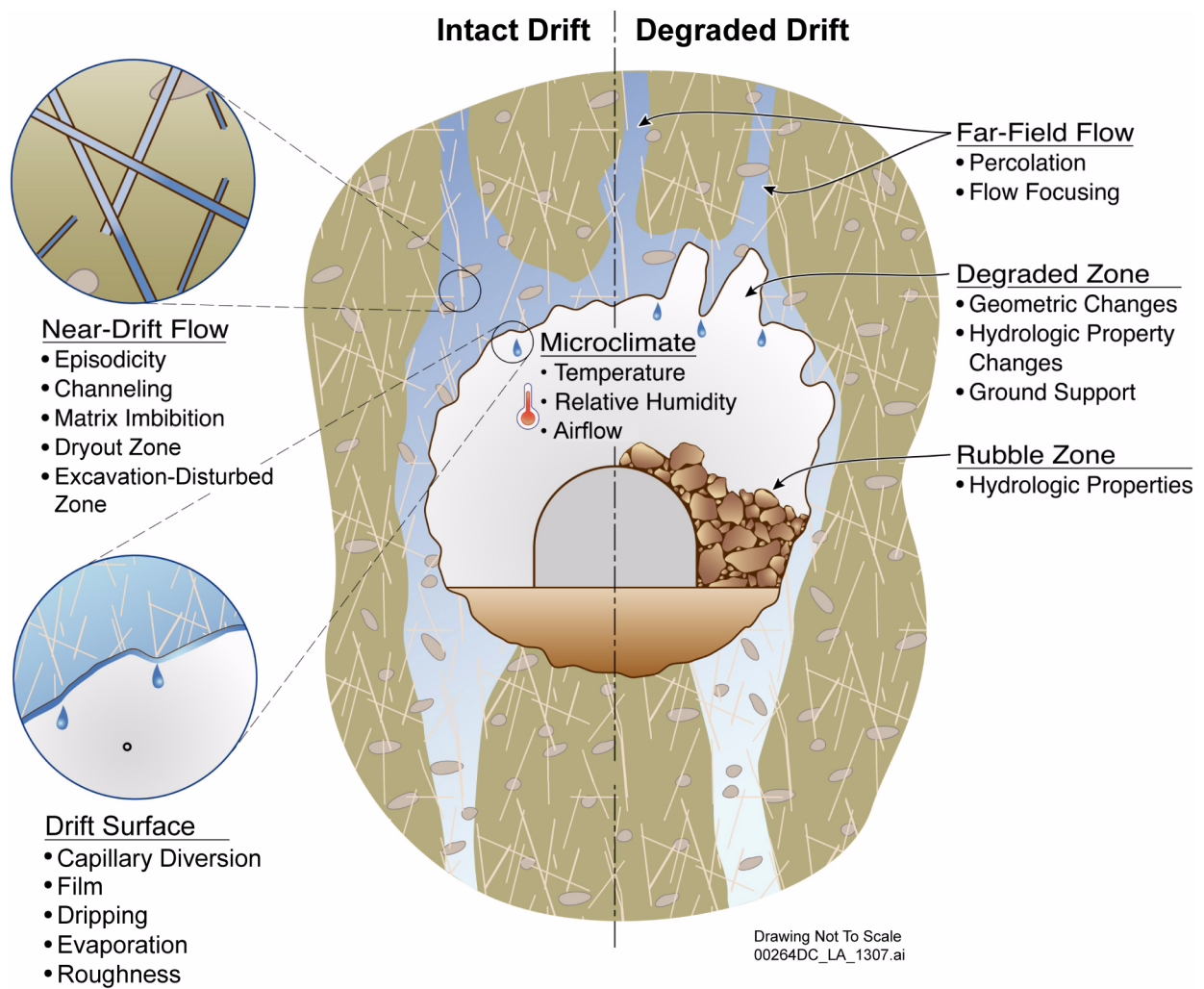
Figure 2.3.3-4. Schematic Showing Seepage Processes and Factors Potentially Affecting Seepage
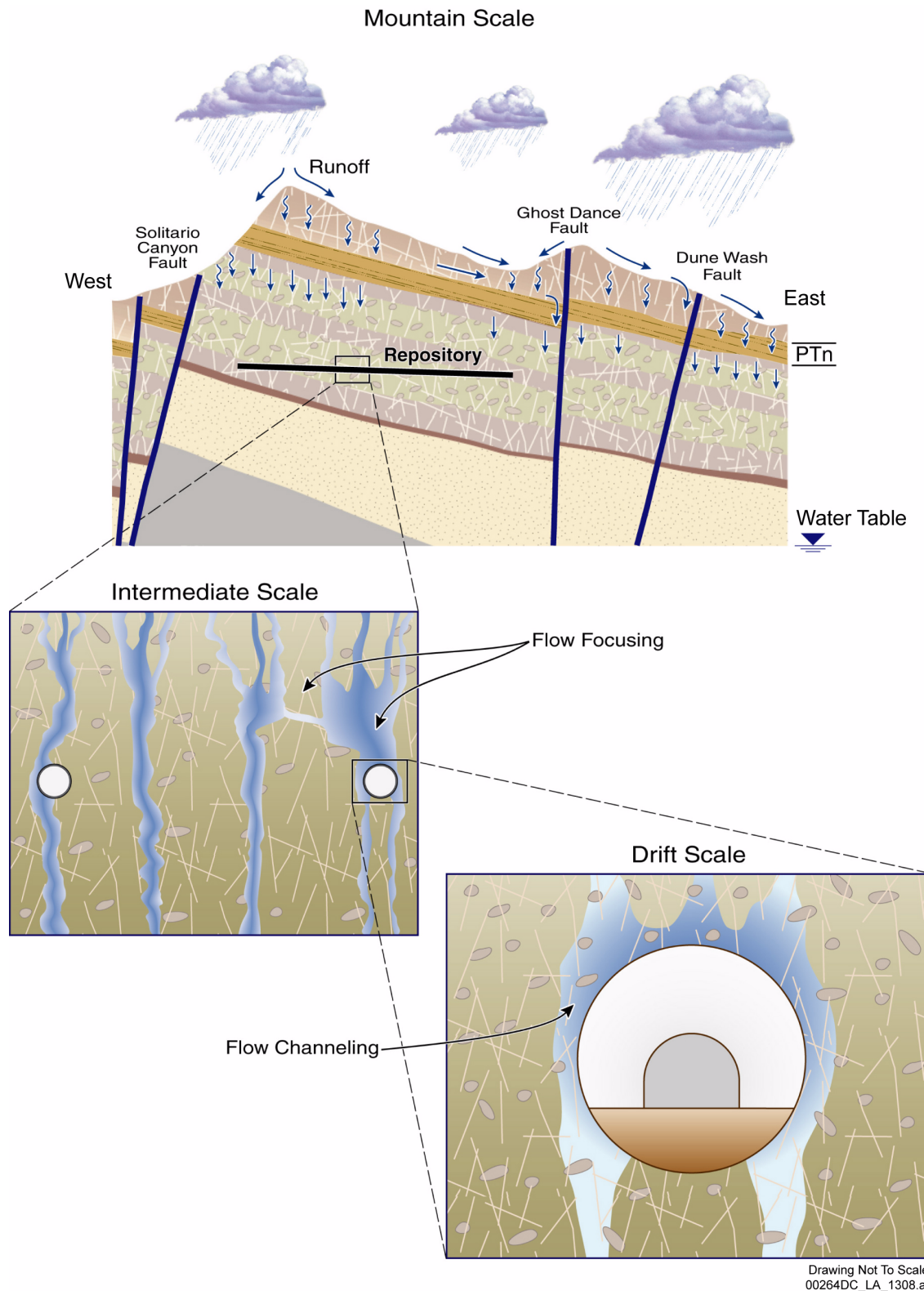
Figure 2.3.3-5. Schematic of Flow-Channeling Effects on Various Scales

NOTE: Flow-focusing factors are applied to account for flow-channeling effects between the intermediate-scale and drift-scale processes.

(a)

(b)

00264DC_LA_1309.ai
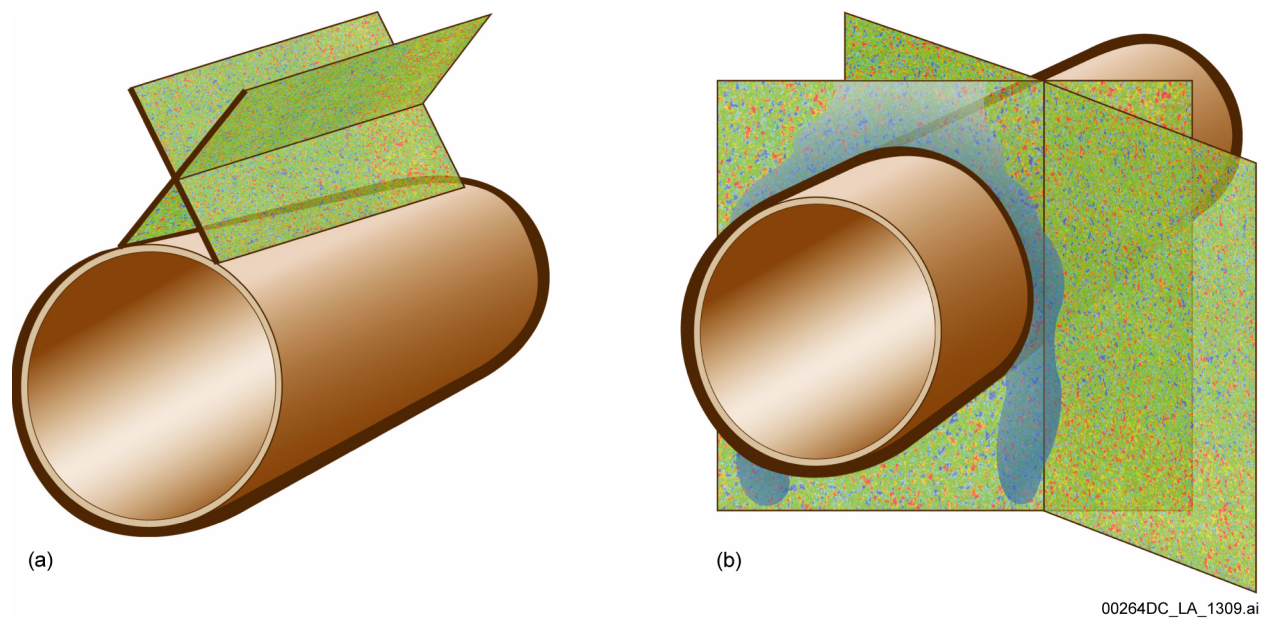
Figure 2.3.3-6. Schematic Showing Two Fractures Intersecting a Drift

NOTE: (a) A two-dimensional fracture network model assumes that all fractures are parallel to the drift axis,
        preventing flow diversion within the fracture plane; (b) a two-dimensional (and three-dimensional) fracture
        continuum model considers flow diversion occurring within multiple fracture planes that are approximately
        perpendicular to the drift axis.

Source: BSC 2004b, Figure 6-1.
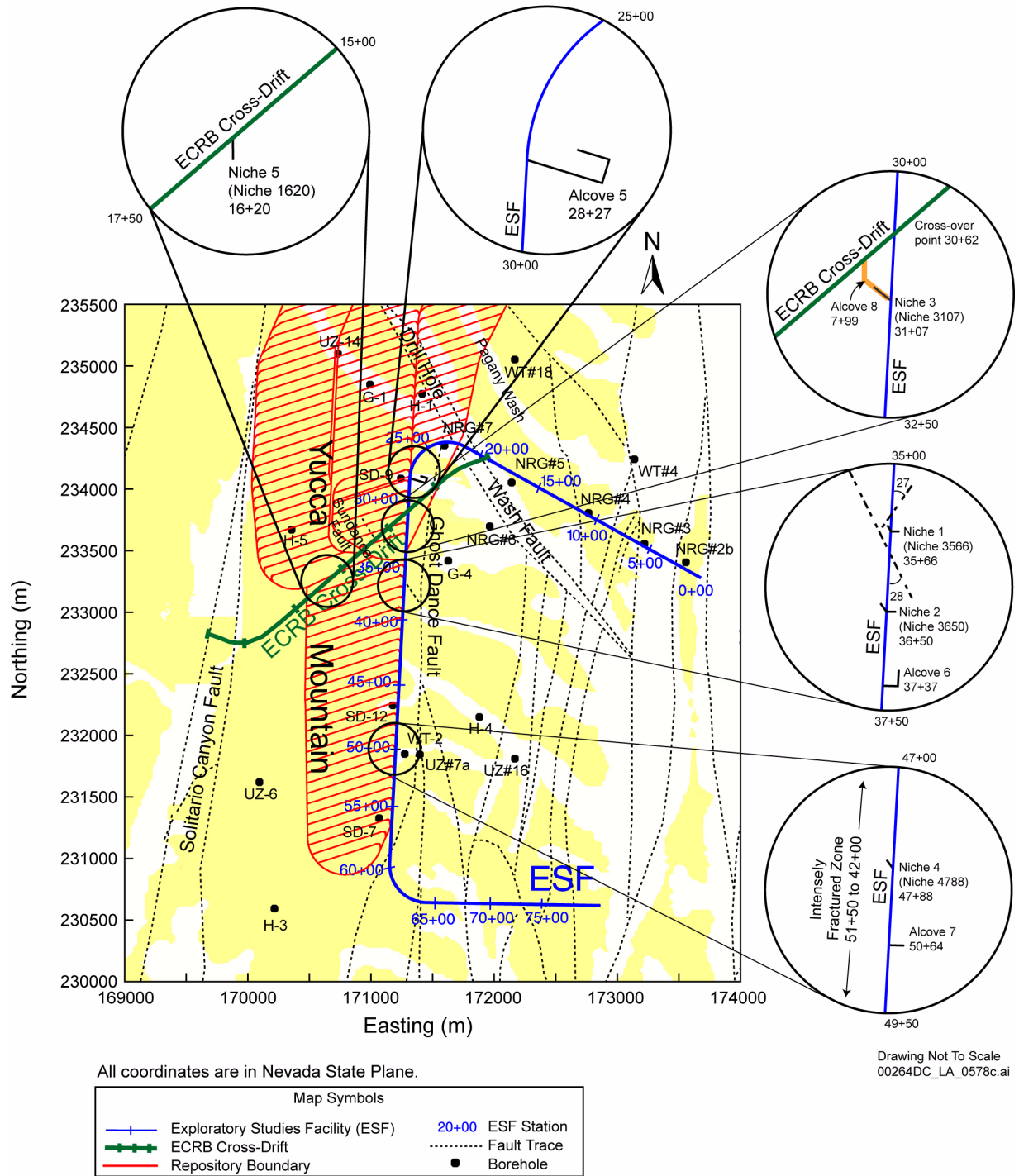
Figure 2.3.3-7. Schematic Showing Approximate Location of Niches and Alcoves 5 to 8

NOTE: The shape of the openings is approximate. Niches 3566, 3650, 3107, 4788, and 1620 are also referred to as Niches 1, 2, 3, 4, and 5, respectively.

Source: BSC 2004f, Figure 6-3.
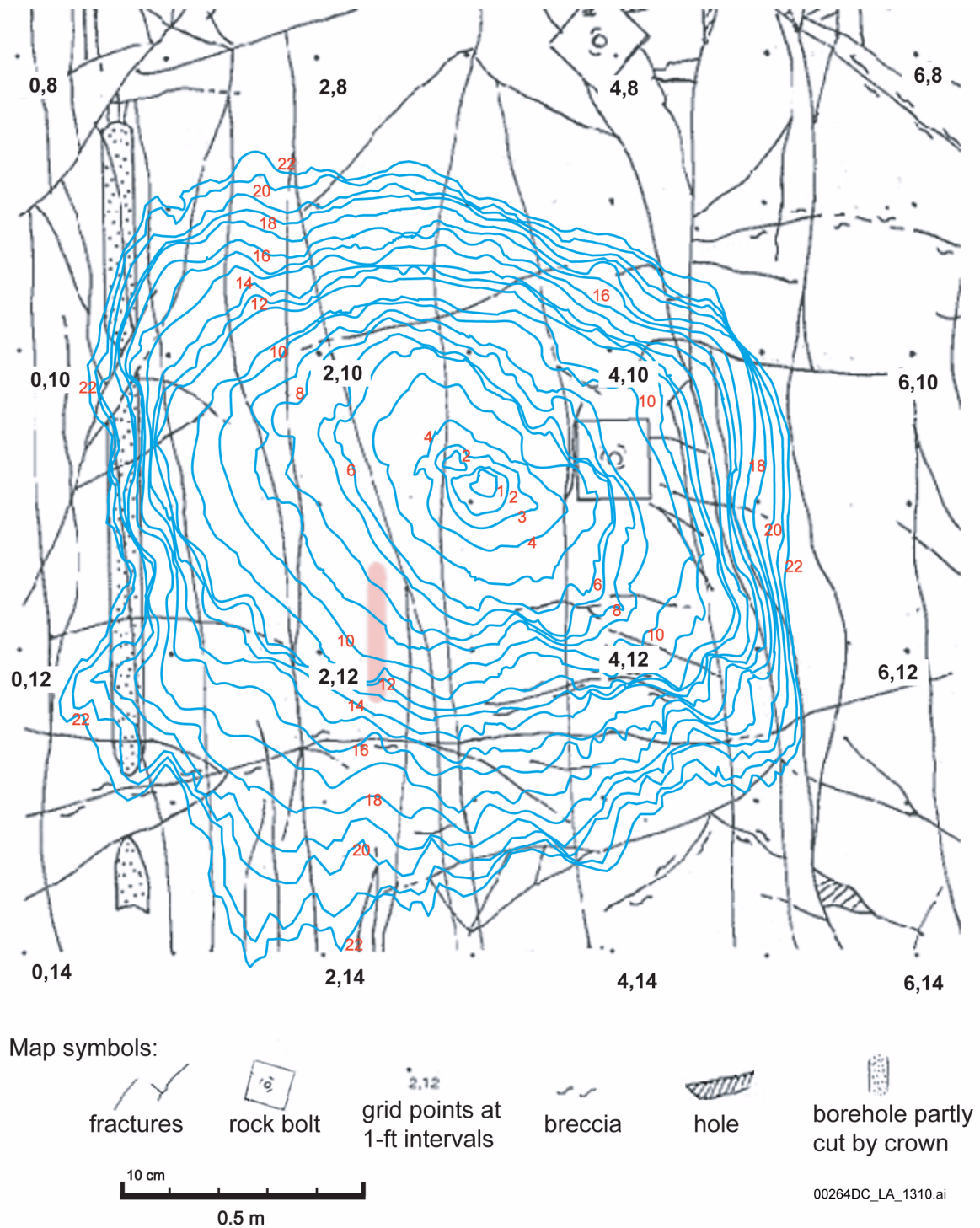
Figure 2.3.3-8. Wetting-Front Sequences Overlying Fracture Map of Niche 4 Crown for a Representative Liquid-Release Test

NOTE: Blue contours are outlines of wetting fronts. Red numbers indicate ordering of the wetting fronts in time (about 12 elapsed days). The pink bar indicates the approximate position of the release interval in the borehole above the niche, projected onto the crown.

Source: BSC 2004f, Figure 6-30.
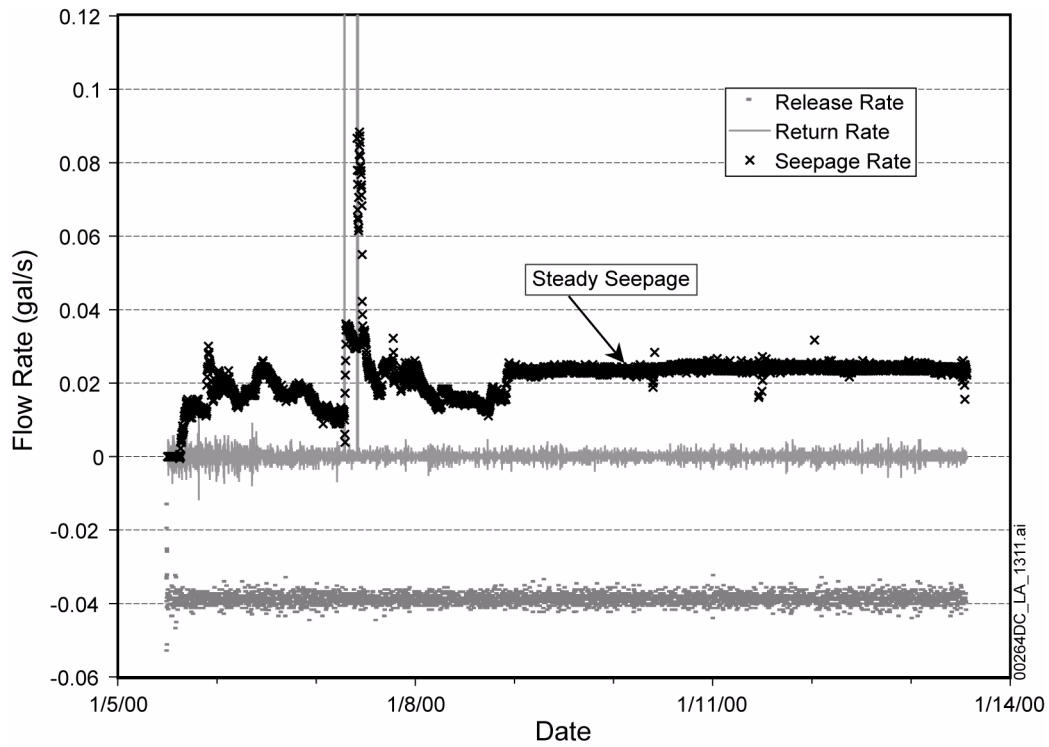
Figure 2.3.3-9.   Release, Return, and Seepage Rates Observed During a Representative
                   Liquid-Release Test Conducted in Niche 4

NOTE: Negative values indicate flow into the formations; positive values indicate flow out of the formation.

Source: BSC 2004f, Figure 6-29.
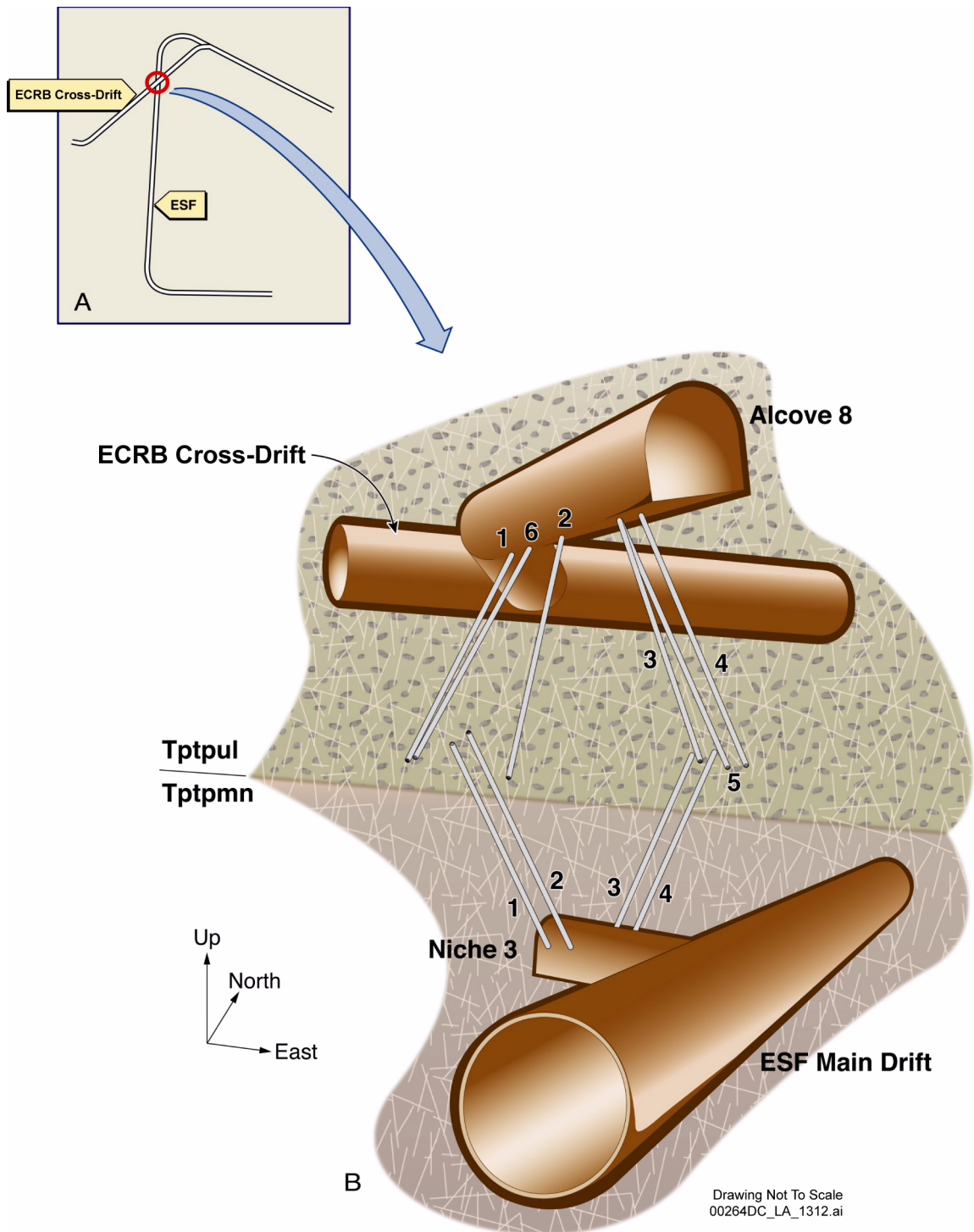
Figure 2.3.3-10. Schematic Illustration of the Alcove 8–Niche 3 Test Configuration

NOTE: Boreholes identified by numbers.

Source: BSC 2004f, Figure 6-149.

Station 25+00

Tunnel Boring Machine
(Hot/Warm)

Station 26+60

Station 26+30

Station 20+00

Station 26+03

Station 25+90

Station 25+60

Station 25+36

Station 25+10

Station 24+40

Station 23+45

Station 22+50

Station 15+00

Station 21+90

Station 21+40

Station 20+40

Legend

X   Relative Humidity/Temperature
     Measurements

     Automated Water Sampler (2 of 6 depicted)
     Stations 24+85 to 24+95

     Electrical Resistance Probe (Saturation Measurement)
     Stations 24+00 to 26+36

     Boreholes with Psychrometers

Station 15+02

Drawing Not To Scale
00264DC_LA_0206a.ai

Figure 2.3.3-11.   Schematic Illustration of the Location of the Tunnel Boring Machine and Monitoring Stations in the Enhanced Characterization of the Repository Block Cross-Drift

NOTE: Not to scale.

Source: BSC 2004f, Figure 6-107.
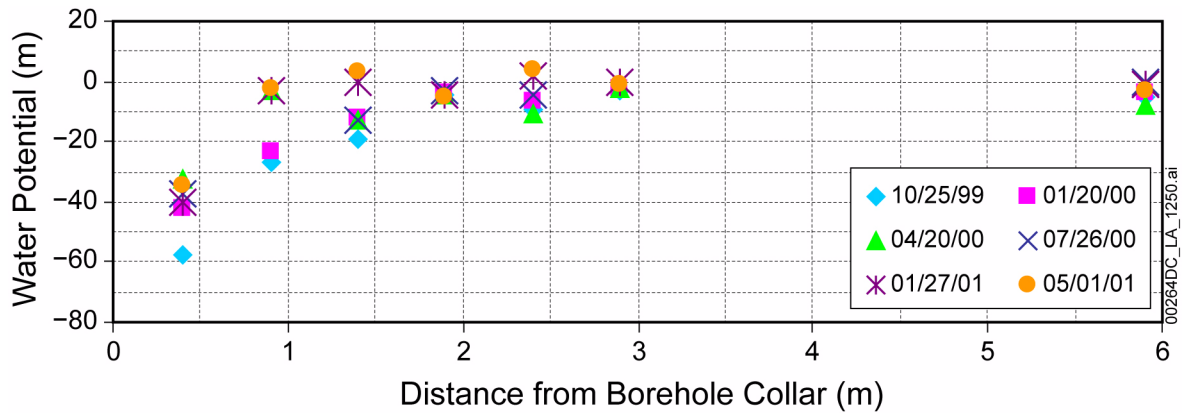
Figure 2.3.3-12.   Water Potential Measurement as a Function of Time and Distance from the Borehole Collar

Source: Modified from BSC 2004f, Figure 6-109b.
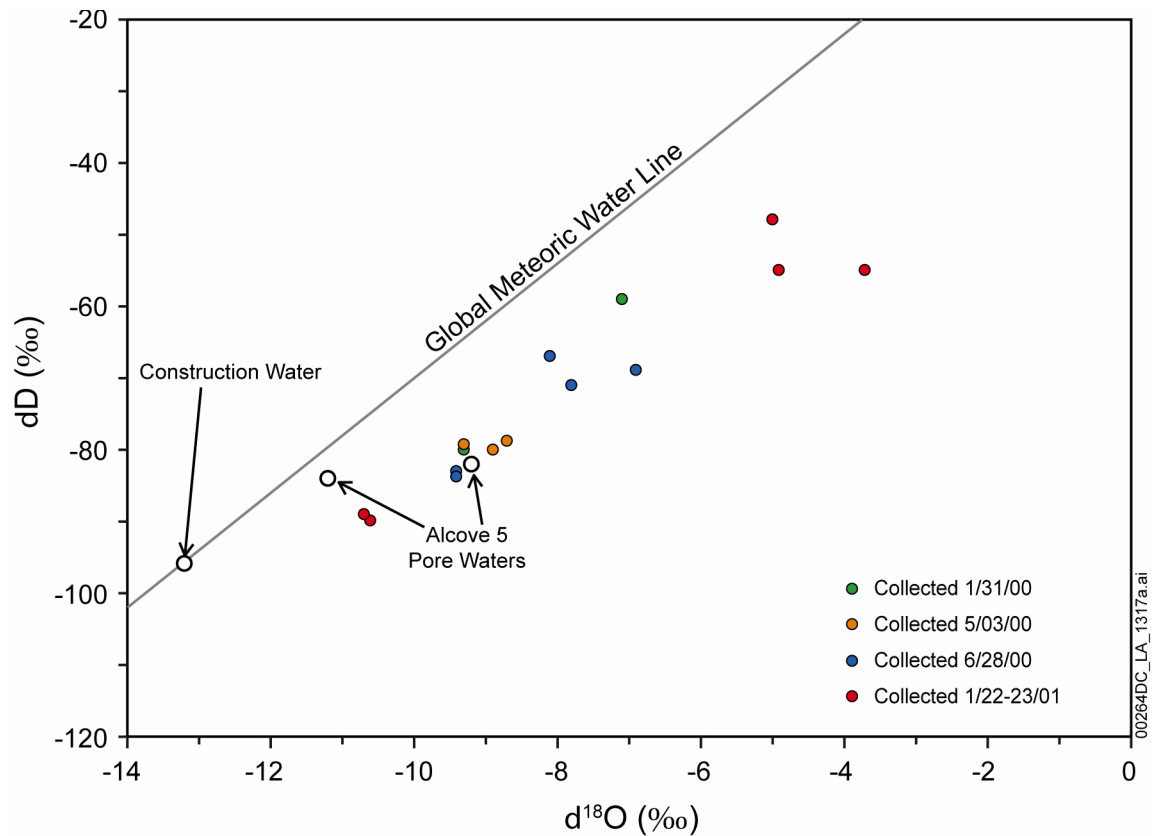
Figure 2.3.3-13.   Plot of the Hydrogen and Oxygen Isotope Compositions of Water Samples Collected from the Enhanced Characterization of the Repository Block Cross-Drift

NOTE: Also plotted is the isotopic composition of construction water, two pore-water samples extracted from core samples from Alcove 5, and the Global Meteoric Water Line.

Source: Modified from BSC 2004f, Figure 6-126.
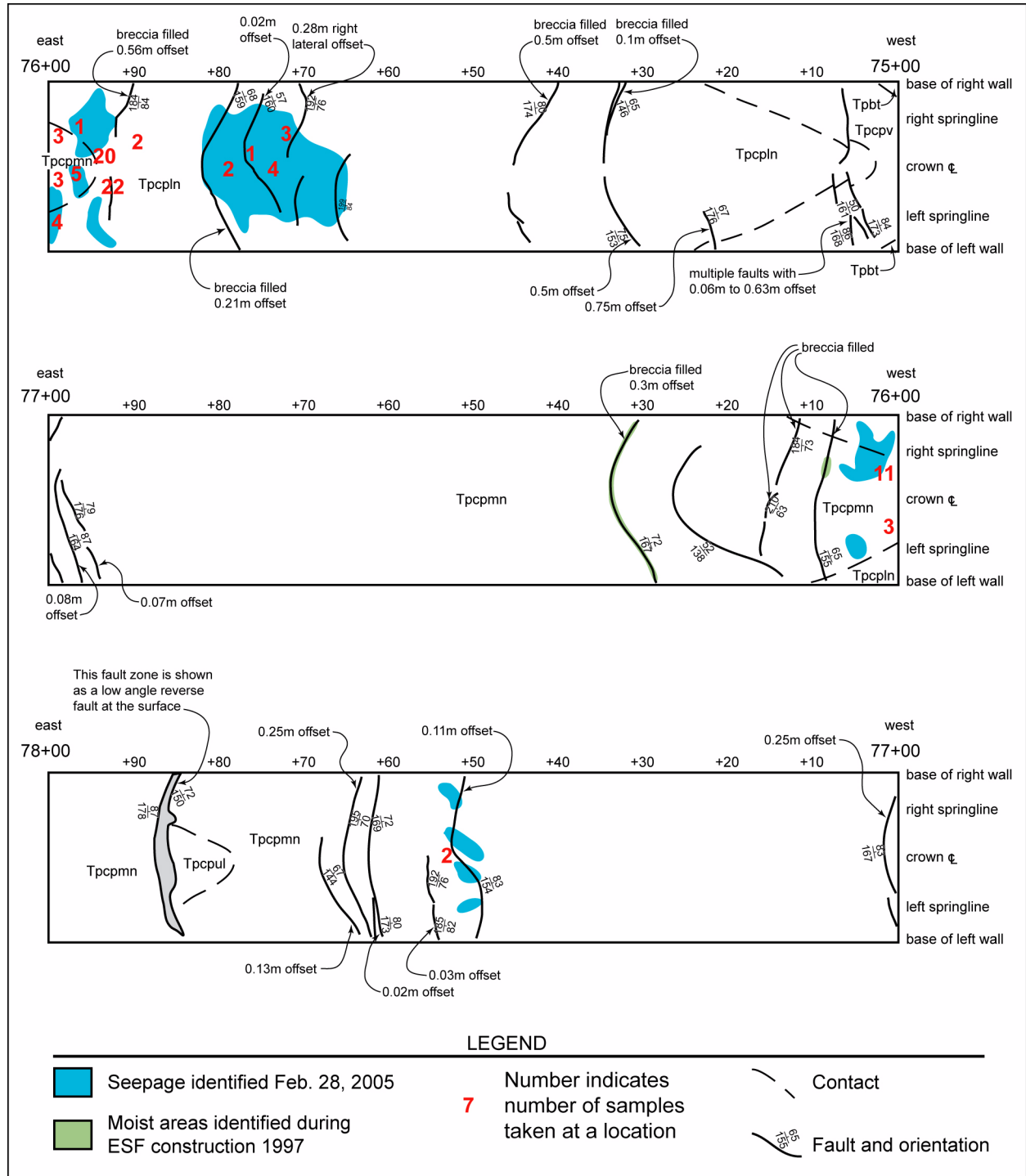
00264DC_LA_0207a.ai

Figure 2.3.3-14.   Full Periphery View of the ESF South Ramp from Station 75+00 to Station 78+00, Showing Seeps Identified Since February 28, 2005

NOTE: Tpcpln = Tiva Canyon Tuff lower nonlithophysal zone; Tpcpmn = Tiva Canyon Tuff middle nonlithophysal zone; Tpcpul = Tiva Canyon Tuff upper lithophysal zone.

Source: SNL 2007a, Figure 7-1[a]
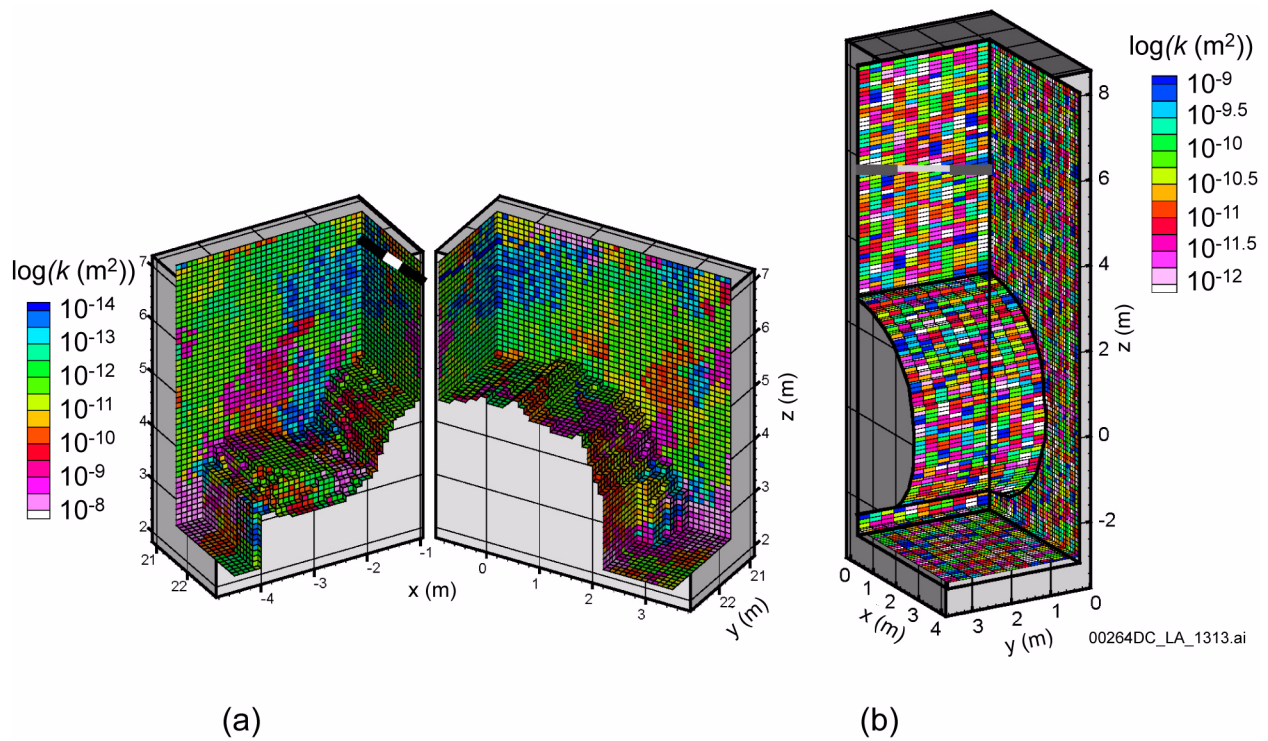
Figure 2.3.3-15.   Examples of the Numerical Grid and One Realization of the Underlying Heterogeneous Permeability Field for the Simulation of Liquid-Release Tests in (a) a Niche and (b) the Enhanced Characterization of the Repository Block Cross-Drift

NOTE: Boreholes are indicated by thick black or grey lines, and the injection intervals are indicated by a thick white line.

Source: BSC 2004b, Figures 6-15b and 6-14.
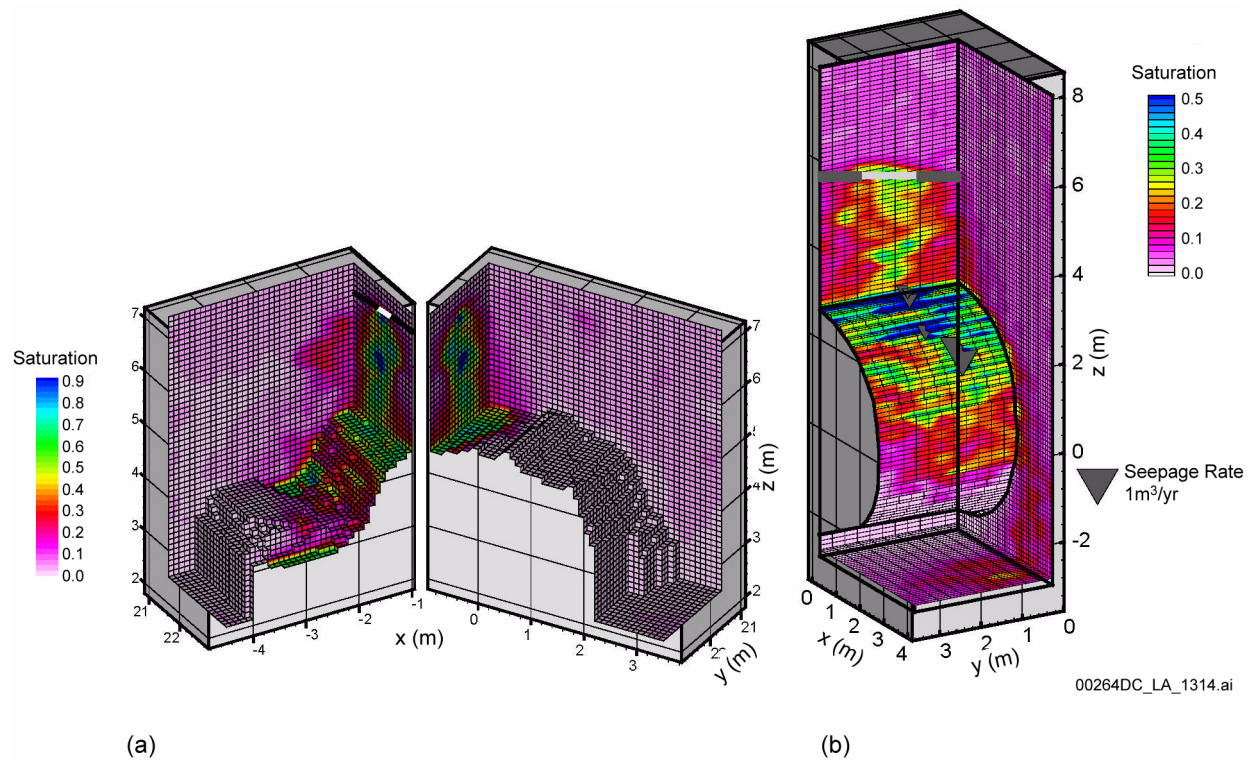
Figure 2.3.3-16.   Saturation Distributions at the End of a Liquid-Release Test Conducted in (a) Niche 5
(at 13 days) and (b) the Enhanced Characterization of the Repository Block Cross-Drift
(at 30 days) as Simulated with the Seepage Calibrated Model

NOTE: Boreholes are indicated by thick black or grey lines, and the injection intervals are indicated by a thick white
line.

Source: BSC 2004b, Figures 6-28a and 6-21d.
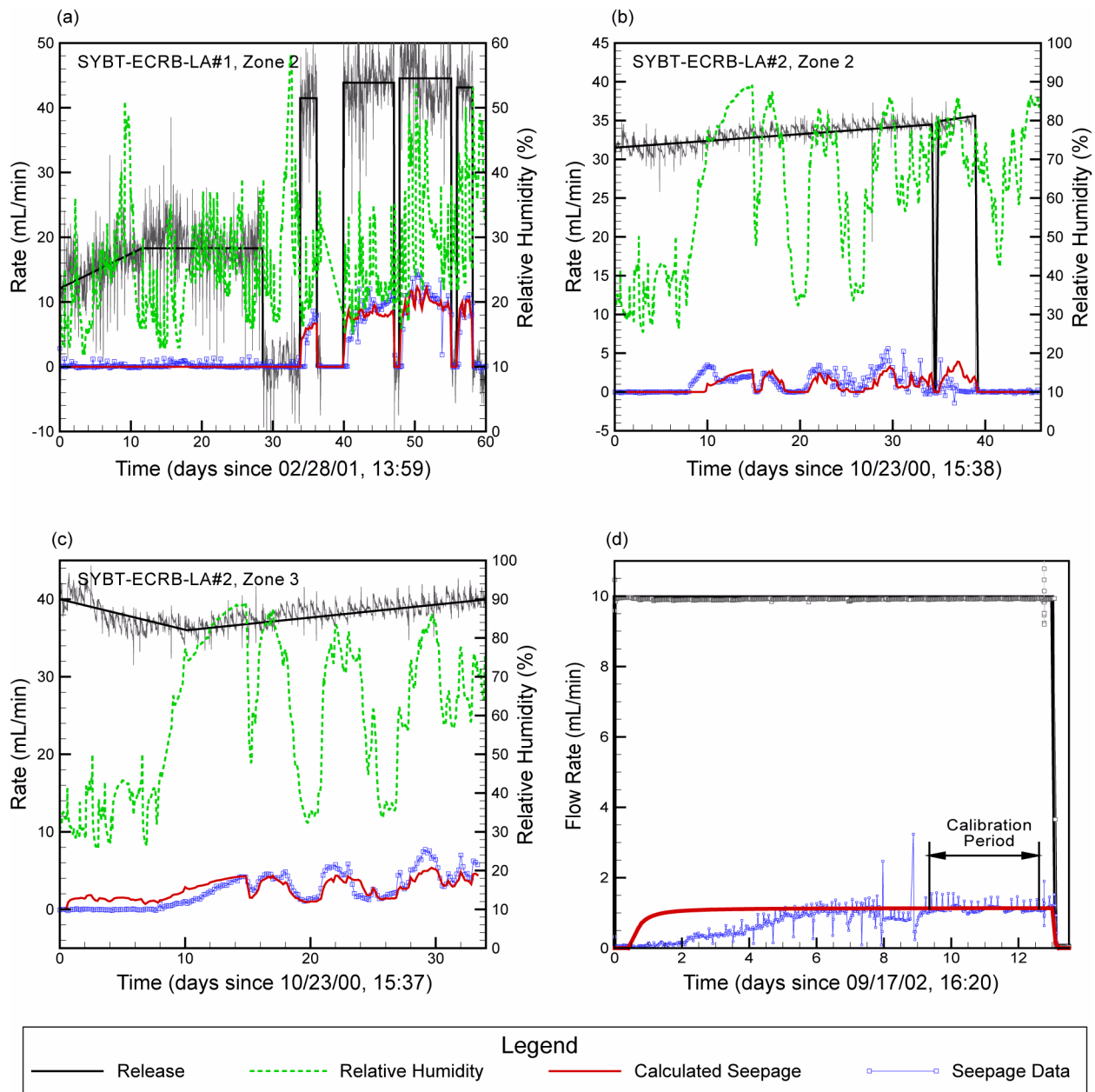
Figure 2.3.3-17.   Calibration of Seepage-Rate Data from Liquid-Release Tests (a) Boreholes
SYBT-ECRB-LA#1, Zone 2; (b) SYBT-ECRB-LA#2, Zone 2; (c) SYBT-ECRB-LA#2,
Zone 3; and (d) Borehole 4 in Niche 5

NOTE: The gray line is the measured release rate, which is approximated in the seepage calibration model by the
black line. Blue symbols represent measured seepage-rate data; the red line is calculated with the seepage
calibration model. The green line is the relative humidity used to prescribe the evaporation boundary
condition. Relative humidity in Niche 5 was constant at approximately 85%.

Source: BSC 2004b, Figures 6-19, 6-22, 6-23, and 6-25.
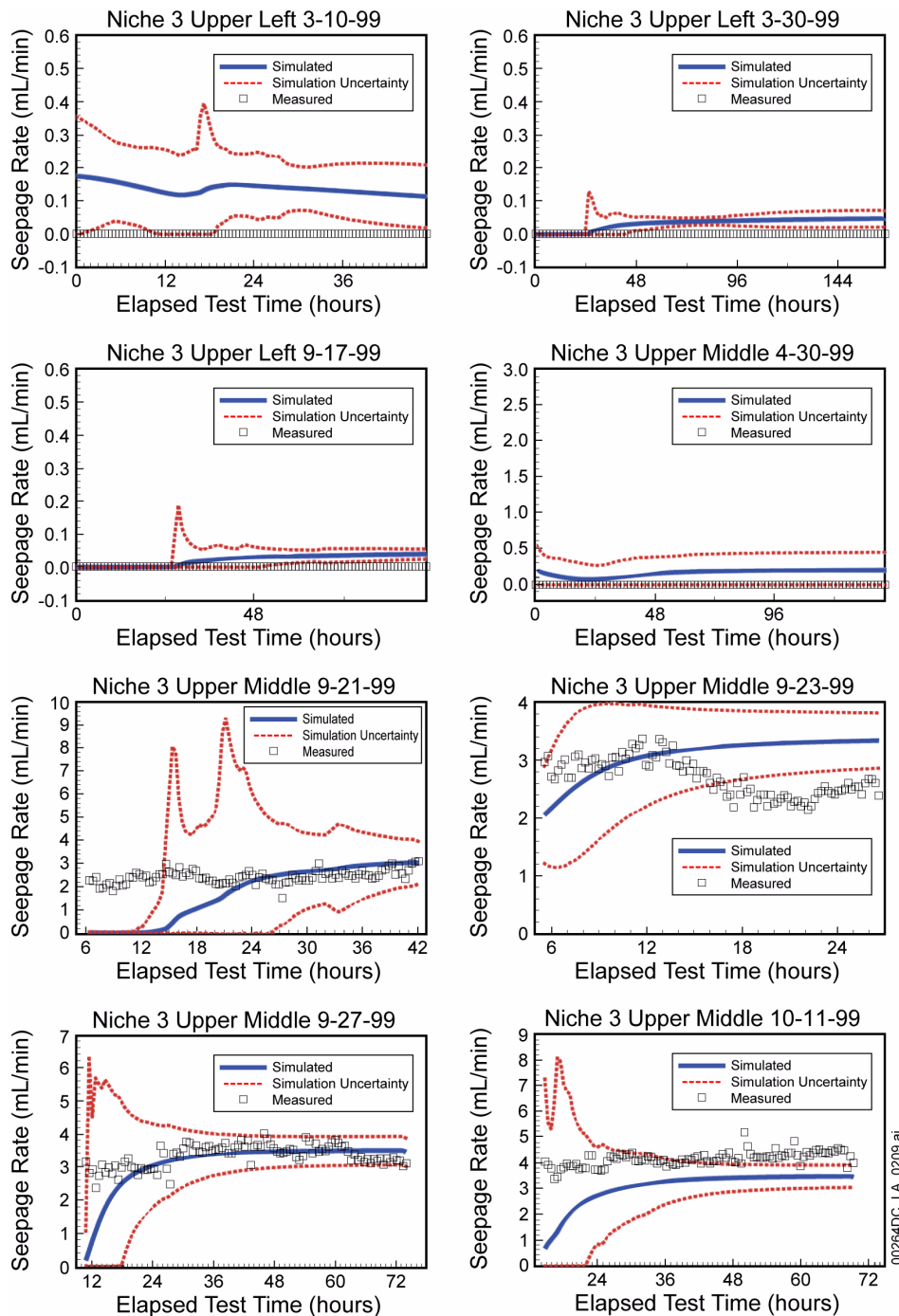
Figure 2.3.3-18.　　Validation of Seepage Calibration Model and Tptpmn Unit Seepage-Relevant
　　　　　　　　　　　Parameters Using Data from Niche 3

NOTE:　Linear uncertainty propagation analysis was used to calculate the uncertainty band of the model estimates.
　　　　　The uncertainty envelope used in the drift seepage abstraction for TSPA is broader than the uncertainty range
　　　　　used for comparison of individual test results with model results. This accommodates the cases in which
　　　　　measured seepage values are greater than the 95% confidence interval around simulated seepage values
　　　　　(Niche 3 Upper Middle 10-11-99).

Source:　BSC 2004b, Figure 7-8.
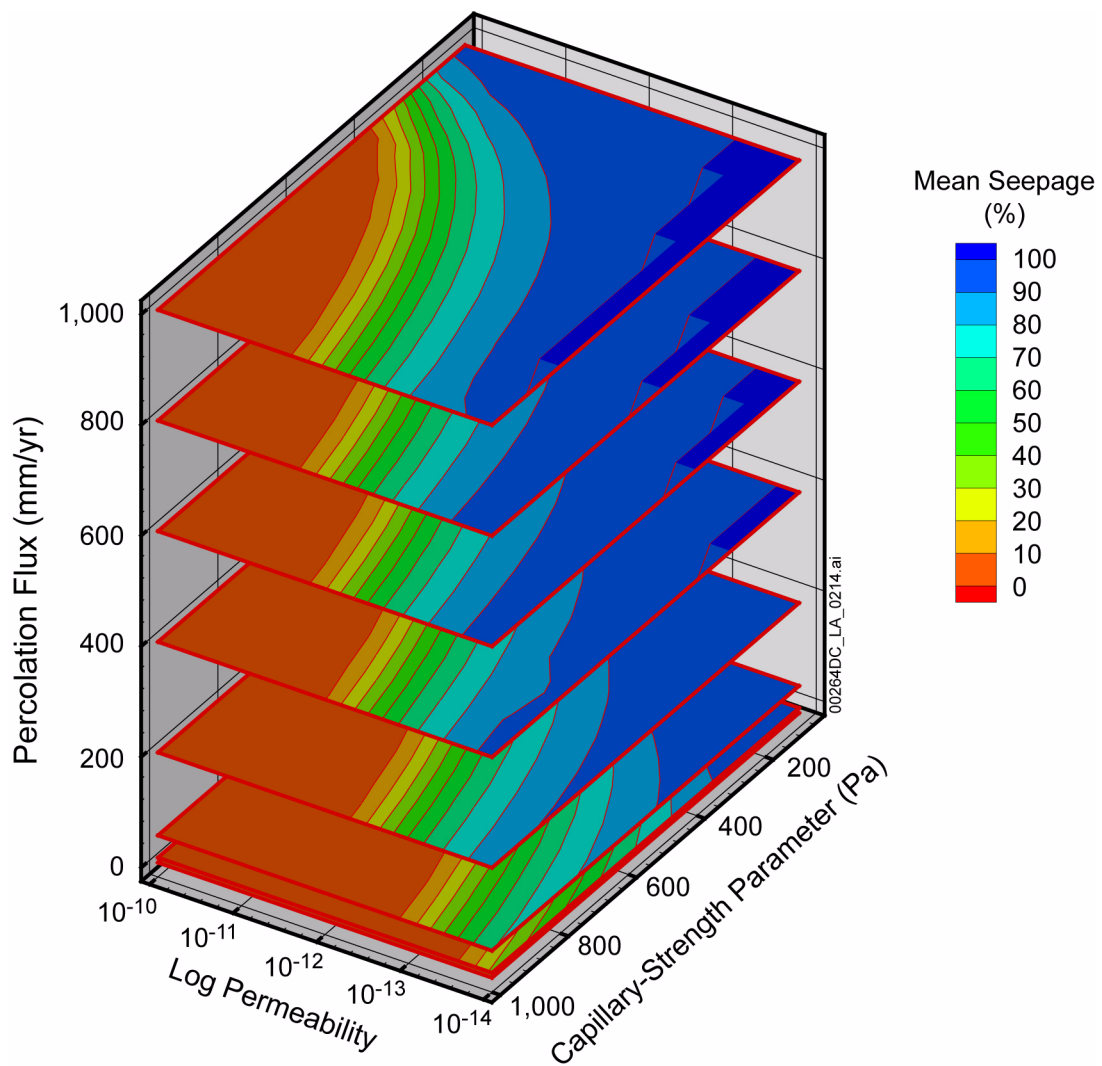
Figure 2.3.3-19. Mean Seepage Percentage as a Function of Capillary Strength Parameter and Log Permeability for Percolation Fluxes of 1, 10, 50, 200, 400, 600, 800, and 1,000 mm/yr

NOTE: Permeability values in log10 of unit m^2.

Source: Modified from BSC 2004a, Figure 6-8.
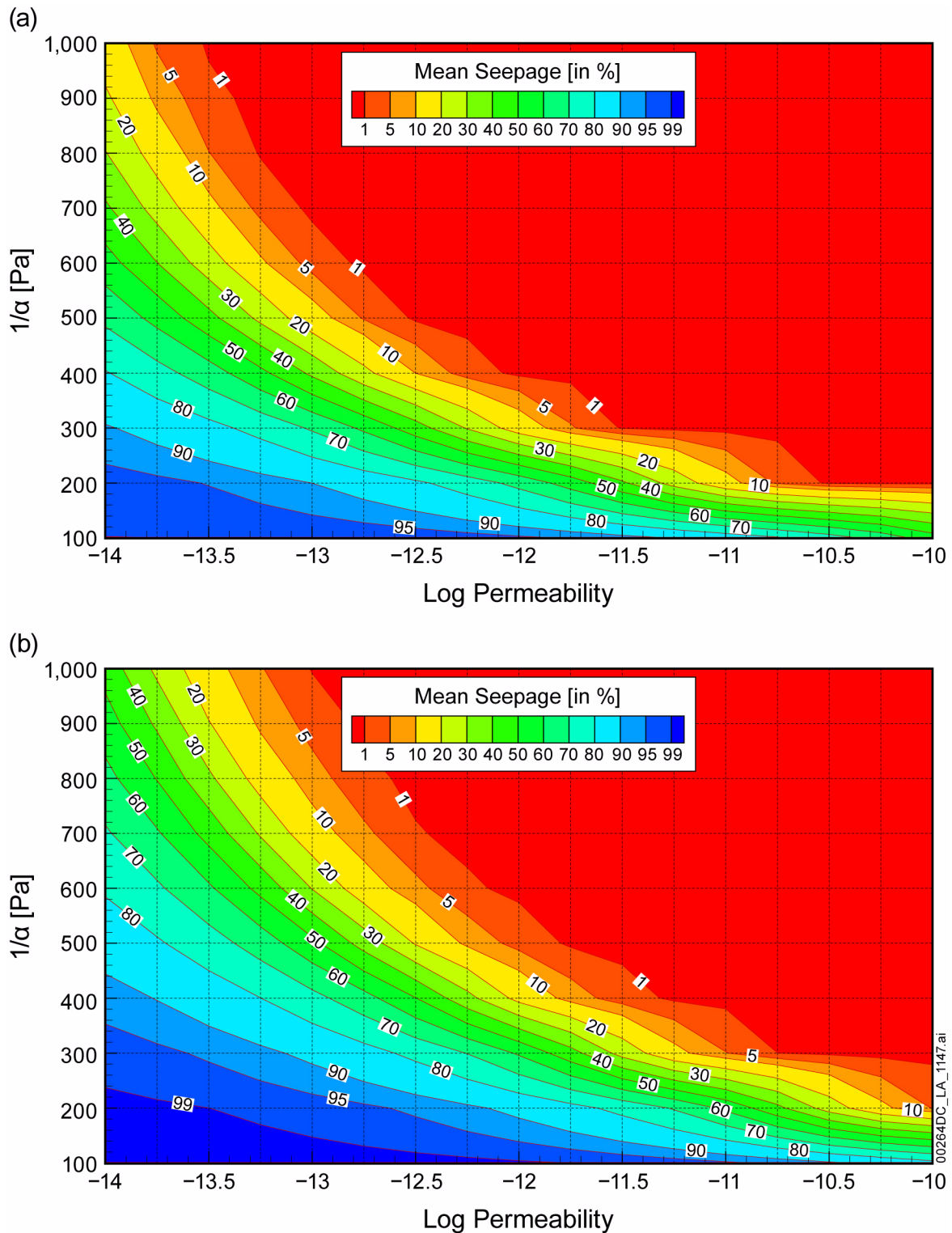
Figure 2.3.3-20.   Seepage Percentage for (a) Intact Drifts and (b) Collapsed Drifts as a Function of
                    Capillary Strength Parameter and Log Permeability for a Percolation Flux of 5 mm/year

NOTE: Horizontal and vertical lines indicate simulated parameter cases. Permeability values in log10 of unit m^2.

Source: Modified from SNL 2007a, Figures 6.4-3 and 6.4-8.
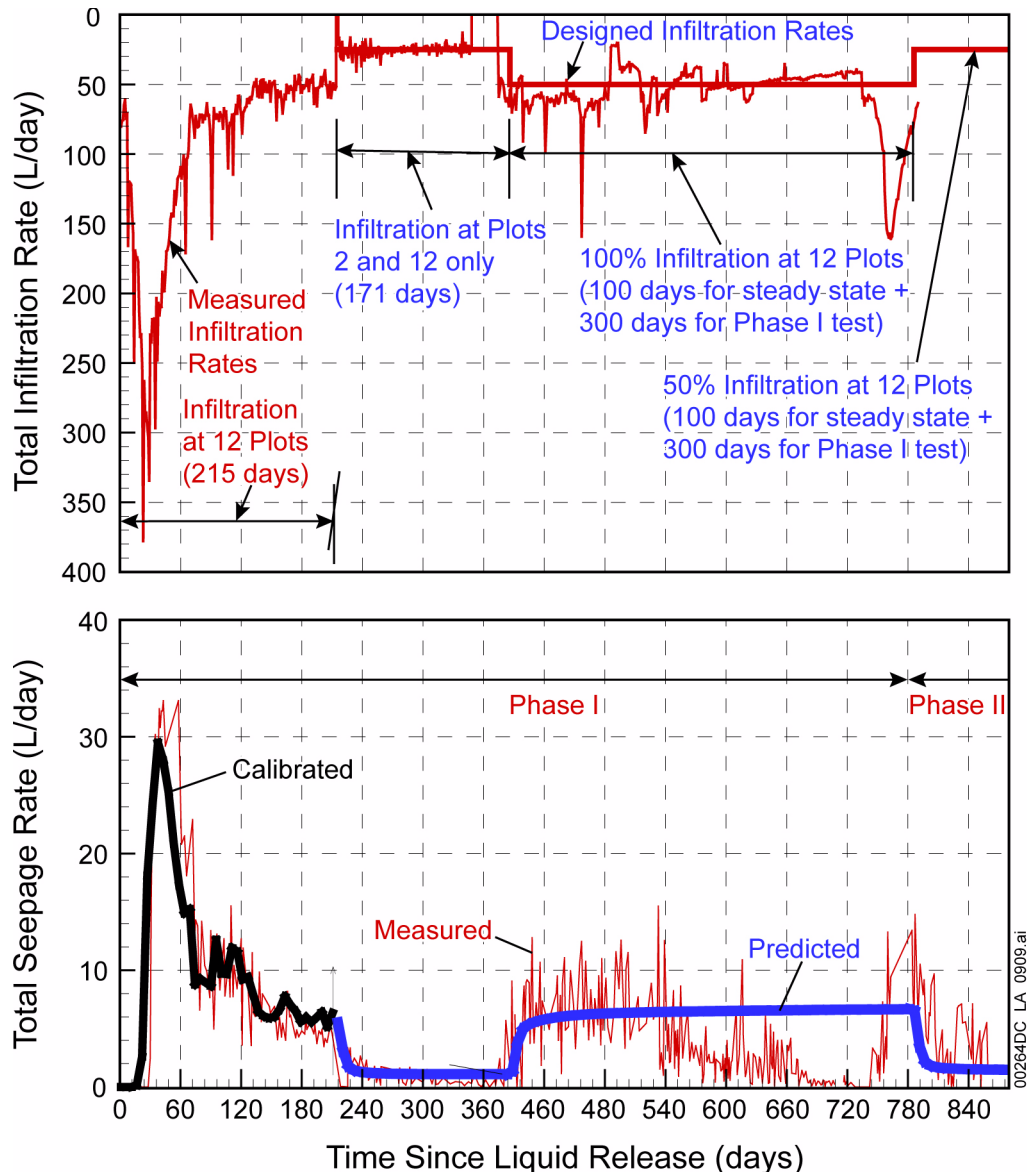
Figure 2.3.3-21. Total Infiltration Rates (top) and Seepage Rates (bottom) in Alcove 8-Niche 3 Testing

NOTE: The bottom plot shows simulated and observed total seepage rates. The model was calibrated for a 210-day period at the beginning of infiltration.

Source: BSC 2006, Figure 6.2-4.
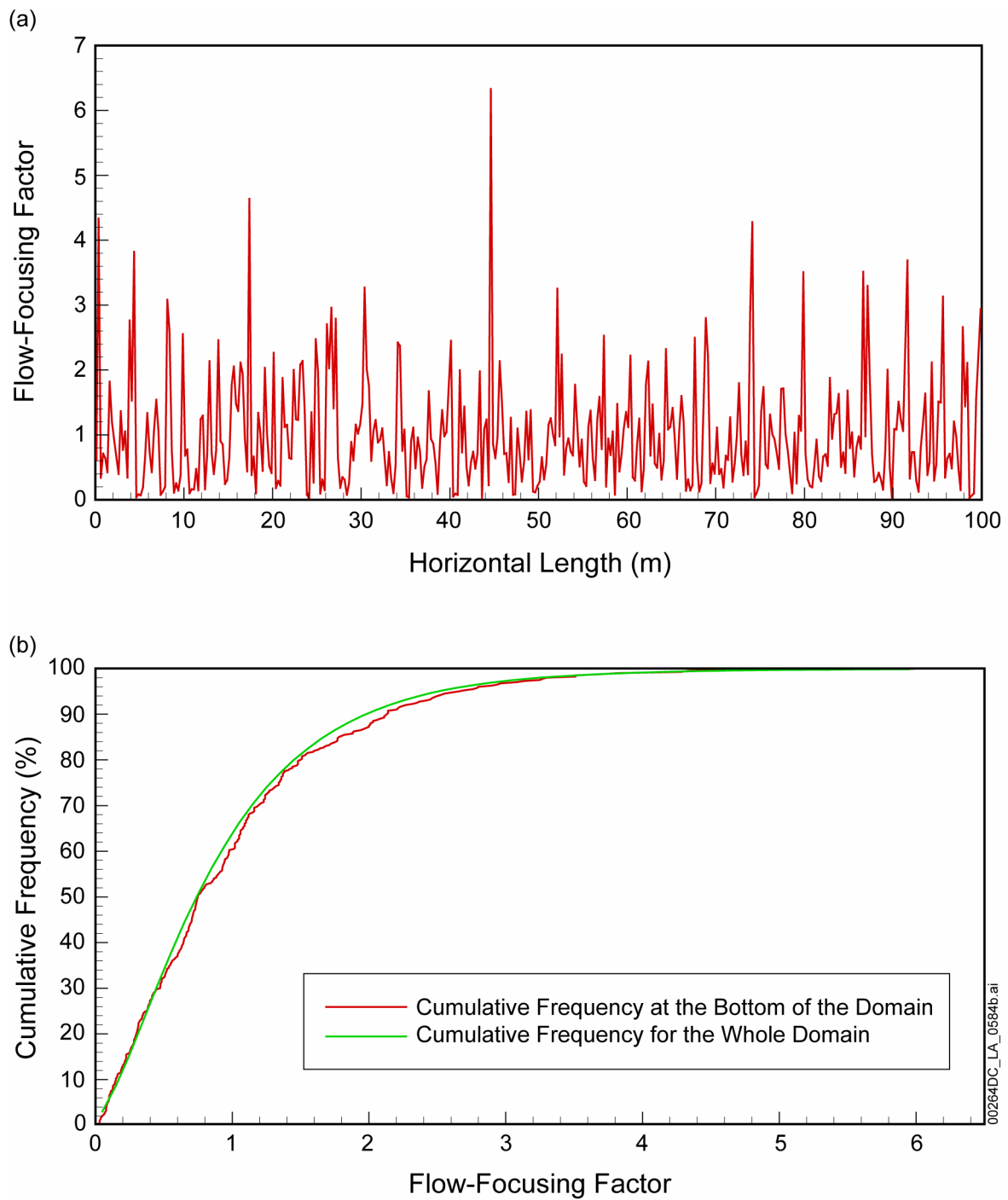
Figure 2.3.3-22.   (a) Spatial Variability and (b) Cumulative Frequency Distribution of Flow-Focusing Factors at the Bottom of the Model Domain for a Simulation Case with 5 mm/yr Infiltration, as Well as Cumulative Frequency for the Entire Model Domain

Source: Modified from BSC 2004a, Figure 6-25.
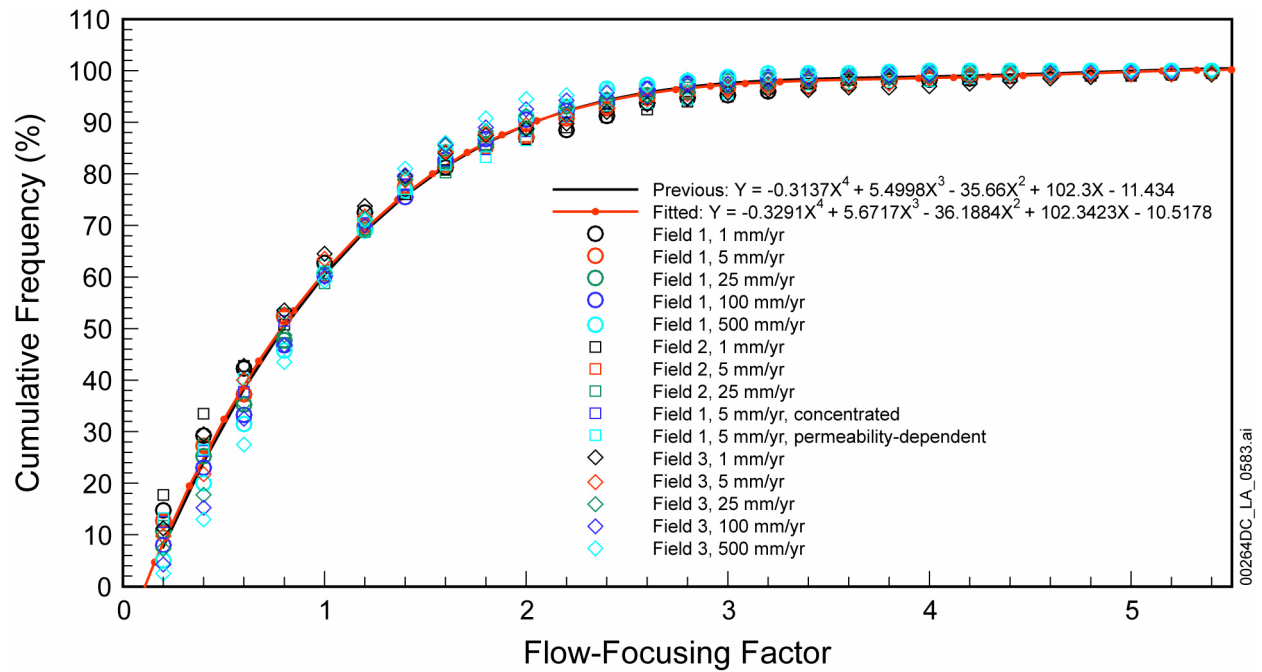
Figure 2.3.3-23.   Regression Curve (and 99% Confidence Band) for Cumulative Distribution of Percolation Flux at the Bottom of the Model Domain, Averaged over All Simulations for Various Flow-Focusing Factors

Source: BSC 2004a, Figure 6-26.
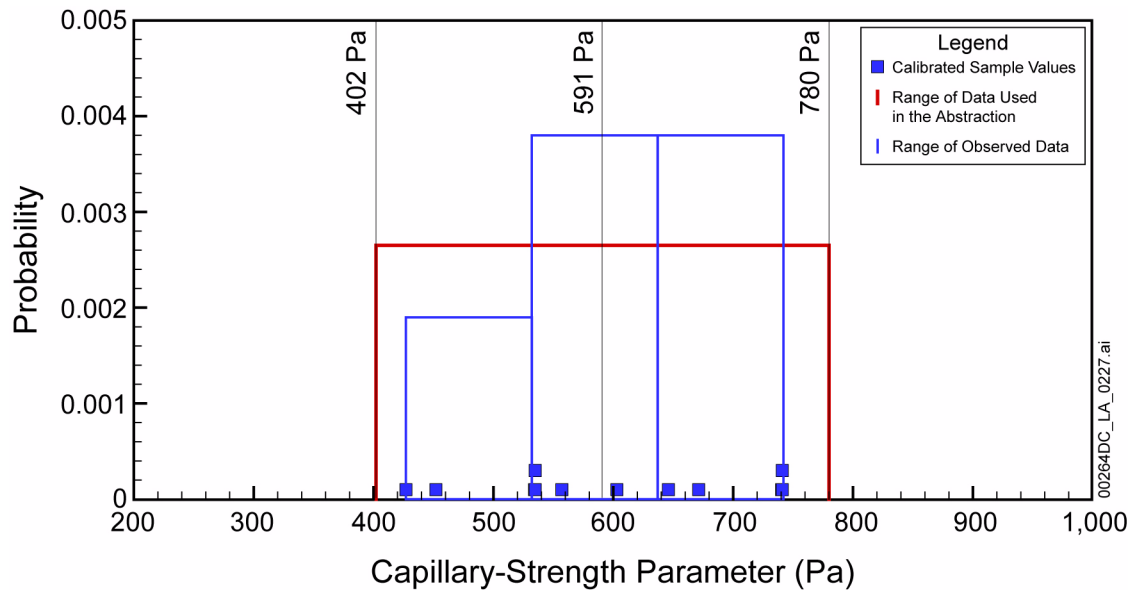
Figure 2.3.3-24.   Histogram and Related Probability Distribution for Spatial Variability of Capillary
                   Strength Parameter, Using Statistical Parameters from All of the Samples from the
                   Tptpmn and Tptpll Units

NOTE: Vertical lines indicate mean and range of distribution.

Source: SNL 2007a, Figure 6.6-2.
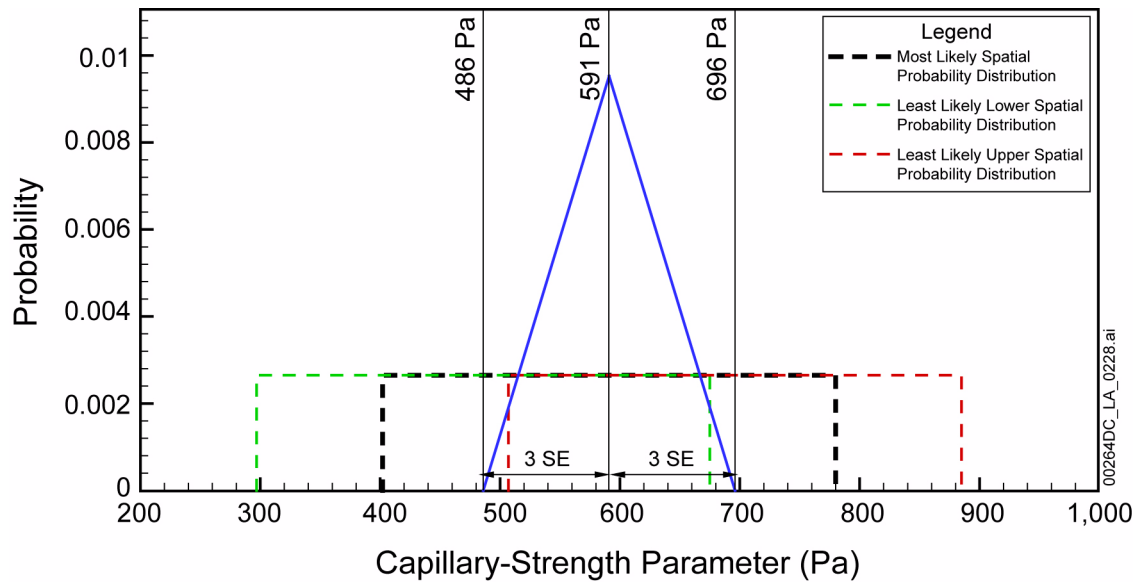
Figure 2.3.3-25.   Triangular Probability Distribution for Covering Uncertainty of the Capillary Strength
                    Parameter by Varying the Mean of the Spatial Probability Distribution, Statistical
                    Parameters Derived from All of the Samples from the Tptpmn and Tptpll Units

NOTE: The least likely spatial probability distributions (at the minimum and the maximum of the triangular distribution)
        are based on statistical parameters summarized in *Abstraction of Drift Seepage* (SNL 2007a, Table 6.6-2).
        SE = standard error.

Source: SNL 2007a, Figure 6.6-3.
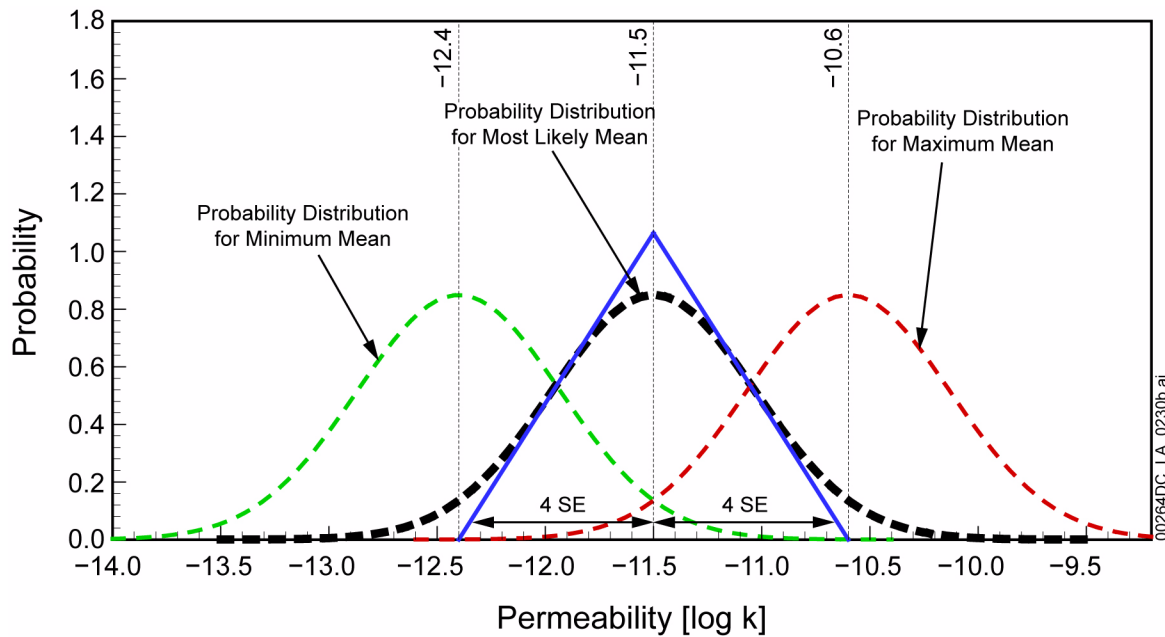
Figure 2.3.3-26.　Log-Triangular Probability Distribution for Covering Uncertainty of Permeability in the Tptpll Unit by Varying the Mean of the Log-Normal Spatial Probability Distribution

NOTE:　The least likely spatial probability distributions (at the minimum and the maximum of the log-triangular distribution) are discussed in *Abstraction of Drift Seepage* (SNL 2007a, Sections 6.6.2.2 and 6.6.2.3). SE = standard error.

Source:　SNL 2007a, Figure 6.6.8.
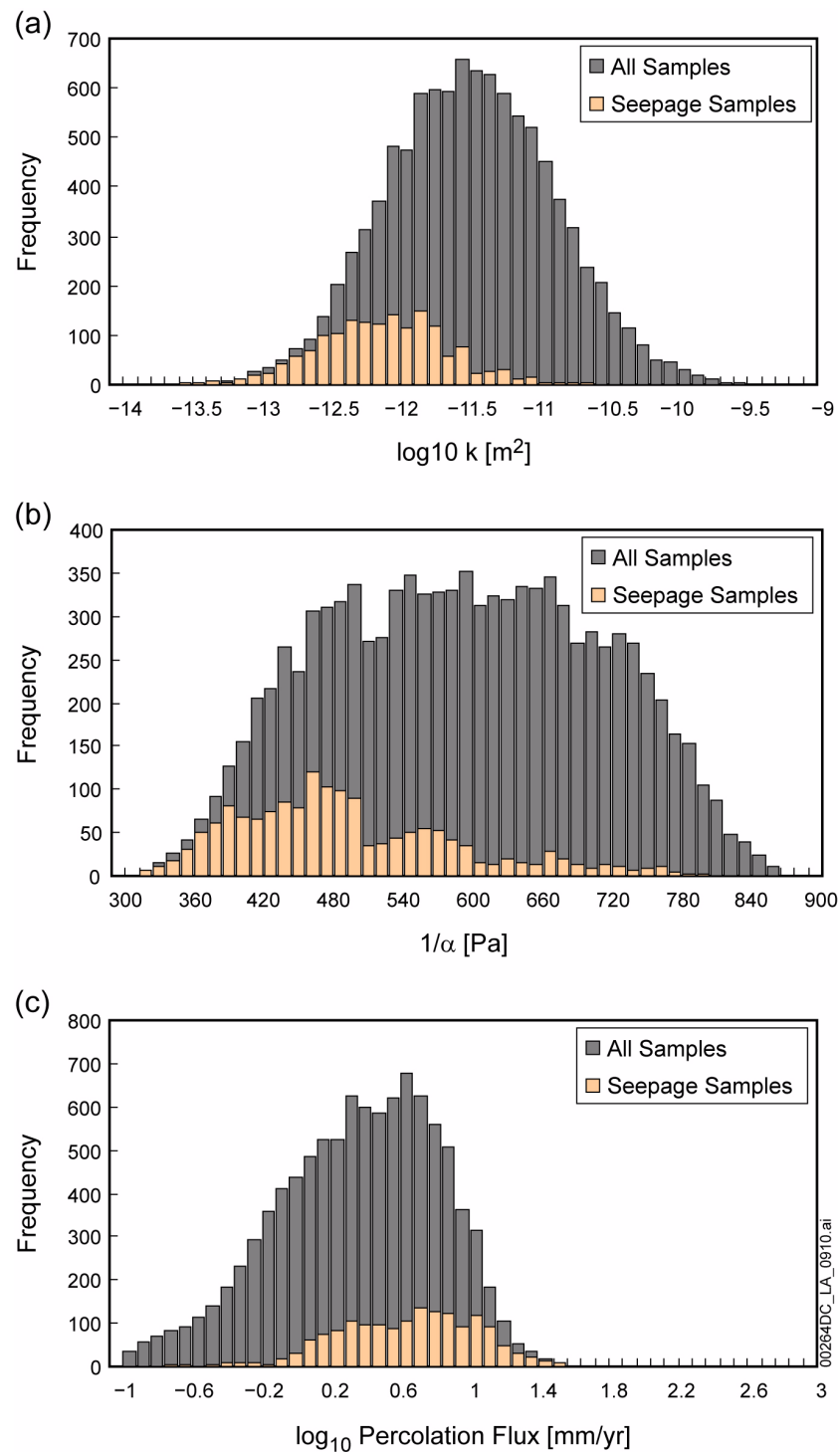
Figure 2.3.3-27.   Histograms of Seepage-Relevant Parameters (a) Permeability, (b) Capillary Strength, and (c) Percolation Flux Including Flow Focusing

NOTE: Results are from the probabilistic calculation for impact drifts in the Tptpll, using flow field from 10th percentile infiltration scenario of the present-day climate. Light-shaded bars indicate parameter combinations giving seepage.

Source: SNL 2007a, Figure 6-12[a].
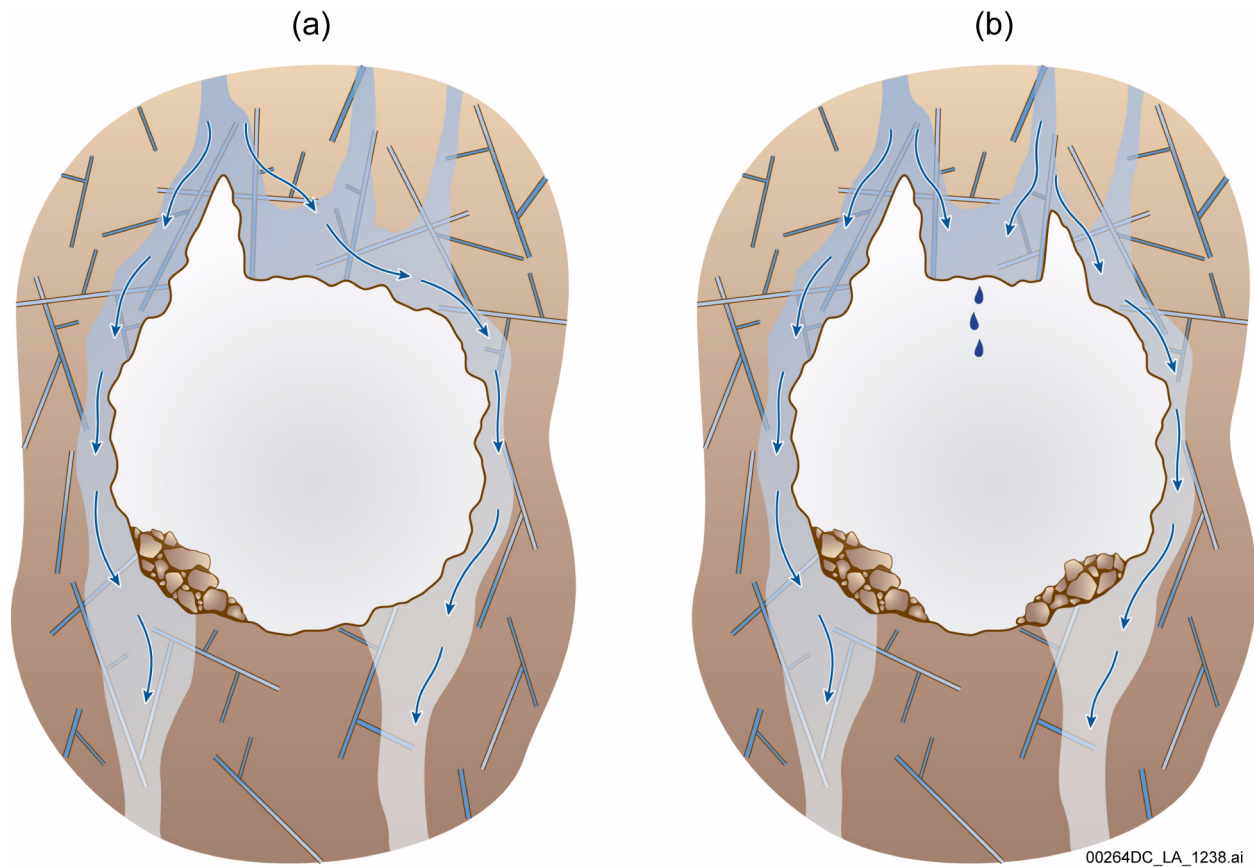
Figure 2.3.3-28.   Schematic of Flow Processes and Seepage in Drifts with Local Wedge-Type Rockfall in Nonlithophysal Rock

NOTE: (a) Single large wedge has shaken loose. (b) Two large wedges have shaken loose, and a topographic low forms at the ceiling, increasing the potential for seepage.

Source: SNL 2007a, Figure 6-7[a].
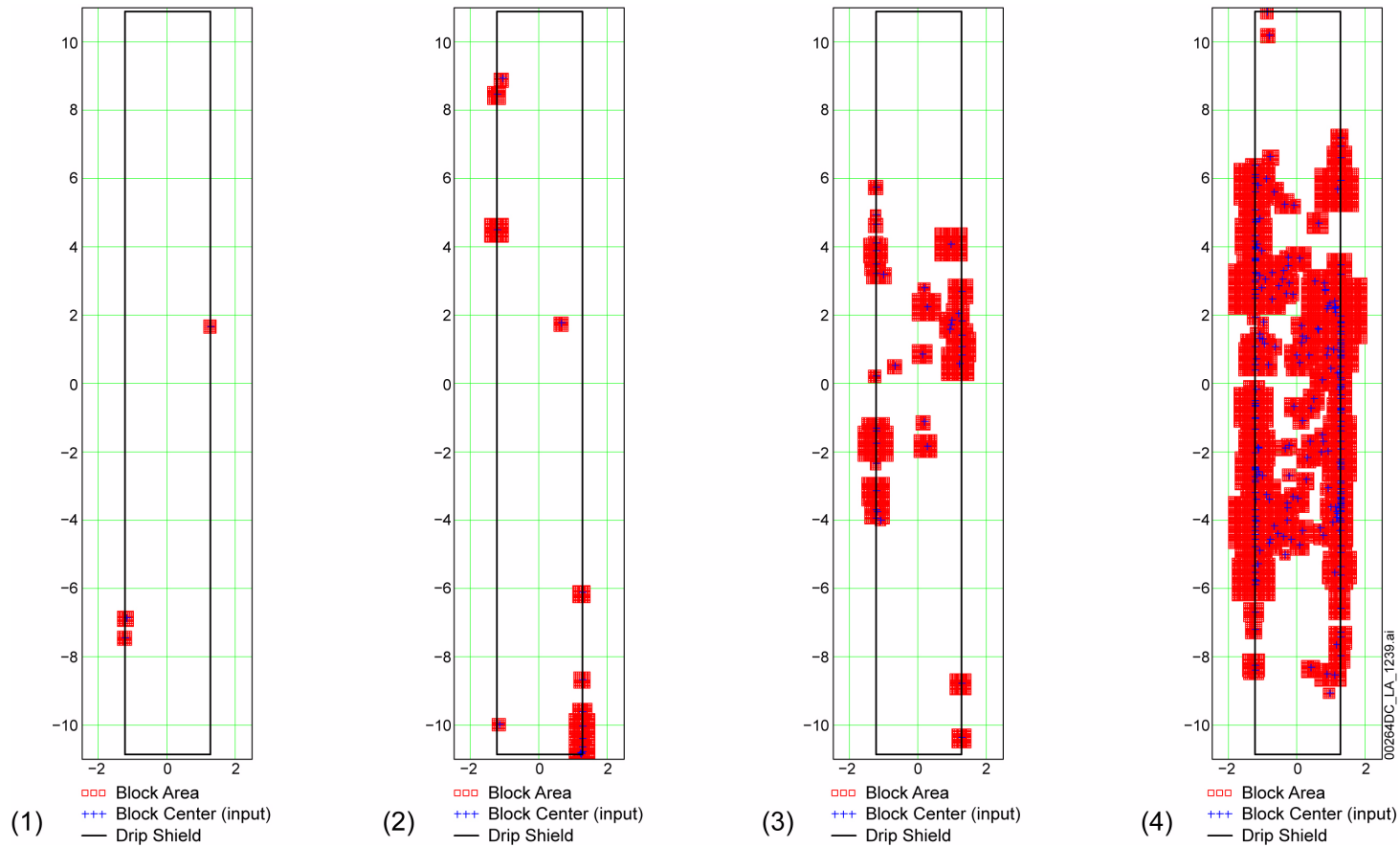
Figure 2.3.3-29. Footprint Plot for Selected Rockfall Cases in Nonlithophysal Rock

NOTE: The axes represent distance along drift centerline and perpendicular to drift centerline. Red areas identify locations where rockfall has occurred. The selected cases are representative of the typical rockfall behavior in the four classes of rockfall severity with (1) PGV = 0.4 m/s, Case 27; (2) PGV = 1.05 m/s, Case 24; (3) PGV = 2.44 m/s, Case 28; and (4) PGV = 5.35 m/s, Case 64. Notice that the PGV level of 5.35 m/s has an occurrence probability of less than 10^{-8} per year. The simulation results derived from the 5.35-m/s PGV level are included in the analyses because they broaden the range of rockfall volumes for evaluation of drift shapes after multiple seismic events. The rockfall volumes for the selected cases are (1) 0.0044 m^3/m, (2) 0.0606 m^3/m, (3) 0.2766 m^3/m, and (4) 2.7281 m^3/m.

Source: SNL 2007a, Figure 6-8[a].